Evolutionary development of palatal bones and *bmp 4* gene-ethanol interaction in cleft palate development: Insights from Mexican cavefish and Zebrafish

by

Nuwanthika Gimhani

A Thesis submitted to the Faculty of Graduate Studies of
The University of Manitoba
In partial fulfillment of the requirements of the degree of

Master of Science

Department of Oral Biology
Faculty of Dentistry
University of Manitoba
Winnipeg, Manitoba, Canada

ABSTRACT

Craniofacial development is a tightly regulated process by several cell singalling pathways. It is therefore highly vulnerable to disturbances by genetic and environmental factors. For example ethanol exposure during pregnancy causes severe birth defects including Cleft Lip and or Palate. Zebrafish (*Danio rerio*) is a well-established model organism for studying craniofacial defects with remarkably high similarity to humans. Mexican tetra (*Astyanax mexicanus*) is another teleost and a promising model organism for evolutionary biology that exists as two morphs: pigmented-eyed surface fish and eyeless cavefish. As an adaptation to dark cave environment cavefish lost their eyes, subsequently these eye lost resulted some craniofacial structural changes in the cavefish. The first objective of my study was designed to understand the effect of early eye degeneration on parasphenoid bone in Mexican tetra. My second objective was deciphering the mechanism of *bmp 4* gene-ethanol interactions on palate development.

Alizarin red-bone staining, micro-CT imaging, Tartrate-resistant acid phosphatase and Alkaline Phosphate staining was conducted to understand bone ossification, articulation, and remodeling within surface and cavefish. The phenotypic effect of ethanol and Dorsomorphin (*bmp 4* inhibitor) in the ethmoid plate was characterized by the alcian blue staining and data was statistically analyzed. Whole-mount in situ hybridization was used to identify the expression of *bmp 4* among different treatment groups. The shape of the parasphenoid bone found to be varies amongst different eye morphs in Mexican tetra. The parasphenoid bone is straightened in cavefish and curved in surface fish. Bone remodeling activity in cavefish increased compared to the surface fish. Ethanol and Dorsomorphin affect the size of the ethmoid cartilage but the severity of the ethmoid cartilage defect increased with the combined effect of both treatments. Reduction of *bmp 4* expression was observed with ethanol and combined treatment in the region of developing ethmoid cartilage.

Our data confirmed the distinct morphological changes of the parasphenoid bone amongst different eye morphs of Mexican tetra fish and these changes might have evolved as adaptation to the nutrition sparse cave environment. Further ethanol does affect craniofacial bone formation and ethanol affects the *bmp 4* pathway and regulate zebrafish plate development.

ACKNOWLEDGEMENT

I express my heartfelt gratitude to my supervisor, Dr. Devi Atukorallaya for the opportunity and the support throughout the last two years. I will fall short of words to express how thankful I am to her. I express my sincere gratitude for her advice and guidance and also for her valuable feedback throughout this project. Her great patience and kind guidance were very important to complete this project successfully.

Secondly, I would like to thank my committee members, Dr. Prashen Chelikani and Dr. Benjamin Lindsey for their encouragement and guidance throughout my research project. Their in-depth analysis of my project further helped me to develop my project.

Next, I also thank our team of smart Summer/Co-op students Jessica Gonzales, Dinu Rajapaksha. Special thanks goes to Rachel Weber, and Can Nguyen for every little support they provided me and for taking shifts with me to take care of our fish.

My thanks also go to Muditha Lakmali, for her valuable support, and for providing the necessary knowledge for the statistical analysis.

I must acknowledge the wonderful lab mates I have made in this journey. Special thanks goes to Anjalee: My word will not do enough justice to express the gratitude that I have towards you. I treasure every bit of lab work we shared. How can I forget Feroz, Manoj, Vivianne, and Nisha for the assistance in laboratory works and helping me with handle the equipment.
This journey won't be possible without you guys Sachithrani Kannangara, Promitha Gosh, Tasnim Becon. Thanks for making this 2-year journey so memorable for me.

Finally, I am much grateful to the University of Manitoba, funding agencies, and my supervisor for taking care of my financial aids.

DEDICATION

Dedicated to my loving parents and my sister for their valuable support, sacrifice and love throughout my academic journey

&

to Asela Weerawardhana, for inspiring me every day to be the best version of myself.

TABLE OF CONTENT

LIST OF FIGURES

LIST OF TABLES

List of copyrighted material for which permission was obtained

1. Chapter 1: Different populations of Mexican tetra and cave location of each population
Reprinted with permission from the company of biologist,
License number- 1102663-1
2. Chapter 1: Homology of zebrafish ethmoid cartilage development compared to the human palate
Reprinted with permission from the company of biologist,
License number- 1102667-1
3. Chapter 1: Alcian blue cartilage stained ventral view and the coronal section of 3 dpf zebrafish
Reprinted with permission from the John Wiley and Sons
License number-5031390956872
4. Chapter 1: Homology of zebrafish ethmoid cartilage development compared to the human palate
Reprinted with permission from the Elsevier Books,
License number- 5024890493751

LIST OF ABBREVIATIONS

~ - Approximately

ADH - Alcohol dehydrogenase

ALP - Alkaline Phosphatase

BMP - Bone morphogenetic pathway (Human & Mouse)

bmp - bone morphogenetic pathway (zebrafish)

Bmpr1a - Bone morphogenetic protein receptor, type IA

Bmpr1b - Bone morphogenetic protein receptor, type IB

Bmpr2 - Bone morphogenetic protein receptor type II

CLP - Cleft Lip and or Palate

CNCC - Cranial Neural Crest Cells

CP - Cleft Palate

DepC - Diethyl pyrocarbonate

dpf - days post fertilization

E - Ethmoid

EDTA - Ethylenediaminetetraaceic acid

EMT - Epithelial-Mesenchymal Transition

FGF10 - Fibroblast Growth Factor 10

hpf - hours post fertilization

Hyb - Hybridization solution

IRF6 - Interferon Regulatory Factor 6

MEE - Median Edge Epithelial

Micro-CT - Micro-Computed Tomography

NCC - Neural Crest Cells

NEFD - Normalized Elliptic Fourier Descriptors

NSCLP - Non-Syndromic Cleft Lip Palate

PAH - Polycyclic Aromatic Hydrocarbon

PBS - Phosphate-buffered Saline

PBST - Phosphate-buffered Saline with Tween-20

PCA - Principal Component Analysis

PC1 - Principal Coordinates 1

PC2 - Principal Coordinates 2

PFA - Paraformaldehyde

SO 3 - Suborbital 3

SSC - Saline-sodium citrate

SD - Standard Deviation

TBS - Tris-buffered Saline

TBST - Tris-buffered Saline with Tween-20

TBX22 - T-box transcription factor 22

TE - Tris-EDTA

TRAP - Tartrate-resistant acid phosphatase

WMISH - Whole-Mount in situ Hybridization

WT - Wild Type

ZO-1 - Zonula occludens-1

CHAPTER 1: INTRODUCTION

Vertebrate skull is a complex structure which can be divide into viscerocranium and neurocranium [1]. Palatal bones are part of the neurocranium which play an important role in the skull by separating the oral cavity from the nasal cavity [2]. These palatal bones are located at the base of the neurocranium [3]. Palatal bones are composed of parasphenoid, ethmoid, vomer, and pterygoid bones [2]. Some of the important roles played by these bones include, serving as muscle attachment sites, providing nerve supply to the neurocranium and also in protecting the brain and brain stem from the ventral side [1]. The human palate consist of the soft palate and hard palate [4]. The soft palate is located at the back of the oral cavity and helps with speech, breathing and swallowing [4]. Hard palate is located at the anterior area of the oral cavity, making up two-thirds of the mouth and facilitate the free movement of the tongue and also it makes the hard floor between oral and nasal cavities so the pressure in the oral cavity does not close off the nasal passage [5]. Unlike palate in humans, the palate is not present in most of the lower vertebrates separating the nasal and oral cavity. Instead it separate brain from the oral cavity [6]. Palatal bones are extremely vulnerable to changes and continue to evolve over time [7]. The evolutionary development of these bones have not studied in detail but the information on morphological and molecular developmental patterns of these bones could provide important insight to the common birth defects associated with these bones.

Palatal bones have evolved in various taxa. In particular, loss of palatal bones, gain of new bones, modified articulation, morphology, and bone positions have evolved as an adaptation to feeding and respiration [7]. From the evolutionary perspective, proper palatal bone arrangement which separates oral and nasal cavity first developed in the reptiles and palate similar to the humans was found in the birds and some mammals [7]. Recently teleost fish has identified as fine animal models to study the evolutionary development of the cranial skeleton. [8]. Among them Mexican tetra fish *(Astyanax mexicanus)* is widely recognized as an excellent model for the evolutionary and developmental biological research [9]. Mexican tetra has two morphs; blind albino cavefish and eyed pigmented surface fish [8, 10]. Cavefish has developed some adaptation to the cave environment by developmental trajectories and limited resources in the inhabiting niche [11]. As a major adaptation to the dark cave environment, cavefish eye has degenerated. Consequently eye degeneration in cavefish leads to some craniofacial changes [12]. For instance, Eye loss directly affect the size, shape and position of the circumorbital bones [1, 13]. The maxillary teeth, the positions of SO 4 to SO 6, and the shape of the opercular bone were found to be unaffected by the eye loss [12]. The effect of eye loss on palatal bone development has not been studied before and Mexican tetra found to be a fine model to

investigate this intriguing question. Comparison between cavefish and surface fish could provide important insights to long-term morphological adaptation. Evolutionary changes in the palatal bones are critical for understanding functional and structural changes that occurred in the oral cavity. These adaptations possibly requiring variation in muscle attachments and relative positioning of the major sensory organs [14].

Embryonic development is a delicate process influenced by the environment. Environmental factors, not only affect the evolution, but also could interfere with normal bone growth and ultimately result in disease conditions. Cleft Palate (CP) formation is one such example. CP develops as a result of improper palate fusion in embryonic palate development. [15]. Both genetic and environmental factors could be at reasons for CP however, the exact etiology still remains unclear. Previous studies have demonstrated that exposure to ethanol in the first trimester of the pregnancy can increase the incidence of CP [16]. According to previous studies, CP condition is linked to a number of genes and environmental factors. The discovery of the possible gene and environmental factors linked to CP development takes us one step closer to understanding how these defects develop and these studies contribute to get a better understanding of the etiology of CP and provide useful information in developing disease mitigation strategies. Therefore, studying evolutionary and clinical aspects of the palatal bone development will be a significant area in understanding the normal development and designing therapeutic regimens in disease conditions. Furthermore, these studies will help to reduce the knowledge gaps in evolutionary and developmental aspects of the palatal bone development.

1.1 Neurocranium of the teleost fish

The cranium or the superior aspect of the skull is one of the unique structures of the gnathostomes (Jawed vertebrate) skeleton. The neurocranium and viscerocranium are the two major parts of the cranium [1]. The neurocranium forms the skull vault and skull base which are structurally arranged to encapsulate vital organs such as the brain and brain stem [1]. The neurocranium is also identified as a rostral continuation of the axial skeleton [1]. In vertebrates, the base of the anterior skull consists of the palate; which is considered to be the roof of the mouth separating the oral and nasal cavities [3]. The palate mainly encompasses ethmoid, vomer, pterygoid and parasphenoid bones [2]. This bone arrangement varies in different phyla. For instance in zebrafish (*Danio rerio*) the anatomical location of ethmoid bone has close proximity to olfactory apparatus of the skull [2]. The vomer is a tear-drop-shaped bone located ventrally to the ethmoid bone. The parasphenoid bone is an unpaired bone, dorsoventrally

flattened and elongated bone located in the midline of the skull [2, 17]. There two lateral wings have extended out from the middle area of the parasphenoid bone [2].

1.2 Palatal bones evolution in vertebrate phyla

In the complex evolutionary history, palatal bones were subjected to a vast array of changes, which include changes in their position, morphology, and articulation [7]. In some cases, bones in different taxa were either lost or gained in response to selective pressure. For example, adult salamanders (amphibian) have well-developed parasphenoid bone which resembles the brachiosaur dinosaur from the cretaceous period, whereas the other amphibians that belong to order Anura (frogs and toads) do not have well-developed parasphenoid bones [7]. Furthermore, the bones in anurans are in the form of struts or rods, which interestingly resembles the early-stage bone differentiation in salamanders [7]. In contrast, the vomer bone is highly developed in both salamanders and anurans [18]. In caecilians (limbless amphibians), the parasphenoid bone is absent but the vomer is well developed [17].

Reptiles have vomer and parasphenoid bones [18]. In these animals, the parasphenoid bone consists of a narrow median portion with a pair of lateral wings located towards the posterior end [17]. This morphology is common among crocodiles, turtles, lizards as well as in birds [17]. The vomer bone is a major supporting bone in the roof of the oral cavity in all the diapsids (reptilian amniotes with two holes on each side of the skull) except crocodilians [19]. Whereas in mammals, the vomer is not a part of the palate and is located in the nasal cavity [19].

Evolutionarily cyclostomata is a group of jawless fish which includes hagfish and lampreys. This group consists of a processes that grow dorsally and rostrally and differentiate into the upper lip, there by pushing the nostril towards the dorsal aspect of the head [20]. For instance, hagfish consists of a posterior process that divides the oronasal septum [20]. In contrast to jawless fish, the craniofacial anatomy of bony fish like teleost fish consists of complex bony structures [10]. Furthermore, in comparison to the primitive skulled fish like the Devonian crossopterygian and actinopterygian (class of bony fish), the skull bones of teleost fish are more complex [10]. The teleost is the largest group of fish that accounts for more than 95% percent of actinopterygians, which accounts for about half of the extant vertebrate species [8]. In addition, the teleost fish also exhibit great diversity in genome, physiology, anatomy, and behavior which validates their use as a model organism in studying vertebrate evolution [8].

Teleost fish exhibits many important characteristics, such as adaptive radiation (adaptation of an organism to spread into other environments) and trophic polymorphism (phenotypic diversification) [21]. Therefore they have been identified as model organisms to study the evolutionary development of the craniofacial structures [21]. Some of the teleost fish groups

are well studied, such as Atlantic salmon (*Salmo salar*), Rainbow trout (*Oncorhynchus mykiss*), Nile tilapia (*Oreochromis niloticus*), and Channel catfish *Ictalurus punctatus* [8]. Genomic studies have been carried out to identify the traits responsible for reproduction, environmental tolerance, disease resistance, pigmentation and growth control [8]. Other than that, zebrafish and Japanese medaka (*Oryzias latipes*) are widely recognized as biomedical models in studies involving a wide range of areas from early development to advanced aging studies [8, 22-24]. Recently, *Astyanax mexicanus* (also known as Mexican tetra, surface, or cavefish) was identified as a promising model organism in evolutionary developmental biology [25, 26].

Phylogenetically Mexican tetra is closely related to zebrafish. Mexican tetra have been used to identify potential markers and gene knock down studies [26]. The craniofacial skeleton of different eye morphs of Mexican tetra has been subjected to many morphological and epigenetic studies due to its intriguing coordinated development with the eye structures [12, 27]. A detailed anatomical study about the structural arrangement of body organs of this fish is not available to date [1]. Mexican tetra make a good model organism because it can be bred and raised in laboratory conditions [1]. Molecular approaches such as transgenic fish line generation and morpholino knock-down can be applied on this species [1]. Furthermore, it has been used in the quantitative trait loci analysis, comparative gene sequence analysis between cave and surface population [1-3, 17]. Therefore, a comprehensive study on Mexican tetra structural organogenesis is vital at this point.

1.3 Mexican tetra *(Astyanax mexicanus)*

Mexican tetra belongs to the order characiform [7]. It is one of the most promising new model organisms for evolutionary and developmental biological researches [18, 20]. Cavefish originated from the ancestral surface-form when their cave-dwelling ancestors became isolated in the limestone caves in the Sierra de El Abra region in Mexico, which resulted in two distinguishable morphs of Mexican tetra: surface fish and cavefish (Fig.1.1) [8, 10]. The divergent event of Mexican tetra resulted in two populations (cave and surface-dwelling forms) dates back to approximately 100,000 years [20]. Five demographic events of colonization, geographically isolated the cavefish that established into nearly 29 caves in northeastern Mexico [19]. Thus far, at least thirty different cavefish populations were found in the limestone caves of the Sierra de El Abra region. Surface fish can be found throughout streams and rivers of northeastern Mexico and southern Texas [19]. Each cavefish population is named based on its cave origin. Namely Pachon, Tinaja, Chica, Los Sabinos, Subterraneo, Molino, etc. (Fig. 1.1) [19].

Fig 1.1: Different populations of Mexican tetra and cave location of each population. **A:** Location of the caves found in the Mexican region, **B:** Pigmented eyed Surface fish population, **C:** Molino cavefish population, **D:** Pachon cavefish population, **E:** Tinaja cavefish population [28].

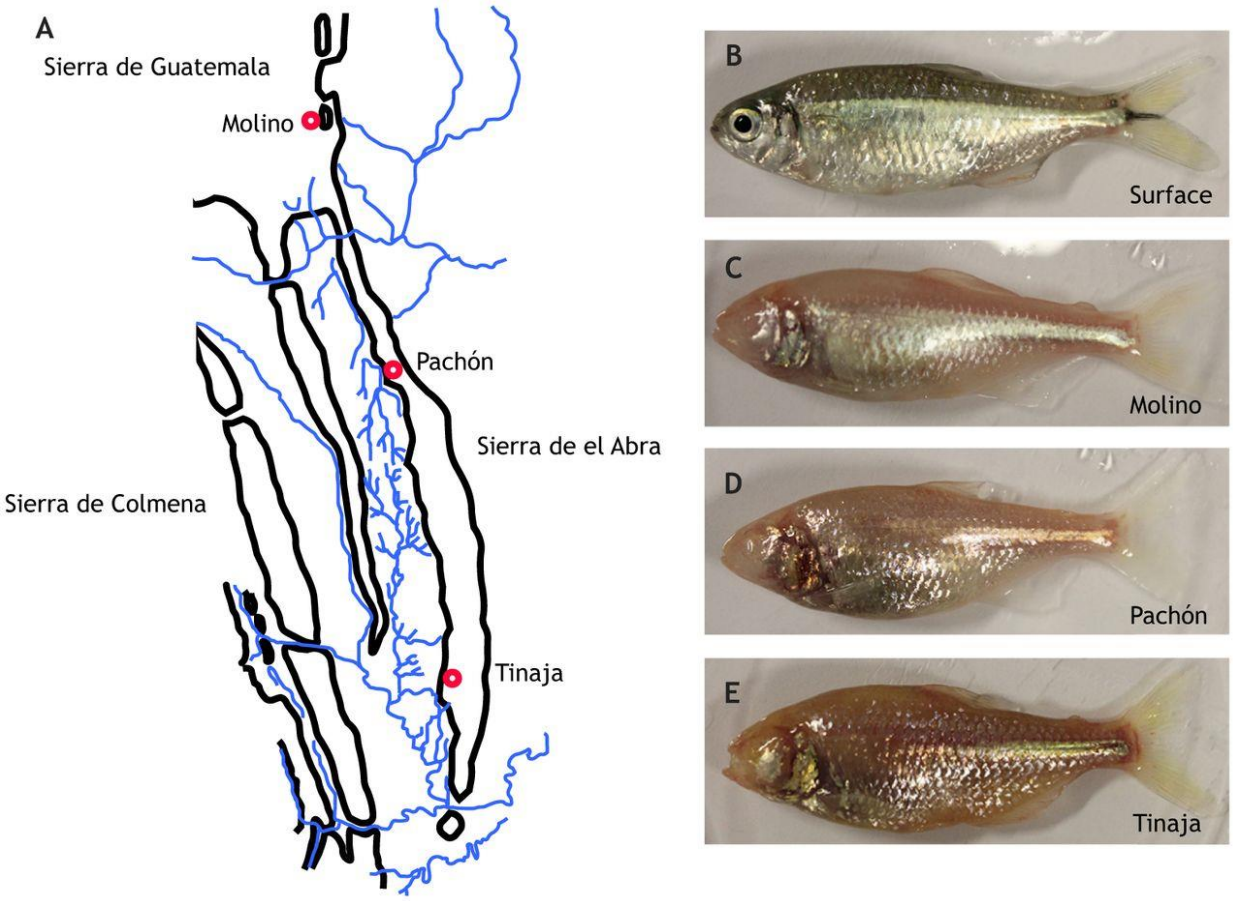

Cavefish have low genetic diversity compared to the surface fish [29]. Gene flow from the surface fish populations to the cavefish population is high [29]. The cavefish population developed adaptations to the constant darkness of the caves (troglomorphic conditions) [30]. In the past, some biotic and abiotic factors in the cave environment triggered the evolution of constructive and regressive traits in the cavefish populations [30]. The importance of biotic and abiotic factors for individual growth has been previously reported [30]. Biotic factors include food source, predation, competition and abiotic factors include physical factors (light and temperature) and chemical factors (pH of water) [30]. The adaptation to the cave environment could have arisen through one founder event that successively disseminated through an entire cave system or two or three convergent founder events resulting in troglomorphic populations (animals that morphologically adapted to live in constant darkness in the cave environment) to evolve within the cavefish populations [8, 24]. Also, it is believed that at least five independent events led to these changes in the cave population over the past 1-2 million years [10]. Physiological traits and behavioral traits gained by cavefish over the evolution are distinct from the surface fish [31]. The physiological traits include low metabolic rates and fat reservoirs, production of larger eggs, increased sensitivity of the olfactory system, and a large number of taste buds enhance chemosensory capabilities and superficial neuromasts in vibration attraction [3, 25, 26]. Constructive behavioral traits include little sleep, a shift from fighting to foraging, and prey capture skills [9, 12].

It has been previously established that the accumulation of functional mutations in the genes related to eye development has led to the loss of eyes in cavefish [12]. The loss of eyes lead to cranial asymmetry in the adult cavefish skull and is displayed as left-right differences and shows the “handedness behavior” in cavefish [13]. Also, it exhibits directional bending with the skull biased to the left [13]. The aberrant development of the Suborbital bone series (SO), late in the ontogeny is also considered as a precursor for the cranial asymmetry in the adult cavefish populations [27]. Bilateral asymmetries appeared in several other cave-dwelling taxas as well. For example, eye size reduction in cave catfish, antenna in cave crickets, asymmetrical mandibular structures in cave silverfish provides evidence for bilateral asymmetry [13]. In contrast, this type of asymmetry was not observed in the surface fish population [13]. Interestingly, this asymmetry is present in the chondrocranium (cartilaginous skull) of cavefish juveniles even before the formation of osteocranium [13]. The chondrocranium in fish supports the early jaw development and the positioning of the bones in the adult skull [13]. Some studies have suggested the asymmetric neural crest cell migration and differentiation could be the reason for this cranial asymmetry [13].

Two unusual ossifications in cavefish cause the unusual development of the bones surrounding the eye socket [32]. The first mechanism is the post-ossification remodeling which includes carvings of channels in the mature bones with a combined increased bone remodeling activity in cavefish [32]. The second mechanism is the sporadic appearance of the independent bony element in the cavefish skull [32]. Furthermore, this explains the indirect effect of eye loss on the orbital collapse or the occurrence of multiple ossification centers [33]. A study has already been performed to check whether eye loss in cavefish affects this bone fragmentation by transplanting the surface fish eyes into cavefish [9]. Although the development of the structural eyes was observed in the cavefish after transplantation, the fragmentation of the SO 3 (Sub Orbital 3) bone was still present. This suggest that the bone fragmentation is not a direct effect of eye loss in cavefish. Also, a more detailed study done on cavefish facial bone fragmentation reveal that facial bone fragmentation most commonly occurs in the third SO bone which is considered as the largest of the suborbital series [9]. SO 3 bone shows the left-right asymmetry in the number, position, and pattern of the ossification centers throughout the ossification process in cavefish [32, 33].

Some cranial changes have occurred from the direct effect of eye loss in cavefish [12, 13, 34, 35]. For example, the size of the olfactory pits influences the position and distance of the nasal and anteriorbital bones [12]. The size and position of the circumorbital bones, ossified sclera, and the shape of both SO 3 and the supraorbital bone are the elements that are directly affected by the eye loss [1, 13]. The maxillary teeth, the positions of SO 4 to SO 6, and the shape of the opercular bone were found to be unaffected by the eye loss [12]. The effect of eye loss on the palatal bones in cavefish has not been broadly studied thus far. Similar to other teleost species, in Mexican tetra base of the neurocranium is made of a series of bones that form the roof of the oral cavity. The parasphenoid bone, basioccipital, vomer, ethmoid, and other bones form the base of the neurocranium (Fig. 1.2) [29].

Fig 1.2: Lateral view of the skull of Mexican tetra 35 dpf surface and cavefish. **A**: Surface fish, **B**: Cavefish

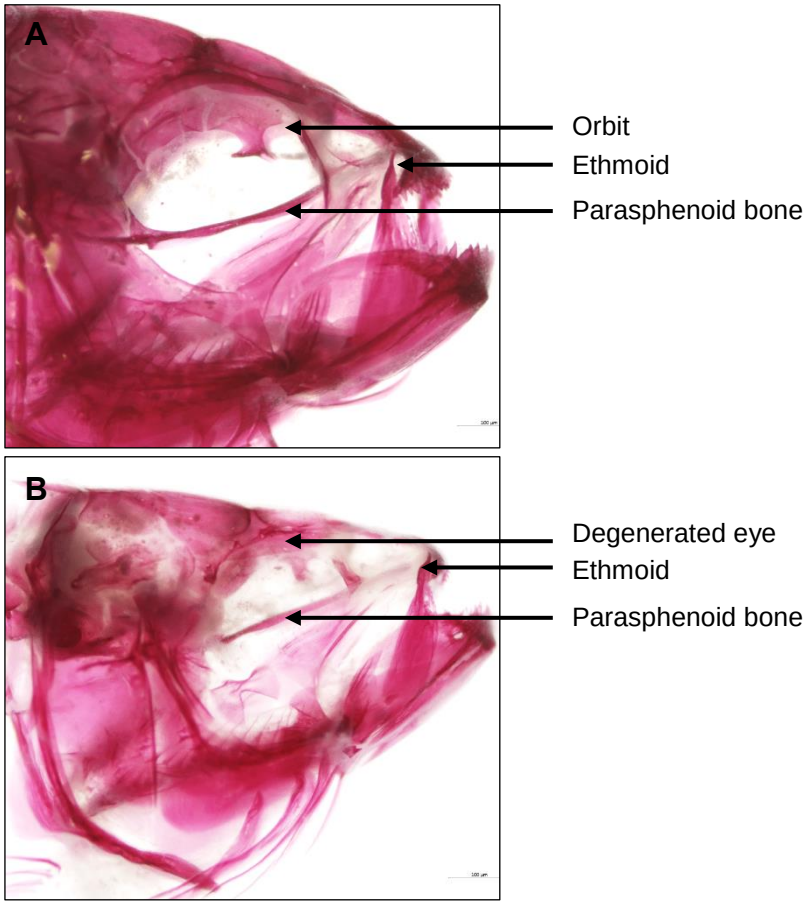

1.4 Zebrafish (*Danio rerio*)

1.4.1 Zebrafish as a model organism

Zebrafish is a small freshwater teleost fish that belongs to the family Cyprinidae [36]. It is widely used as a model organism in biological research [36]. Zebrafish is well established in developmental biology research field as it has externally developing, optically transparent eggs, which are convenient for high-resolution optical imaging and genome editing [37]. Also compared to other model organisms, the development of zebrafish is a rapid process [37]. During the first 5 days of development, all the major organ systems of the fish body begin to function [37]. Zebrafish breed throughout the year and after each successful breeding event females lay a few hundred eggs, making it a robust model to reach large sample size [37]. The genome of zebrafish consists of approximately 26,000 protein-coding genes [38]. In addition, it has approximately 70% of the human genome counterpart [38].

1.4.2 Zebrafish as a model organism to study the palate development

Zebrafish is considered as a model organism to study the development of the craniofacial structures, which include craniofacial skeleton, dentitions, and soft tissue morphogenesis [22, 39-41]. The genes that express in the development of the human and murine palates were found to be analogous to the genes that express in the development of the zebrafish ethmoid plate. [42]. Furthermore, several homologous features in the plate development in zebrafish and amniotes have been discovered [42, 43]. Also, the cranial neural crest cells (CNCCs) location in the zebrafish around 36 hpf (hours post fertilization) was found to be homologous to the amniotes [42]. Zebrafish anterior neurocranium is formed by CNCCs, which is considered to be common to all vertebrates [1, 44]. Anterior neurocranium includes the ethmoid plate, the paired trabeculae, and the optic capsules [2, 44]. The posterior and medial structures of the neurocranium are formed from the mesoderm [44]. The ethmoid cartilage of zebrafish consists of two main parts, the lateral ethmoid, and the median ethmoid (Fig: 1.3). Paired trabeculae are two longitudinal rods made from chondrocytes [44]. From the posterior side trabeculae articulate with the basiocapsular commissures and parachordal cartilages [44]. Trabeculae are fused in the midline and develop towards the anterior direction to form the lateral ethmoid [44].

Fig 1.3: Alcian blue cartilage stained ventral view and coronal section of 3 dpf zebrafish. **A**: Alcian blue-stained zebrafish neurocranium. **B**: Toluidine blue-stained coronal section of zebrafish oral cavity. At this stage, the ethmoid plate is fully formed. Lateral and medial ethmoid plates fused. In **B** the asterisk indicates the oral epithelium, which lines the roof of the oral cavity. The oral epithelia are intact on the midline. **B:** brain, **E:** ethmoid cartilage, **O:** oral cavity, **Mc:** Meckel's cartilage (Scale bar: 100 µm) [45].

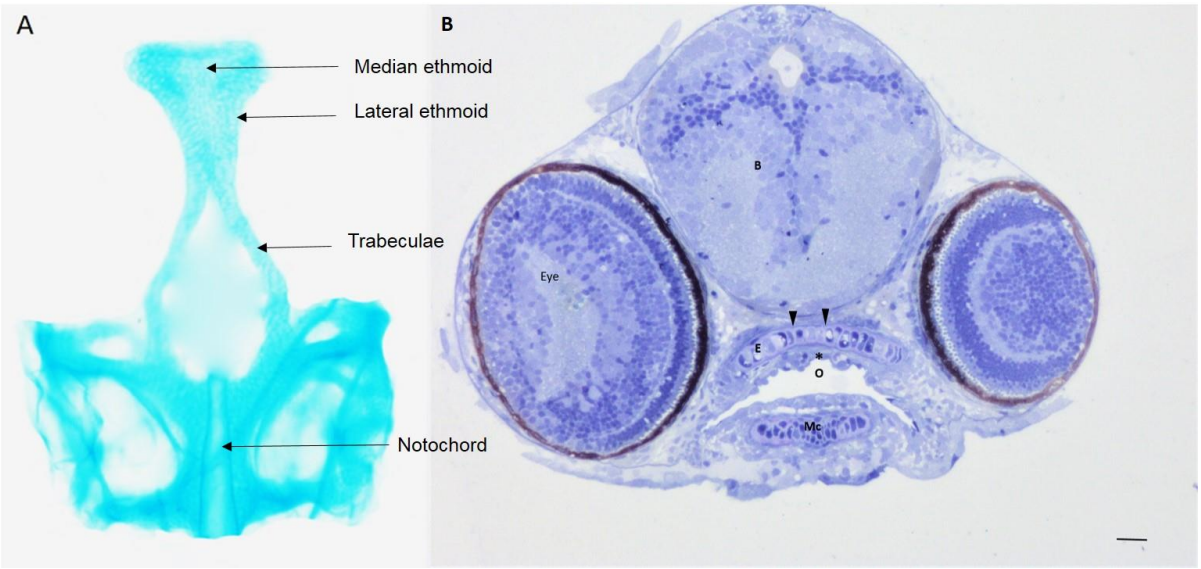

During median ethmoid cartilage development, the discrete pairs of CNCCs in the anterior lateral direction merge and converge towards the midline [44]. After that, this group of cells makes a sharp 180˚ turn at the anterior boundary while condensing further into one group, streaming into the caudal direction to fuse with the paired lateral ethmoid cartilage [44]. Once the median ethmoid cells reach the paired lateral ethmoid region, integration of these parts begins to complete the fusion of the ethmoid cartilage [44]. During this integration, juxtaposed columnar shaped cells in the lateral ethmoid and cuboid-shaped cells in the median ethmoid undergo a morphological transition [44]. Palate development in humans is homologous to the zebrafish ethmoid cartilage development [46]. Furthermore, the human primary palate is homologous to the zebrafish medial ethmoid region. Previous research has suggested that the human secondary palate is homologous to the lateral ethmoid region of zebrafish (Fig 1. 4: A & B) [46]. The V-shape fusion seam of the frontonasal process and the bilateral maxillary processes of the human palate are analogous to the V-shaped junction found in the zebrafish ethmoid cartilage (Fig: 1. 4 C) [47].

Fig 1.4: Homology of zebrafish ethmoid cartilage development to the human palate. **A**; Zebrafish ethmoid cartilage, **B**; Human palate. Homologous area in **A** and **B** indicate by the same color. **C** indicate the ventral view of 3 dpf of zebrafish neurocranium and enlarged view of the ethmoid cartilage of zebrafish. In **C** the highlighted area shown the V-shaped junction found in the zebrafish ethmoid cartilage fusion. The green color area in **C** indicates the lateral ethmoid cartilage where the red color indicates the medial ethmoid cartilage [46, 47].

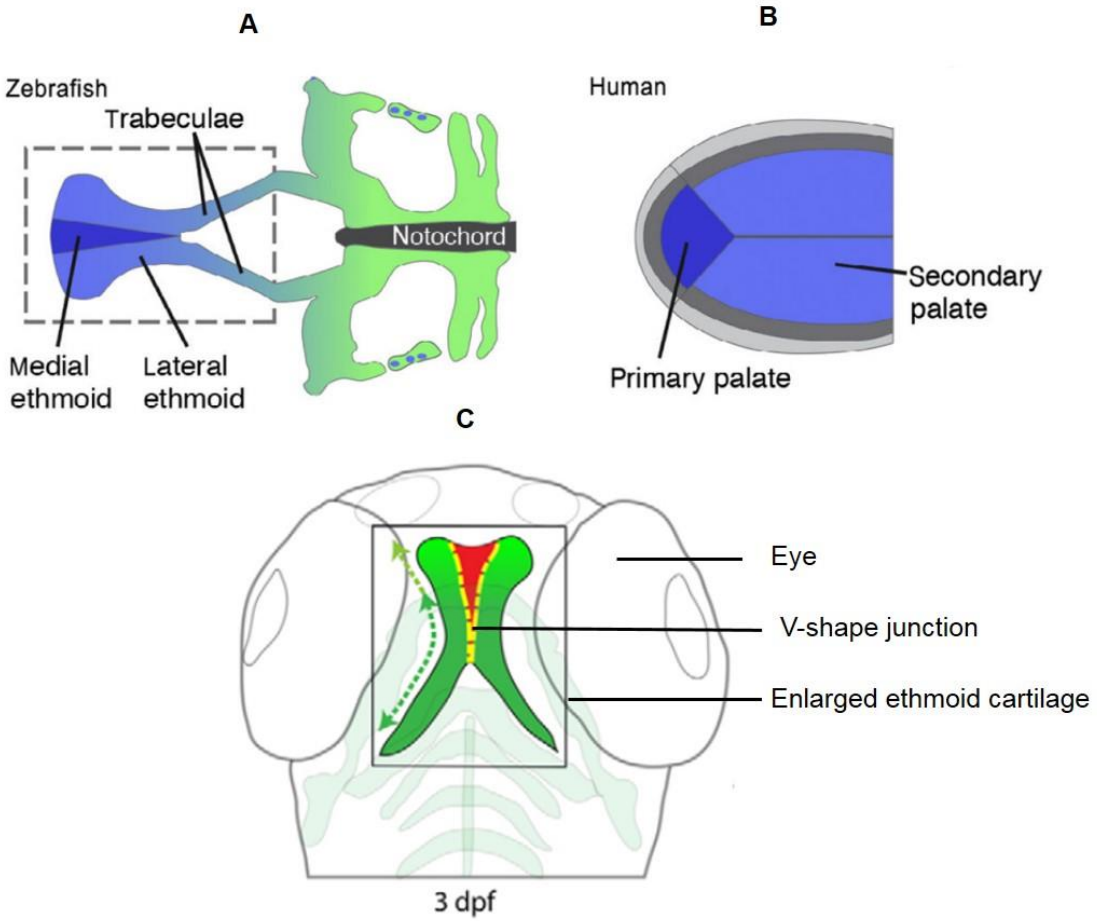

1.4.3 Palatal bone development and articulation in zebrafish

The adult zebrafish has 73 cranial bones, which exceeds the number of bones that form a mammalian skull [48]. Zebrafish cranial bones develop from the 74 ossification centers [2]. The parasphenoid bone in zebrafish is located in the midline of the skull and create a suspension between orbits and trabeculae communia [2]. Ossification begins from the center of the cartilaginous plate and grows towards the anterior direction, and the bifurcates of ossification grow towards the posterior and fuse to the basioccipital [2]. From lateral ossifications, wings grow medially to fuse with median ossification centers and form the lateral wings of the parasphenoid bone [2]. This general morphology of single median portion and paired lateral wings are conserved in teleost fish [2]. Anteriorly, parasphenoid bone articulates to the orbitosphenoid bone and anterior-laterally to vomer [2]. Anterior-dorsally, it articulates to the ethmoid bone. Posteriorly it articulates to the basioccipital bone (Fig: 1.5) [2]. In zebrafish, parasphenoid bone appears early in the ossification sequence around 4 dpf [2]. Zebrafish ethmoid bone dorsally articulates to the supraethmoid, posterolaterally with lateral ethmoid, in ventral vomer and parasphenoid bone (Fig:1.5). The vomer anteriorly articulates with pre-ethmoid bone. The dorsal edge of the vomer curling over the ethmoid bone from the antereo-medial edge. Posteriorly bone meets the anterior parasphenoid and ethmoid (Fig:1.5) [2].

Fig 1.5: Neurocranium of adult zebrafish. **A**: Dorsal side of the neurocranium **B**: Ventral side of the neurocranium. (**ac**: auditory capsule, **boc**: basioccipital, **bp**: basal plate, **eoc**: exoccipital, **epb**: epiphyseal bar, **ep**: ethmoid plate, **f**: frontal, **k**: kinoethmoid, **le**: lateral ethmoid, **nc**: a notochord, **os**: orbitosphenoid, **p**: parasphenoid, **pro**: prootic , **pto**: pterotic, **pts**: pterospenoid, **sph**: sphenotic, **tc**: trabeculae cranii, **tma**: tania marginalis anterior,, **tmp**: taenia marginali posterior, **v**: vomer) [49]

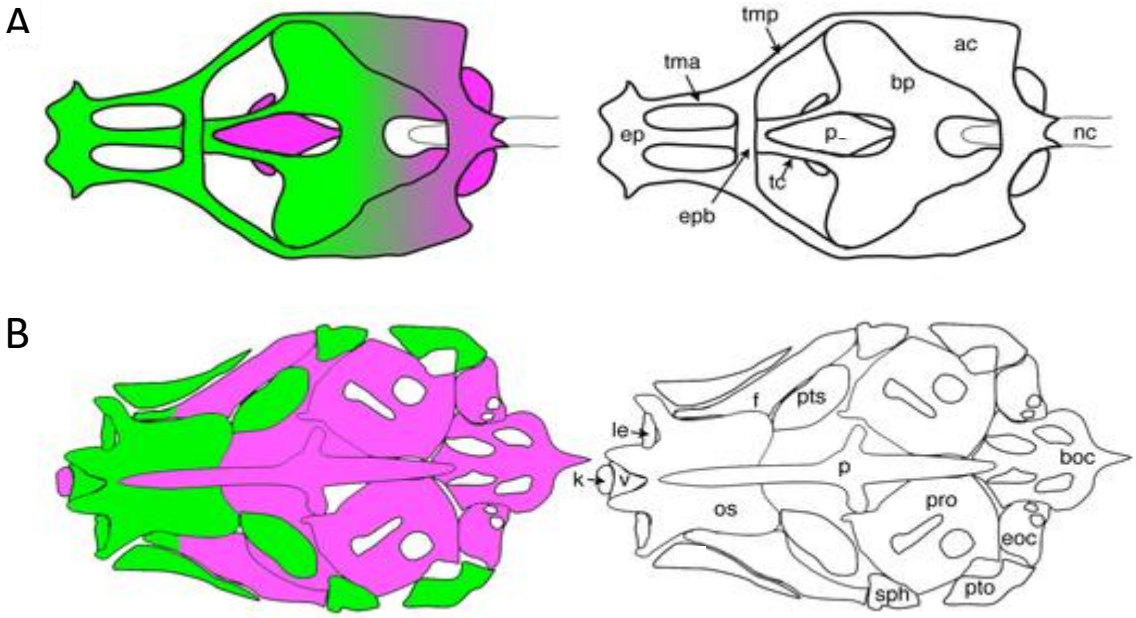

1.5 Palate development in human and pathogenesis of Cleft Lip and or Cleft Palate (CLP)

Palatal bone development occurs within the first three months of embryonic development [50]. The palate consists of two main parts namely the primary palate and secondary palate [50]. The anterior part of the palate is made of bone and name as hard palate and the posterior part is made of the muscular connective tissue, hence name as soft palate [50]. The left and right maxillary processes fuse with the frontonasal process on the midline to form the primary palate [50]. Primary palate formation begins around the 6th week of embryonic development [50]. At the beginning developing maxillary processes contact with the lateral nasal processes [50]. Next it is contacted with the globular shape medial nasal processes form the primary palate [51]. Secondary palate formation starts around the 6th week and completes around the 12th week of embryonic development [50]. Secondary palate forms from the inner maxillary prominences named as palatal shelves [50]. Initially, those prominences grow on the vertical side of the developing tongue. Secondly, it reorients the position by palatal shelves elevation by reorienting the horizontal position above the tongue. After that these palatal shelves grow towards each other [50]. Palatal shelves are tissues that originated from the neural crest cell-derived mesenchyme and the oral epithelium [52]. Palate fusion occurs in the midline either by the apoptosis of median edge epithelial cells (MEE) or by the epithelial-mesenchymal transition (EMT) [53, 54]. EMT is described as the process of phenotypic transformation of an epithelial cell into a mixture of mesenchymal cells [53]. Palatal shelves fusion begins anteriorly with the primary palate in week 9 and is completed posteriorly by week 12 [51]. Then bone extends into the lateral palatine processes to form the hard palate but the posterior portions of the lateral palatine processes do not become ossified, instead of that, it extends to the nasal septum and fuse to form the soft palate [51].

Any defect in proliferation, migration, and survival of the neural crest cells and any malfusion+ between the medial nasal and maxillary processes may cause Cleft Lip and or Cleft Palate (Fig:1.6) (CLP) which is a common birth defect that is occurring 1 out of 700 infants [55]. According to the world health organization, CLP is varying between the different geographical regions and different ethnicities [56]. Global annual prevalence for orofacial clefting is 7.94 cases for the 10,000 live births. Different ethnicities have different prevalence for the CLP. For example, in Europe, the prevalence is 0.3 per 1000 live births. Within USA the average prevalence of CLP is 7.75 for 10,000 live births [57]. A detailed study identified the ratio of Cleft Palate (CP) and CLP in different ethnic groups using the total number of 8,043,393 live births. In the non-Hispanic population, the CP ratio is 7.6 and the CLP ratio is 8.76, the

Hispanic population CP ratio is 4.79 and the CLP ratio is 7.5, the prevalence for CP in Asia/Pacific population is 4.9 and CLP 6.68, the African American population has a prevalence of 4.1 for CP and 6.7 for CLP. The CP ratio is equal to 2.1 among native Africans, while the CLP ratio is equal to 6 [56].

Fig 1.6: Subtypes of orofacial clefting. **A:** Normal palate, **B:** Cleft Palate alone, **C:** Unilateral Cleft Lip and Palate.

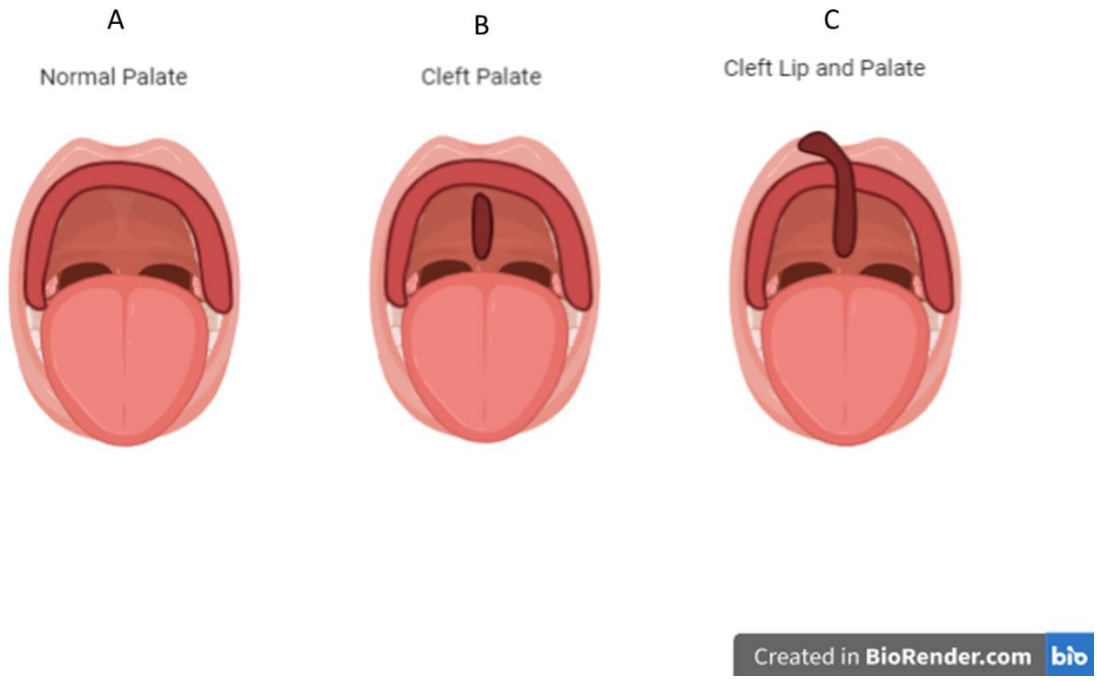

1.6 Etiology of CLP

Both genetic predisposition and environmental factors affect CLP development, but the exact etiology still remains unclear [58]. Literature suggests that alteration of growth factors and metabolic enzymes are responsible for palate development and could increase the risk of CLP [59-61]. Moreover, some studies found that transcription factors of, TBX22 (T-box transcription factor 22), Poliovirus Receptor Like-1 (PVRL1), and Interferon Regulatory Factor 6 (IRF6) could contribute to the development of Non-Syndromic Cleft Lip Palate (NSCLP). TBX22 is highly expressed in the palatal shelves during the growth of the palatal shelves [60]. The involvement of TBX22 in NSCLP is identified by the genome-wide sibling pair analysis [60]. Further, Mutation analysis revealed that the involvement of the TBX22 in the NSCLP [60]. The PVRL1 is responsible for cell adhesion [62]. The PVRL1 has been expressed in the MEE in developing palatal shelves [62]. Heterozygous mutation in PVRL1 was found to be associated with the NSCLP [60]. The IRF6 gene also acts as a mediator for Transforming Growth Factor Beta 3 (TGFβ3) in palate development [63]. Further, IFR6 regulates the EMT in the palatal shelves fusion process subsequently affecting the expression of Snail Family Transcriptional Repressor 2 (SNAI2), which is an EMT regulator [63]. SNAI2 expression affects the various epithelial markers such as E-cadherin, Plakophilin, and Zonula occludens-1 (ZO-1). This data suggests that IRF6 regulates the EMT process in the fusion of the palatal shelves to form the palate [63]. Further IRF6 gene is involved in the MEE cell apoptosis through degradation of the ΔNp63 transcription factor [59]. Also, Transforming growth factor-alpha (TGF-$\boldsymbol{\alpha}$), 5,10- Methylenetetrahydrofolate reductase (MTHFR), and Sequence-binding protein-2 gene (SATB2) were found to be the candidate genes and the loci for the NSCLP [60].

Gene vs. Environmental interaction in CLP development is an area that a handful of studies have explored but plays a major role in the alteration of gene expression [64]. Gene vs Environmental interactions have also been found for several genes associated with NSCLP [64]. Haplotype analysis and single-nucleotide polymorphism (SNP) analysis data reveal that maternal Environmental Tobacco Smoke (ETS) can alter the IRF6 expression that can cause CLP [61]. Deficiency of the nutrients such as folic acid and zinc increases the risk whereas the multivitamin supplement is confirmed as not a protective factor [64]. Also, chemical substances such as exposure to agricultural chemicals, retinoids, corticosteroids, and some anticonvulsants drugs can increase the risk [52, 65]. Furthermore, the studies found that ethanol consumption in the first trimester of the pregnancy could increase the risk of CLP by direct and indirect interaction with genes [66]. However, the underlying mechanism remains unclear.

Some environmental factors can directly affect CLP development. Smoke contains polycyclic aromatic hydrocarbons (PAHs), carbon monoxide, tar, and nicotine [48]. These compounds can pass to the amniotic fluid through the placenta [48]. Studies that expose zebrafish to PAHs, carbon monoxide, and nicotine chemicals revealed that these chemicals have an impact on the ethmoid cartilage of the zebrafish [48]. Also, a cleft in the zebrafish ethmoid region was observed in the early developmental stages under hypoxic conditions [48]. Exogenous retinoic acid exposure (5 nM) in zebrafish at the period of 4 and 96 hpf causes severe damage to the neurocranium. The cell in the ethmoid plate was found to be disorderly arranged [48]. The ethmoid plate in those fish was found to be shortened and resemble a single rod [48, 61]. During the period of pregnancy, intake of VAP (mood stabilizer) and anti-epileptic drugs were found to increase the risk of a craniofacial defect. Specially, VAP was found to be associated with facial abnormalities including CLP [48]. VAP act as an inhibitor for histone deacetylases which can affect the genes that are required for craniofacial development [48]. Zebrafish that exposed to VAP (30 μM) during 4-96 hpf resulted in a shortened ethmoid cartilage [48].

1.6.3 Effect of ethanol on CLP development

Ethanol is an organic compound that acts as a teratogen to the human body depending on the time and amount of exposure [67]. There are different mechanisms for ethanol teratogenesis, (i) Ethanol can increase oxidative stress, (ii) Ethanol can disturb glucose, protein, lipid, and DNA metabolism, (iii) It can impair neurogenesis and induce cell apoptosis, (iv) Disturb hormonal regulation, and (v) Affect gene expression [67]. Ethanol induces oxidative stress by forming free radicals, and those free radicals can react with the different compounds in the body [67]. Ethanol can reduce cellular signaling by affecting the transcription factors, retinoic acid, or growth factors by down regulation of ribosome and proteasome pathways, up-regulated glycolysis and pentose phosphate pathway, regulation of tight junctions, and Wnt signaling pathway [68]. Furthermore, ethanol has the ability to disrupt cell-cell interactions in the body and subsequently affects cell proliferation and increases cell apoptosis [68]. The same study revealed that ethanol can alter genes such as zinc finger protein, mitogen-activated protein kinase (MAP kinase), and metabolic genes, namely lactate dehydrogenase and aldolase [68]. Ethanol is teratogenic to multiple organs, specially it affects the central nervous system [67]. Length of ethanol exposure and amount of ethanol exposure determine the severity of the disease [67]. Studies have already demonstrated that maternal exposure to ethanol increases the risk of birth defects in an infant [16]. Heavy maternal ethanol exposure can cause fetal alcohol syndrome, which characterizes the wide array of craniofacial anomalies: postnatal, and

prenatal growth retardation, and central nervous system disorder [16]. Ethanol was detected in the fetus after one to two hours of maternal ethanol consumption [69]. But the rise of blood ethanol is slower in fetuses compared to the maternal blood ethanol concentration [69]. But within one to two hours, concentrations become equal to each other [69]. Ethanol enters the fetus through the placenta [67, 69]. The chemical structure of the ethanol allows it to enter the placenta through dispersion [69]. Also, ethanol can reduce the activity of endogenous antioxidants in organs including the cerebellum and placenta [67, 69]. An increase of the oxidative free radicals in the placental villous stromal cells can increase the passage of ethanol molecules through the placenta and reach the developing fetus [67, 69]. Increased oxidative stress damage DNA and proteins [67]. The fetus contains the same enzymes that are responsible for ethanol metabolism in the mother's body, but the concentration and level of activity, are not the same. [69, 70]. First, 90-95% of ethanol metabolize into acetaldehyde by the enzyme Alcohol dehydrogenase (ADH) [70]. 5-10% of the ethanol metabolism in the liver is carried on by Cytochrome 450 enzymes (CYPs) mostly [70]. CYP2E1 and P450 were detected in the embryo at the 19th, 23rd, and 24th weeks of gestation [69]. Ethanol oxidation in the body can also be done in the non-oxidative conversion of ethanol into fatty acid ethyl esters [70]. The amount of ethanol metabolized in this pathway is minor compared to the oxidative pathway [70].

Once ethanol has entered into the amniotic fluid ethanol metabolism starts using the ADH enzyme (Present in the fetus from 2 months of gestation) [69]. Ethanol in the amniotic fluid will enter the fetus by three main mechanisms. Initially, ethanol absorbs into the fetus through un-keratinized skin in the first half of gestation [69]. Then absorbed ethanol will circulate through amniotic fluid unchanged via fetal urine and pulmonary excretions in the second half of gestation [69]. Fetal swallowing of ethanol will starts by the 11th week of embryo development [69]. Prenatal ethanol exposure has been divided into three different categories according to the amount of ethanol ingestion. The first category is heavy drinking of ethanol where the ingestion of 48-60 grams of ethanol per day can develop fetal alcohol syndrome. The second category is moderate ethanol drinking equal to 24-48 grams of ethanol per day. The third category is binge drinking, defined by occasional drinking of 4-5 drinks of ethanol, which equals 90 grams per drink. Binge drinking is found to increase the incidence of CLP [67].

1.7 Role of Bone Morphogenetic Protein (BMP) family in palatogenesis and CLP formation

The BMP was first discovered in 1965 by Marshall Urist by remarkable osteoinductive activity in the demineralized membrane [71]. BMPs belong to the Transforming growth factor β (TGF-β) family of ligands [72]. To date, at least 20 different BMP ligands are identified [72, 73]. BMPs are involved in skeletal development and other biological functions in the body [72, 73]. Also, BMPs are involved in a wide array of developmental functions such as apoptosis, cell proliferation, differentiation, and morphogenesis [72, 73]. BMP pathway transduces the signal through transmembrane serine/threonine kinase receptors [73]. These receptors are of two types: Type 1 receptors and type 2 receptors [71]. Type 1 receptors have four different receptors (Bmpr1a, Bmpr1b, Acvr1, and Alk1) and type 2 receptors have three different receptors (Bmpr2, Acvr2a, and Acvr2b) [74]. SMAD 1, 5, and 8 act as downstream molecules of the BMP pathway [75]. Bmpr1a expression was found in the anterior region of the palate [76]. Literature suggests that Bmpr1a is important for the cell proliferation and patterning of the palate. The loss of the Bmpr1a in the anterior region showed decreased cell proliferation. [63]. In signal transduction, type 1 and type 2 receptors form a dimerized structure [75]. Upon binding the ligand with the receptor SMAD 1, SMAD 5, and SMAD 8 protein complex phosphorylates and binds with SMAD 4 and then whole complex translocates into the nucleus and interacts with transcriptional factors (Fig:1.7) [75].

1.7.1 Bmp 4 function in palatogenesis and CLP formation

Bone Morphogenetic Protein 4 (BMP 4) is a member of the BMP family protein that plays a major role in palate development [63]. Bmp 4 expression starts around 6.5 days of embryonic development (ED) in mice [77]. Further, Bmp 4 expression in mice was found in palatal epithelium and mesenchyme around ED12.5, and expression was only found in the mesenchyme in ED13.5 to ED14.5 [78]. Expression of Bmp 5 and Bmp 7 was found in the branchial arches in early gastrulation [63]. In palate development, Bmp 4 expression shifts from the anterior to the posterior region but the Bmp 2 expression can be found in both the anterior and posterior regions [78]. In the developing palatal shelves, Bmp 4 expression is overlapping with the T- Box transcription factor 3 (Tbx3) expression [78]. These two genes regulate each other's expression. Tbx3 inhibits the expression of Bmp 4 in palatal mesenchyme whereas Bmp 4 induces the expression of Tbx3 in anterior palatal shelves [78]. These regulatory loops are important for cell proliferation in the development of the anterior palatal region [78]. Transcription factor 63 (T63) regulates the Bmp 4 expression in the anterior palatal

region [79]. Studies suggest that loss of expression of T63 leads to improper expression of Bmp 4 and subsequently leads to cleft formation in the palate [79]. Also, the absence of the Wnt5a down-regulates the expression of Bmp 4 in the anterior palatal region around ED13.5 whereas expression seems up-regulated in the posterior palatal region [80].

Noggin acts as an inhibitor molecule for the BMP family that competes with the signaling molecules (BMP) and prevents signal transduction [63]. More specifically linkage analysis and Genome-Wide Association Studies (GWAS) found an association of gene polymorphism in the BMP 4 and Noggin related to the NSCLP [63]. Dorsomorphin was identified as the first known small molecular inhibitor for the BMP pathway [81]. Dorsomorphin has the ability to selectively inhibit the type 1 receptors (ALK2, ALK3, and ALK6). Binding of Dorsomorphin to the ligands blocks the signaling of SMAD 1/5 and 8 (Fig. 1.7) [81]. This regulates the expression of genes responsible for osteogenic differentiation [81]. In zebrafish inhibition of osteogenic differentiation alters bone mineralization [81]. Dorsomorphin has an effect on craniofacial morphology when zebrafish are exposed to it during the endodermal-Bmp responsive window of development [82].

Fig 1.7: BMP pathway signal transduction. Upon ligand binding, type 2 receptor phosphorylates and dimerizes with type 1 receptor. Subsequently SMAD1, SMAD5, and SMAD8 protein complex phosphorylates and forms a complex with SMAD4 and the whole complex then translocates into the nucleus and interacts with transcriptional factors. BMP signal interrupts when a ligand binds with antagonists.

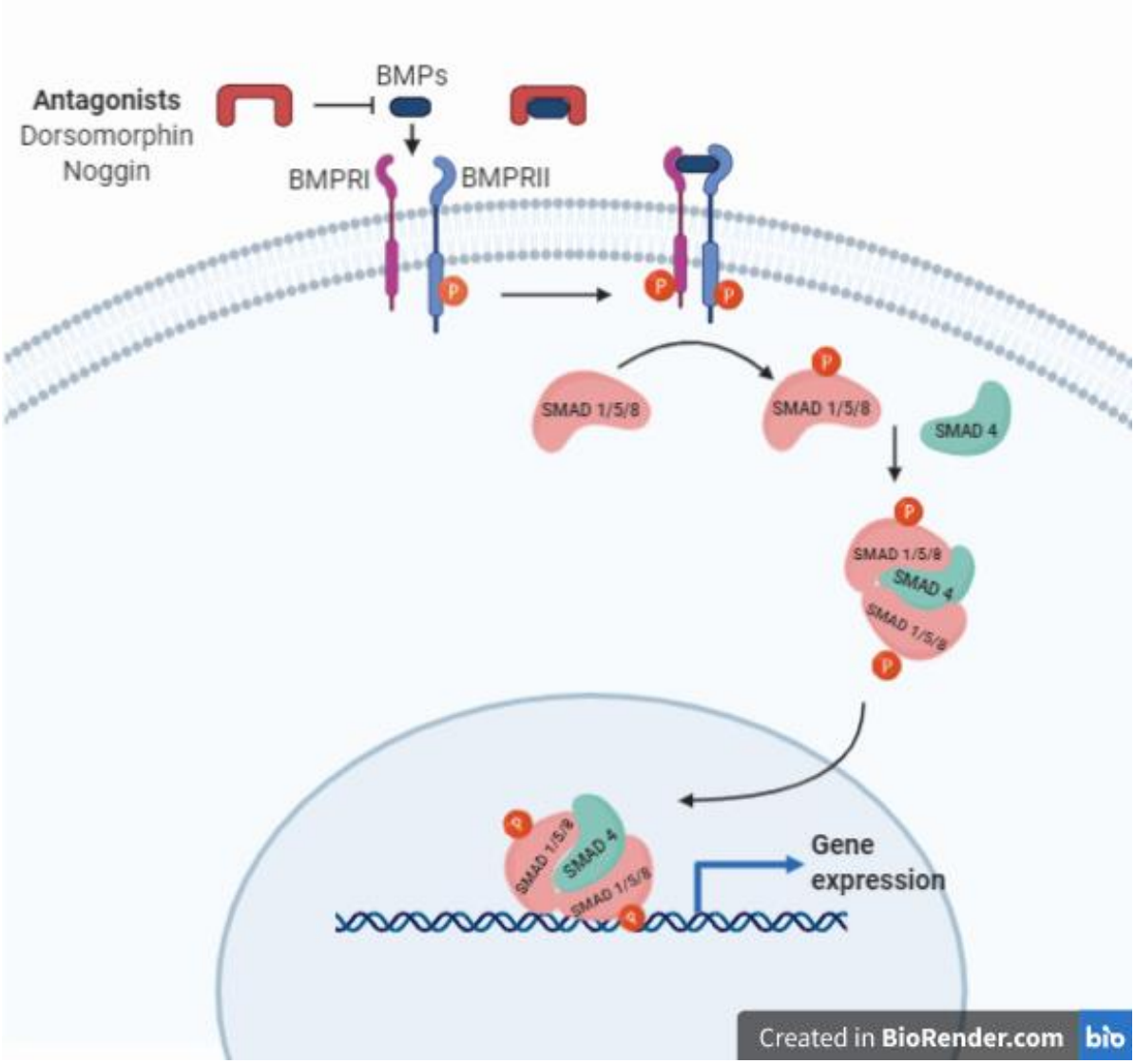

CHAPTER 2: OBJECTIVES, HYPOTHESIS AND RATIONALE

Objective

Environmental factors have the potential to affect long-term bone evolution as well as have a profound effect on normal bone development. Cavefish have degenerated their eyes as a result of their adaptation to the dark cave environment. Consequently eye degeneration in cavefish leads to some craniofacial changes. Therefore, my first objective was to examine the effect of early eye degeneration on the growth, articulation, and bone remodeling activity of the parasphenoid bone in different Mexican tetra eye morphs.

Defects in bone development is also a major manifestation of the variable environmental factors. The effect of maternal ethanol exposure is one such occurrence that may increase the risk of cleft palate. As a result in my second objective I used zebrafish as a model organism to investigate the mechanism of the *bmp 4* gene-ethanol interaction on cleft palate development.

Objective 1: To understand the effect of early eye degeneration on the development, articulation, and bone remodeling activity of parasphenoid bone of different eye morphs of Mexican tetra.

2.1 Rationale for objective 1:

Mexican tetra is a promising model organism in various fields of research. The existence of surface-dwelling and cave-dwelling morph make it unique and allow comparative experiments to be carried out between two populations of the same species. Eye degeneration in cavefish leads to some craniofacial structural changes in cavefish populations. These structural changes can be identified as eye-dependent structures and structures that did not get affected by this eye loss identified as eye independent structures. Several studies have outlined the effect of eye degeneration on facial bone development and the development of skull asymmetry due to aberrant bone development [32] [33] . However, there are no studies that focus on the effect of eye degeneration on palate formation even though palate play a significant role in the craniofacial region. Palate is a collection of several bones such as parasphenoid, ethmoid, and vomer. The parasphenoid bone forms the largest part of the palatal bone that borders the ventral neurocranium. To addressed the first objective of my project, I used the several techniques such as, alizarine red bone staining, TRAP staining, ALP staining and micro-CT imaging. Alizarin red bone staining is a standard method to study mineralized bones. Furthermore, TRAP and ALP staining can be used to determine the bone remodeling activity. Similarly, micro-CT imaging is an advanced imaging technique, which is invaluable in understanding the 3-D structural anatomy.

2.2 Hypothesis:

We hypothesize that eye degeneration in cavefish has an effect on parasphenoid bone morphology in different populations of Mexican tetra.

2.3 Sub-objectives:

1. To understand the parasphenoid bone development and articulation in Mexican tetra cave and surface fish populations.
2. To determine the effect of eye degeneration on parasphenoid bone shape in Mexican tetra cave and surface fish populations.
3. To understand the bone remodeling activity of parasphenoid bone in Mexican tetra cave and surface populations.

Objective 2: To decipher the mechanism of *bmp 4* gene-ethanol interactions in cleft palate development: Insight from Zebrafish (*Danio rerio*).

2.4 Rationale for objective 2:

Craniofacial development is an intricate process that is tightly regulated by several genetic factors and signaling pathways. It is therefore highly vulnerable to disturbances by genetic and environmental factors. Various environmental factors have been identified to regulate craniofacial development. Among them, ethanol is known as the most abused drug that causes severe defects in craniofacial development depending on time and amount of exposure. Importantly maternal ethanol exposure was found to increase the incidence of CLP development in the infant. CLP is the second most common birth defect. Infants born with CLP face numerous challenges in their early life such as feeding problems, breathing problems, susceptibility to infections, hearing problems, and dental defects. Zebrafish is a well-established model organism for studying craniofacial defect with remarkably high similarity to humans. Currently available data confirmed that BMP 4 is important in palatogenesis in humans. In the second objective of my project, I investigated the mechanism of *bmp 4* gene-ethanol interactions on cleft palate development using the zebrafish as a model system. To investigate objective two, I used several techiniques such as alcian blue cartilage staining one-way ANOVA and Tukey's pairwise comparison. Further WMISH was used to locate the *bmp 4* gene expression.

2.5 Hypothesis for objective 2:

We hypothesize that *bmp 4* gene-ethanol interaction affect for the ethmoid plate development in zebrafish.

2.6 Sub - objectives

1. To analyze the morphological differences of ethmoid cartilage upon differential chemical exposure.
2. To analyze morphometric differences of the ethmoid cartilage upon differential chemical exposure.
3. To determine the expression of the *bmp 4* gene upon differential chemical exposure.

CHAPTER 3: MATERIALS AND METHODS

3. Materials and Methods

3.1 Fish husbandry Mexican tetra (*Astyanax mexicanus*)

The surface fish, Pachon and Tinaja cavefish breeding colonies at the Bannatyne Campus University of Manitoba are the second and third-generation wild-type (WT) fish that were obtained from Dr. Richard Borowsky (New York University) and Dr. William Jeffery (University of Maryland). These fish were raised in the Techniplast standalone rack system and adult fish were maintained at 21°C on a 12-hour light and a 12-hour dark cycle. The water parameters in the system were maintained constant at a water conductivity at 900 µS and a pH of 7.6. Fish were fed twice a day in the morning and the evening with flake food (Tetramin). In the priming season, fish were fed three times a day in the morning with flake food, afternoon and evening with a variety of food such as brine shrimps, blood worms, black worms, and Mysis shrimps. After two weeks of priming, spawning was induced by increasing the tank temperature to 26°C and one male was added to a tank containing one female. Gravels and pot pieces were added to the tank bottom. Tanks were carefully examined for the next few days for eggs. Once eggs were laid, adults were transferred to a separate tank. Eggs were collected and washed three times thoroughly in 0.01 methylene blue (Cat. No. BP117-100; Fisher Chemicals) solution prepared in the system water. Then the eggs were separated and pooled into small batches (~25 eggs per each) and kept in the glass cups containing the aforementioned methylene blue solution. The hatching occurs around 24 hours and feeding was started at 5 dpf. At 5 dpf to 2 weeks of age, the larvae were fed twice a day with hatched brine shrimps (*Artemia fransicana*). The fish containers were cleaned every day and dead larvae were removed. Between 2 weeks to 4 weeks, the fish were fed with brine shrimps and finely crushed flake food. Post one month fish were transferred into the Techniplast rack system and continued feeding with crushed flake food and shrimps and then fed only with the flake food.

For the first objective, fish of 5 dpf, 10 dpf, 20 dpf, 35 dpf, 60 dpf, and adult fish of 5-7 years of age were euthanized using 0.1% Tricaine methanesulfonate (MS222) (Cat. No. 118000500; Fisher Chemicals) solution made with system water. The samples were fixed in the 10% Neutral Buffered Formalin solution (NBF) (Cat. No. 22050105, Fisher Chemicals) overnight. Next, the samples were stored in 70% ethanol (Cat. No. P006EAAN; Commercial Alcohols, Greenfield Specialty Alcohols).

Of note, some of the 35 dpf and 60 dpf surface fish and Pachon cavefish used in this study were received as 4% PFA (Paraformaldehyde) fixed samples from Dr. Nicholas Rohner (Stower's Institute for Medical Research, Kansas City). Fixed samples were used for Alizarin

red bone staining. Adult (5-7 years of age) fish were used for the Micro-CT imaging. All the protocols and guidelines followed in this study were according to the Canadian Council of Animal Care (CCAC) and the protocol number 17-030 (AC11301) by the Animal Care Committee, University of Manitoba.

3.2 Alizarin red bone staining (Appendix 1)

Mexican tetra samples were fixed at different time points ranging from 5 dpf, 10 dpf, 20 dpf, 35 dpf, 60 dpf, and adults (5-7 years of age). Fixed samples were stored in 70% ethanol. Alizarine red bone staining was conducted according to the available standard protocol [83]. The fish were bleached overnight in 3% hydrogen peroxide (Cat. No.:1767; Sigma-Aldrich) and 1% potassium hydroxide solution (Cat. No.134060010; Fisher Chemicals). The following day, after a single rinse in tap water, the samples were soaked in saturated sodium tetraborate solution (Cat. No. B9876; Sigma-Aldrich) overnight. Next, the samples were stained overnight in 0.05% Alizarin red (Cat. No. A5533; Sigma-Aldrich) prepared in 1% KOH solution followed by incubation of samples in 1% Trypsin-Borax solution (Cat. No. 9002-07-7; Fisher Scientific) for 3 days at 37ºC. The specimens were processed through an ascending series of glycerol solutions (Cat. No.BP229-4; Fisher Chemicals), which were prepared in 1% potassium hydroxide solution and then transferred to a storage solution consisting of 100% glycerol. Once the samples were sufficiently cleared, the samples were dissected using fine forceps under the dissection microscope to visualize the parasphenoid bone. The development of the parasphenoid bone were observed and the following characters were noted to trace the developmental sequence; the number of ossification centers, the direction of the progression of the ossification. Images were taken by using the stereomicroscope (Zeiss Discovery V8).

3.3 Micro-Computed Tomography (micro-CT) imaging

Adult Mexican tetra (Surface fish, n=6, Pachon cavefish, n=7, Tinaja cavefish, n=5) were used for this analysis. The high-resolution 3D tissue visualization was performed using the SKYSCAN 1176 micro-CT imaging system located at the small animals imaging facility at the Bannatyne campus, University of Manitoba. For imaging, fixed fish samples were taken out of 70% ethanol and excess ethanol removed using tissue papers. Then the sample was inserted into the polystyrene tube and sealed with parafilm for better orientation. The polystyrene foam tubes were placed on the half tube (180°) of the carbon fiber sample stage in the machine. After that, the region of interest was selected and the scanning process initiated. Condition for the micro-CT imaging was high resolution, no filters, a flat field of 70˚, and pixel size was 9 µm.

The axial, coronal, and sagittal x-ray images were collected and analyzed using Bruker's Data Viewer software and 3D structures were reconstructed using Bruker's NRecon, and the 3D micro-CT images were analyzed using CT Analyzer and CT Vox software.

3.4 Principal Component Analysis

Principal Component Analysis (PCA) was conducted using micro-CT images. The shape of the upper neurocranium and the contours of the parasphenoid bone of the three Mexican tetra were extracted by CorelDRAW 2018 (64-Bit). Images were processed through the SHAPE Ver 1.3 software following the procedure as described in the manual. Briefly, images were uploaded into the chain coder. Next, the chain-coded file was uploaded to the "Chc2Nef". In the "Chc2Nef", the contour of the pictures was converted to the normalized elliptic Fourier descriptors (NEFDs) form. After that, the NEFD file was uploaded to the PrinComp. PrinComp performs the principal component analysis for the NEFD file and generated the PC coordinates. PCA coordinate data was drawn in the form of a scatter plot, using the R Studio, 3.6.2.

3.5 TRAP staining

The paraffin-embedded horizontal sections from the skulls of 60 dpf surface fish and Pachon cavefish were used to analyze the bone growth and remodeling pattern of the parasphenoid bone. TRAP staining was conducted according to the available standard protocol 17049327. Slides were deparaffinized and TRAP staining was carried out inside a humid box for a period of two hours at 37˚C in a Hybridization oven. Sufficient care was taken to avoid the drying of the sections. TRAP solution consisted of adding 25 ml of 0.2 M Sodium acetate (Cat. No. BP333-500; Fisher Chemicals), 10 mg of Naphthol AS-BI phosphate Sodium salt (Cat. No.415311000; Acros), Fast red-violet L.B salt (Cat. No. F3381-1G; Sigma-Aldrich) dissolved in 20 ml of distilled water. After that, 375 mg of L-tartaric acid (Cat. No.202875000; Acros) was added. Then the pH of the solution was adjusted to 5.0-5.4 using 1 N Sodium Hydroxide (Cat. No. 83076-300; VWR). Finally, distilled water was added to top up the total volume to 50 ml. The solution was aliquoted into 1 ml eppendorf tubes and stored at -80˚C for long-term storage. The sections were thoroughly washed with the distilled water followed by one quick rinse in 100% ethanol to remove non-specific binding. Sections were counter stained with 0.01% methylene blue solution (Cat No.BP117-100; Fisher Scientific). The sections were mounted with the glycerol solutions (Cat. No. BP229-4; Fisher Chemicals) as a mounting solution, and samples were observed under the stereomicroscope attached to a Nikon DSFi2 camera to identify the site of bone resorption.

3.6 ALP staining

The above-mentioned sections were used to identify the osteoblast cells using ALP staining. ALP staining was done according to the standard protocol which was available [84]. Briefly, the slides were deparaffinized and incubated overnight at 37˚C in 1% magnesium chloride (Cat. No.M33-500; Fisher chemicals) solution made in 100 mM Tris-maleate buffer. Tris-maleate buffer was prepared by adding 24.2 g Tris (Cat. No. BP152-500; Fisher Chemicals) to 23.2 g of maleic acid (Cat. No. 25, 263-8; Sigma Aldrich) diluted in distilled water and adjusted pH into 9.2 using 0.2 M Sodium Hydroxide (Cat. No. 83076-300; VWR). After that, sections were incubated for two hours at 37˚C in BCIP/NBT Liquid substrate solution (Cat. No. ICN980771; Fisher Scientific) followed by several vigorous washes with distilled water. The section was mounted on glycerol and observed under the stereomicroscope attached to a Nikon DSFi2 camera.

3.7 Zebrafish Rearing and Breeding

The WT AB zebrafish breeding was purchased from the hospital for sick children (SickKids), University of Toronto. Fish were maintained in the Tecniplast rack system colonies at the Bannatyne campus, University of Manitoba. Water in the system circulates through the UV filters. Water conductivity was at 764 µS, and the pH of the system was at 7.4 and the water temperature was maintained at 27 ˚C. The fishes were fed twice a day with commercially prepared zebrafish food (Gamma micro 300 ZF, SKRETTING). The following feeding regimen was followed for feeding fish of different ages. Adult breeders were fed with Gamma 300 food and live *Artemia fransicana* (brine shrimps). Fish (1-3 months old) were fed with Gamma 150 food (Gamma micro 150 ZF, SKRETTING) and live *Artemia fransicana*. Fish below one month were fed with *Artemia fransicana*, *Rotifera*, and Gamma 75 (Gamma micro 75 ZF, SKRETTING). Larval fish of 5 dpf to 14 dpf were fed with *Rotifera* and gamma 75.

Adult fish (~3 months of age) were started to prime two weeks before breeding. Feeding frequency was also increased by an additional feeding in the afternoon with brine shrimp. For the breeding purpose, two males and females were selected based on external appearance. Females who seem to be carrying more eggs with distended bellies were selected as good females. The breeding was set up in the evening and two males and two female fishes were placed in breeding tanks, which were half-filled with the system water, males and females were separated by a divider. The breeding tank was set up inside a 27˚ C water bath for overnight. The following morning dividers were removed and the breeding tanks were slightly tilted to get the characteristic beach breeding where the female fish prefer to lay eggs. After three hours

of removing the divider, the bottom of the tanks was checked for the eggs, and breeders were removed from the tanks. Embryos were collected using a plastic pipette and transferred to a clean Petri dish containing 0.01% methylene blue water prepared using system water. Eggs were washed three times using the above media. After that, eggs were examined under a microscope to determine their age and the dead and damaged eggs were removed. The eggs were transferred into a clean Petri dish (25 eggs per dish) containing embryo media (0.01% methylene blue in system water) and raised in an incubator at 27˚C. The fish specimens used for this experiment comes under the animal care protocol number 17-041 (AC11315) and 18-021 (AC 11360).

3.8 Treatments (Ethanol, BMP pathway agonist)

The samples were subjected to three different chemical treatments after 10 hpf. Namely, 1% of ethanol solution, 10 µm Dorsomorphin and a combined treatment of 1% ethanol and 10 µM Dorsomorphin. 1 ml of absolute ethyl alcohol was added to the 99 ml of distilled water to make the 1% ethanol solution. The 10 µM Dorsomorphin (Cat. No. 866405-64-3; TCI America) solution was prepared by dissolving 0.4 x 10^{-3} g in 100 ml of 1% DMSO (Cat. No. F-515; Fisher Scientific). Combined treatment was prepared by mixing the 25 ml of the aforementioned 1% ethanol solution and 25 ml of the aforementioned 10 µM Dorsomorphin solution. Of note in the combined treatment initial concentrations of 1% ethanol and 10 µM Dorsomorphin were diluted to half to avoid the chemical lethality and to avoid increased mortality of embryos. Approximately 50 embryos, were placed in the petri dish containing each of the above solutions. Treatments were terminated after 14 hours, (at the age of 24 hpf). Embryos were washed three times with 0.01 % methylene blue solution (embryo medium) to remove any residual solutions. The embryos were separated into two batches and grown separately in embryo medium and the following experiments were pursued. (i) Bone staining to perform the morphological and morphometric analysis (fixed at 5 dpf) (ii) To perform Whole-Mount in situ Hybridization (WMISH) (fixed at 48 hpf).

3.9 Whole-mount cartilage staining (Appendix 2)

Alcian blue stain was used to stain the cartilage anterior neurocranium of 5 dpf zebrafish. Stanadard protocol for alcian blue cartilage staining was used for the experiment [85]. Briefly, control (n = 8), 1% ethanol (n= 13), 10 µM Dorsomorphin (n= 5) and combined treated (n= 11) samples were fixed several hours in 10% NBF. Staining was carried out overnight in Alcian blue staining solution for 16 hours. Alcian blue staining solution was made using 0.1 g of

Alcian blue powder (Cat. No. 400460250; Fisher Scientific) dissolved in 80 ml ethanol and 20 ml glacial acetic acid solution (Cat. No. 64-19-7; Fisher Chemicals). Then samples were rehydrated gradually through ethanol series (75%, 50%, and 25%) following PBS washes. PBS buffer was prepared with 4.0 g of Sodium chloride (Cat. No; MSX04201; EMD Millipore) 1.0 g of potassium chloride (Cat. No. BP366-500; Fisher Chemicals) 0.693 g of Sodium phosphate dibasic (Cat. No. BP332-500; Fisher Chemicals), and 0.1 g of Potassium dihydrogen phosphate (Cat. No. BP362-500; Fisher Chemicals). The final volume was topped up to 500 ml by adding distilled water. After that, samples were kept in a bleaching solution for 1 to 3 hours containing 3% hydrogen peroxide and 1% potassium hydroxide solution. Next, the tissues were placed in 0.05% trypsin solution (Cat. No. J60402; Alfa Fisher scientific) made in PBS until clearing for 1 to 2 hours. All specimens were processed through an ascending series of glycerol in a 1% potassium hydroxide solution, and then transferred to a storage solution of 100% glycerol. The samples were examined under the stereomicroscope to observe the associated phenotypes. Associated phenotypes were noted and photographed (Zeiss Discovery V8). The ethmoid plate of these samples was dissected out from the skull using fine tungsten needles. The extracted ethmoid plates were mounted on the slide with Glycerol and covered with the coverslip. The sample was examined under a stereomicroscope under 20x and 40x magnification and images were captured (whole ethmoid cartilage: Zeiss discovery V8 and enlarged using stereomicroscope attached with Nikon DSFi2 camera).

3.10 Statistical analysis

The height and width of the ethmoid cartilage were measured using the ZEN microscope software. Height was measured as the maximum length from the tip of the ethmoid cartilage to the caudal end of the ethmoid cartilage marked with the widest point. Similarly, the width was measured as the maximum width of the ethmoid cartilage perpendicular to that of the rostral-caudal line drawn from the midline. Data obtained were subjected to the one-way ANOVA using R Studio, 3.6.2. The p-value of <0.05 was considered statistically significant. Tukey's Pair-wise comparison for each treatment was conducted using R Studio, 3.6.2. For Tukey's test also p-value of <0.05 was considered as statistically significant. Data was visualized in the form of an interval plot.

3.11 Protein probe preparation

3.11.1 *bmp 4* probe preparation

Probes were prepared according to the manufactures instructions (DIG RNA Labeling kit, SP6/T7, Cat. No. 11175025910; Roche). Briefly, 1 µg of zebrafish template DNA was mixed with 2 µl of 10X NTP labeling mixture, 2 µl of 10x Transcription buffer, 1 µl of protector RNAase inhibitor, and 2 µl of RNA polymerase. The mixture was mixed gently and centrifuged at 12,000x g for 1 minute. Samples were incubated for 2 hours in a 37˚C water bath. 2 µl DNAase was added and incubation was continued for another 15 minutes and then the reaction was stopped by adding 2µl of 0.2M EDTA (Cat. No. 37560; VWR).

3.11.2 Detecting *bmp 4* probe

The probe strength was detected using the dot blot techniques according to the standard procedure (Appendix 3). Briefly, 1 µl of diluted *bmp 4* probes was added to the positively charged Nylon membrane (Cat. No.11209299001; Roche). The paper was placed in a glass container and incubated for 40 minutes in the 100˚C hybridization oven. Next, the paper was soaked in 20 ml of maleic acid buffer and incubate at room temperature for 2 minutes with shaking. Maleic acid buffer was made using 1.1607 g of 1 M Maleic acid, 0.8766 g of 0.15 M Sodium chloride, 0.3 ml of Tween-20 (Cat. No. BP337-100; Fisher Scientific), and the solution was topped up to 100 ml using Diethyl pyrocarbonate (DepC water). Paper was incubated in the blocking buffer for 20 minutes with shaking. The 100 ml of blocking buffer was made by adding 2 ml of 2% Sheep serum (Cat. No. BP2425; MP Biomedicals) 3 g of milk powder (Skimmed milk powder, commercially available) and topped up the solution with 10 x TBST in DepC. TBST buffer was made by adding 6.05 g of Tris (Cat. No. BP152-500; Fisher Chemicals) and 8.76 g of Sodium chloride in 800 ml of DepC water. The pH was adjusted to 7.5 with 1 M hydrochloric acid (Cat. No. SA48-1; Fisher Chemicals) and volume was made up to 1 L with DepC water. Finally, 10 ml of tween-20 was added to 1L of TBS buffer. Paper was washed with TBST for 5 minutes with shaking. Paper was incubated in 10 ml of the antibody solution (Cat. No. 11093274910; Roche) for 30 minutes followed by two washes in washing buffer for 15 minutes for each wash. The antibody solution was made by adding 2 µl of antibody into 10 ml of TBST buffer. The washing buffer was made by adding 1.1607 g of 1M Maleic acid, 0.8766 g of 0.15 M NaCl, 0.3 ml Tween-20. The final solution was made by adding DepC water to 100 ml. Paper was incubated in the detection buffer for 5 minutes.

Detection buffer was made by adding 10 ml of 0.1 M Tris-HCl, 0.5844 g of 0.1 M NaCl, and the final volume was top up to 100 ml with DepC water. The 1 ml of BCIP/NBT Liquid substrate solution (Cat. No.ICN980771; MP Biomedicals) was added on top of the paper, kept in dark, and checked for a color reaction every five minutes. The first dot was detected at the highest concentration within 5 - 10 minutes. The reaction was stopped by adding TE buffer. TE buffer was made by adding 1 ml of 10 mM Tris-HCl, 0.2 ml of 1 mM EDTA (Cat. No. 37560; VWR) and the solution was top up with DepC water to 100 ml.

3.12 Whole-Mount in situ Hybridization (WMISH)

3.12.1 Embryo Fixation

WMISH was performed on the 48 hours WT zebrafish embryos. All the solution for this procedure were made in DepC water. The 48 hpf zebrafish were euthanized using 0.01% MS222 solution and fixed in 4% PFA overnight. Samples were bleached using 0.5% Potassium hydroxide, 3% hydrogen peroxide solution made in DepC water. Next, samples were dehydrated gradually through methanol (Cat. No. BP1105SS-28; Fisher chemicals) series in PBS (25%, 50%, 75%), and samples were stored in 100% methanol for more than three months before used for the experiment.

3.12.2 Whole-mount in situ Hybridization (WMISH) (Appendix 4)

WMISH was conducted according to the established protocol in the lab (Appendix 4) [86]. Briefly, samples were rehydrated to PBS gradually through the methanol (Cat. No. BP1105SS-28; Fisher Chemicals) series (75%, 50%, 25%). Then samples were permeabilized using the proteinase K (1 µl proteinase K / 1000 µl of DepC, Cat. No.BP1700-100; Fisher Chemicals). Then the samples were incubated in the Hyb (-) solution. Hyb (-) solution was prepared by adding 50 ml of Deionized Formamide 100% (Cat. No.327235000; Acros) 25 ml of Saline-sodium citrate 20X (SSC) (Cat. No. BP1325-1; Fisher Chemicals), 0.1 ml Tween-20 final solution was top-up to 100 ml by adding 24.9 ml of DepC water. After that, samples were incubated with *bmp 4* probe in Hyb (+) solution at 70˚C, overnight. Hyb (+) solution was prepared by adding 3.56 ml of Hyb (-), 0.4 ml of Yeast tRNA (5mg/ml) (Cat. No. 10109509001; Roche) 0.04 ml of Heparin (50 µg/ml, Cat. No. BP2425; Fisher Chemicals) 0.0368 ml Citric acid and the final volume was adjusted to 6 ml with DepC water. After that, high stringency washes were performed to remove the non-specific binding of the probe. Next samples were incubated in the blocking buffer. Blocking buffer was made by adding 3920 ml of 1x PBST solution, 80 µl of 2% Heat inactivated sheep serum (Cat. No. BP2425; MPBiomedicals),

0.008g Bovine serum albumin (2 mg/ml) (Cat. No. SH30574.01; GE Life Sciences, HyClone Labs). The final volume was adjusted to 6 ml by adding DepC water. 1 µl of Antibody solution (Cat. No.11093274910; Roche) was added to 9 µl of blocking solution. From that 1 µl was added to each tube. Substrate solution of NBT/BCIP staining was used as a colorimetric detection of RNA. The reaction was conducted in the dark until proper color expression was detected. The color reaction stopped after 40 minutes. The samples were fixed in 4% PFA and dehydrated through methanol series. Whole-mount images were captured using a stereomicroscope in a solution prepared with 50% ethanol and 50% glycerol (Zeiss discovery V8).

3.13 Cryosectioning

3.13.1 Sample preparation for Cryosections

To locate the exact tissue distribution of the *bmp 4* expression, WMISH samples were sectioned which was embedded in the agarose gel. The agarose gel was prepared using 1g of agarose powder (Cat. No. BP160-100; Fisher Chemicals) in 100 ml of distilled water. WMISH zebrafish samples were embedded in the agarose gel. The desired orientation of the embryo was arranged manually using tungsten needles. Small gel blocks with an embedded sample were cut using a surgical blade. Then samples were dipped in the 30 % sucrose solution made in distilled water (Cat. No. AC41976000, Acros) and gel blocks were kept in the sucrose solution until blocks sink to the bottom of the tube.

3.13.2 Cryosection of the whole-mount sample

Cryostat machine (CM1850: Leica Biosystems) in Dr. Hao Ding's lab, Department of Biochemistry and medical genetics, University of Manitoba was used for cryosectioning. Premade agarose gel blocks containing samples were arranged on the specimen disc in the right orientation. Samples were covered with the OTC mounting solution (Cat. No. 75806-668; Leica). Next, the specimen discs were kept inside the cryostat machine at -20˚C to freeze. In the meantime, pre-cooled microtome blades were inserted into the knife holder and clamped (Cat. No. 28-617-21; Thermo scientific, MB22). Specimen disc was inserted into the specimen's head. The knife holder angle and distance were adjusted with specimens. The cryostat was adjusted to 15 µm thick cryosections. Sufficient care was taken to ensure that the block is completely frozen to the specimen's disc (the OCT medium will turn white) before beginning sectioning. Then sections were trimmed down to the required plane by turning the handwheel. The distance between the Anti-roller guide and cutting edge was adjusted to

prevent sections from rolling. Cryosections were carefully placed on glass slides by using a small paintbrush. Slides were air-dried and kept overnight at -4˚C. Next, sections were mounted with glycerol solution to observe under a light microscope in X20 magnification stereomicroscope attached with a Nikon DSFi2 camera. The region of *bmp 4* gene expression in the developing oral region was identified with color intensity (Purple). Pictures were taken using a stereomicroscope attached with a Nikon DSFi2 camera.

CHAPTER 4: RESULTS

4.1 Growth series of Alizarin-red bone staining

Fig 4.1: Two Alizarin red bone stained populations of Mexican tetra*;* Surface fish and Pachon cavefish ventral view of the skull, over ontogeny. **A** & **B**; 5 dpf, **C** & **D**; 10 dpf, **E** & **F**; 20 dpf, **G** & **H**; 35 dpf, **I** & **J**; 60 dpf. **BOC:** Basioccipital, **E:** Ethmoid, **LW:** Lateral wings of the parasphenoid bone, **MP:** Mid parasphenoid, **N:** Notochord, **O, :** Otoliths, **OC:** Ossification center, **P:** Parasphenoid, **V:** Vomer. Parasphenoid bone in both the surface and cavefish populations is developed from the two median ossification centers circled in **C** and **D** (OC). Two anterior projections and two posterior projections were developed from the ossification centers. Projections grew towards the anterior direction and fused in the midline and continued to grow as a single projection. Bifurcates grew towards the posterior direction individually. Fully developed parasphenoid bone was observed in the 35 dpf samples. The median portion of the parasphenoid bone was narrow compared to the anterior and posterior portions. Scale bar for **A, B, C, D, E, F** is 200 µm. Scale bar for **G, H, I, J** is 600 µm.

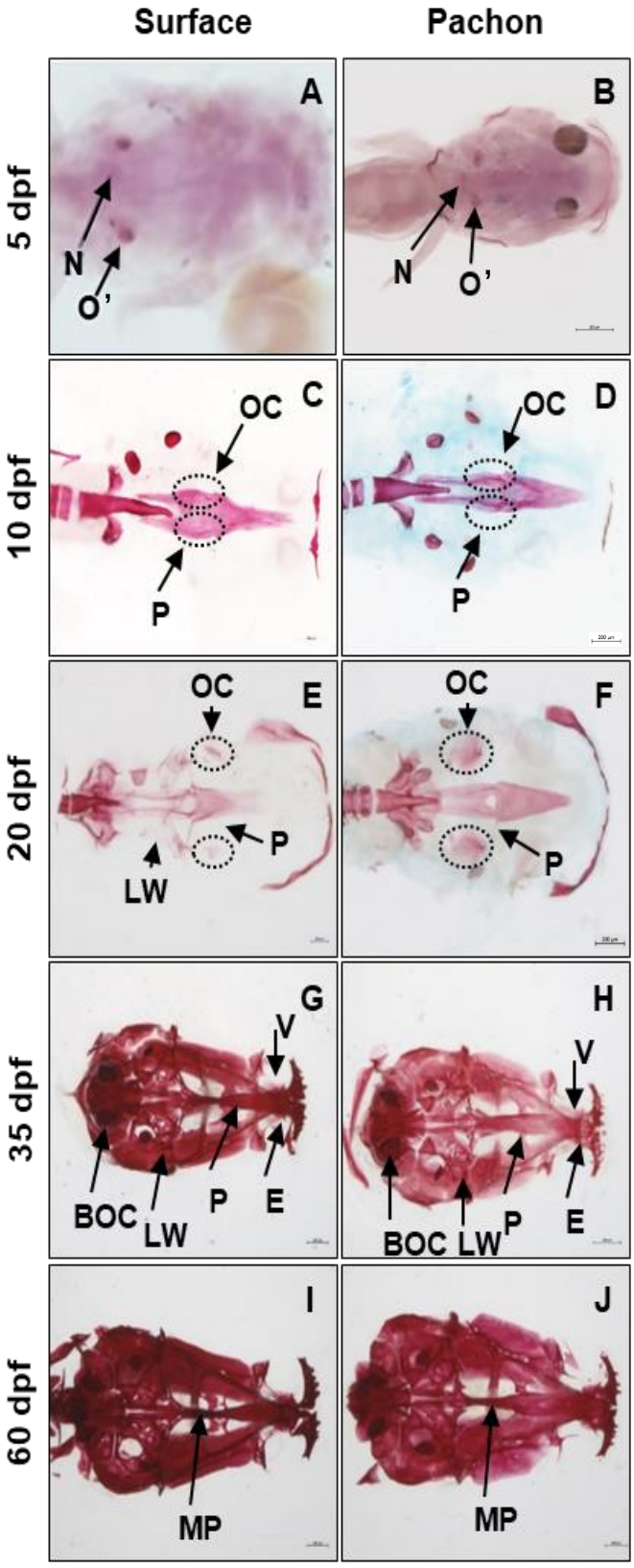
Surface
Pachon
5 dpf
10 dpf
20 dpf
35 dpf
60 dpf
A
B
C
D
E
F
G
H
I
J
N
O'
OC
P
LW
V
BOC
E
MP

Alizarin red bone stained samples were used to understand the anatomy and development of parasphenoid bone in the surface and cavefish populations. According to the bone staining results, the ossification of parasphenoid was not detected in surface fish and Pachon cavefish at 5 dpf (Fig 4.1: A & B). Ossified otoliths and the anterior notochord were observed at this stage in both Mexican tetra populations (Fig 4.1: A & B). Otoliths were located on either side of the base of the neurocranium (Fig 4.1: A & B). The anterior notochord was observed in the posterior base of the neurocranium (Fig 4.1: A & B). Two ossification centers (primary ossification centers) were found in both cave and surface fish populations at 10 dpf in the center of the parasphenoid bone from where the the left and right posterior wings of the parasphenoid bone would eventually emerge (Fig 4.1: C & D). The two spiny projections extended from ossification centers to the anterior and posterior directions (Fig 4.1: C & D). Projections that grew towards the anterior direction fused in the midline and extended towards the ethmoid bone (Fig 4.1: C & D). The two projections grew towards the notochord fused with the basioccipital bone located laterally to the notochord (Fig 4.1: C & D). A pair of ossification centers (secondary ossification centers) appeared in 20 dpf fish mediolaterally to the parasphenoid bone (Fig 4.1: E & F). Specially in surface fish, paired lateral projections from the primary ossification centers protruded at 20 dpf to fuse with secondary ossification centers on either side, but these protrusions could not be observed in Pachon fish at 20 dpf (Fig 4.1: E & F). In 35 dpf, both cave and surface fish had completely developed parasphenoid bone, which articulated anteriorly into the ethmoid bone, anterolaterally to vomer and dorsally to orbitospenoid bone. And, posteriorly it articulated to the basioccipital bone (Fig 4.1: G, H, I & J). Thicker parasphenoid bone was observed in the ventral view of the 35 dpf and 60 dpf surface fish samples compared to the cavefish (Fig 4.1: G, H, I & J). Apart from a few developmental delays, the development and articulation of the parasphenoid bone in Mexican tetra surface and cavefish populations were nearly identical. By the age of 60 dpf, these ossification delays in cavefish had already been recapitulated.

4.2 Micro-CT imaging

Fig 4.2: Micro-CT images of the three populations of adult Mexican tetra, surface fish, Pachon, and Tinaja. **A, B**, and **C** showing the lateral view of the skull. **D**, **E**, and **F** showing the lateral cross-view of the skull, and **G**, **H**, and **I** showing the ventral view of the base of the neurocranium. The encircled area in **A, B, C** shows the circumorbital bones. The white line on **D, E,** and **F** indicates the hypothetical, straight line drawn from the bottom of the parasphenoid bone. The white line in the **G, H,** and **I** mark the skull symmetry in Mexican tetra. Fragmented circumorbital bones in two different cavefish populations were observed **A** and **B**. Intact circumorbital bones of the surface fish observed in **C**. Parasphenoid bone in two cavefish populations found straightened in **D** and **E**. Parasphenoid bone in surface fish is curved to dorsal direction from both anterior and posterior points. Ventral view of the base of the neurocranium shown the asymmetrical skull in two cavefish populations and the symmetrical skull of surface fish found in **G, H** and **I**.

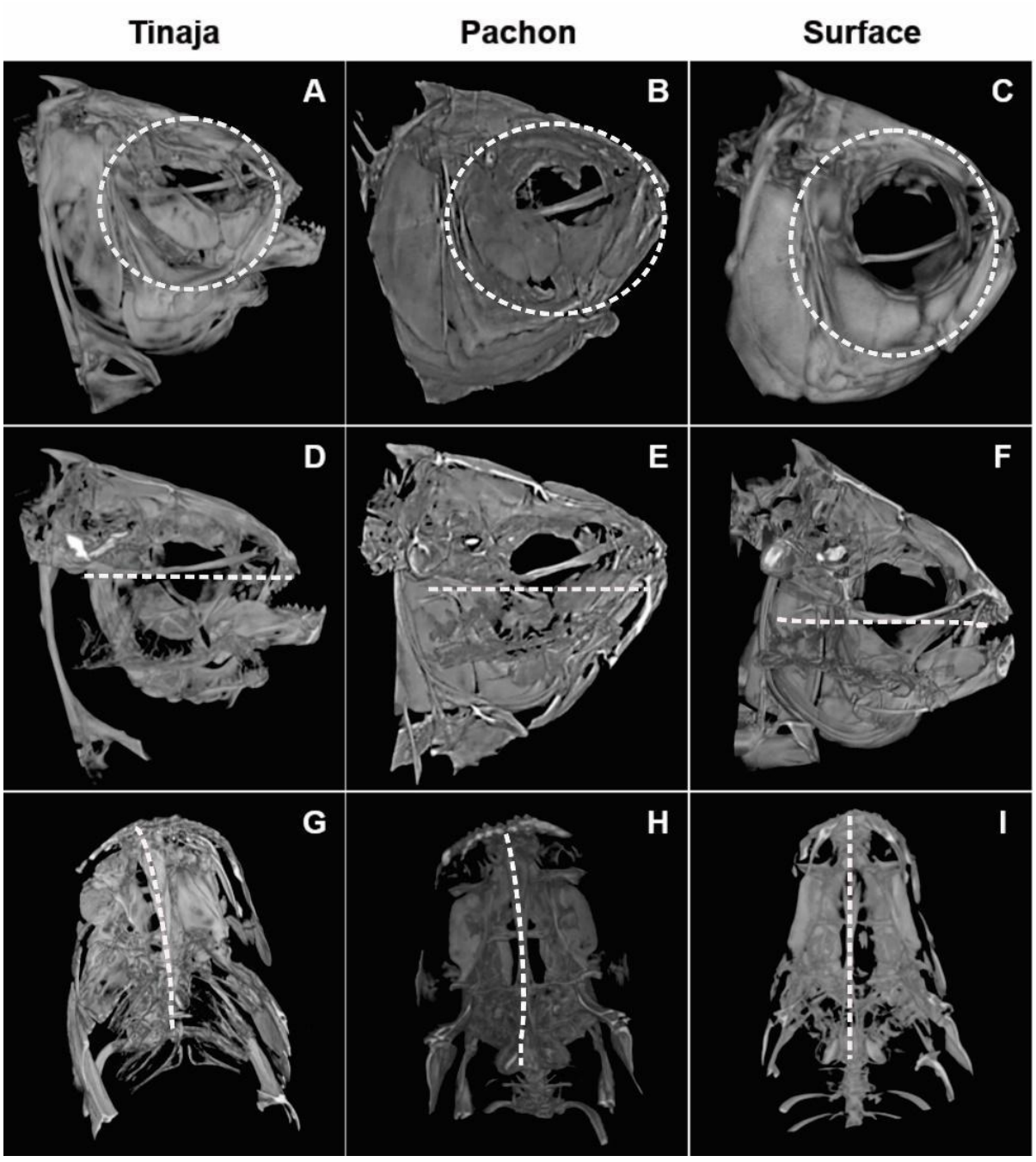
Tinaja
Pachon
Surface
A
B
C
D
E
F
G
H
I

To understand the morphological variation in the parasphenoid bone associated with different eye morphs, micro-CT images of the lateral skull (Fig 4.2: A, B, & C), a lateral cross-section of the skull (Fig 4.2: E, F, & G), and the ventral view of the skull (Fig 4.2: G, H & I) were analyzed in surface fish and compared with the two cavefish populations; Pachon and Tinaja. In the lateral skull view, fragmented circumorbital bones were observed in both cavefish morphs (Fig: 4.2: A & B). Mainly, suborbital 3 (SO3) bone (Largest circumorbital bone) fragmentation was found in two cavefish populations. 3D images of the lateral skull of surface fish showed the intact circular arrangement of circumorbital bones (Fig 4.2 C). More specifically intact SO3 bone was observed in surface fish (Fig 4.2: C). The lateral cross-view of micro-CT images revealed the distinct difference in morphology of parasphenoid bone among different eye morphs (Fig 4.2: D, E & F). The two cavefish populations exhibited straightened parasphenoid bone (Fig 4.2: D & E). In Pachon cavefish, parasphenoid bone was straightened and it has raised towards the anterior-dorsal direction relative to the Tinaja, allowing approximately 20˚ ascending angels of elevation to hypothetically drawn, straight line to the anterior side from the bottom point of the parasphenoid bone (Fig 4.2: E). In Tinaja, parasphenoid bone was perpendicular to the premaxilla (upper jawbone) and the elevation of bone was smaller compared to the Pachon (Fig 4.2: D). Right after the lateral spread of the parasphenoid bone to form its two wings, it took a more horizontal path towards the posterior direction in both cavefish morphs (Fig 4.2: D & E). In contrast to the cavefish, the parasphenoid bone was curved beneath the eye socket in surface fish (Fig 4.2: F). Also, the bone marked the lowest point from the ventral side where the place that lateral wings spread out and anterior to the lowest point and posterior to the lowest point, bone curved to the dorsal direction (Fig 4.2: F). This curve was much more noticeable beneath the eye socket (Fig 4.2: F). Further, the ventral view of the micro-CT images showed asymmetry of the cavefish skull (Fig 4.2: G, H & I). Both cave morphs had left side asymmetry with apparent bone collapsed in cavefish (Fig 4.2: G & H). More interestingly, the asymmetry of the parasphenoid bone was observed (bent towards the left side from the anterior) (Fig 4.2 G & H). In Pachon cavefish bending towards the left was less than Tinaja (Fig 4.2: H). In surface fish, horizontal, symmetrical parasphenoid bone driven from posterior to anterior direction was observed (Fig 4.2: I). Pachon and Tinaja cavefish populations had a wider skull relative to the ventral view of the surface fish skull (Fig 4.2: G, H & I). As seen in micro-CT photographs, different populations of Mexican tetra had different parasphenoid bone morphology in the lateral and ventral views of the skull.

4.3 Principal component analysis (PCA)

Table 4.1: The principal component 1 (PC1) and principal component 3 (PC3) values for the shape of the parasphenoid bone in different Mexican tetra populations

Populations	PC1	PC3
Pachon 1	1.12E-02	3.25E-03
Pachon 2	9.81E-03	1.85E-03
Pachon 3	2.27E-02	8.35E-04
Pachon 4	2.52E-02	1.51E-02
Pachon 5	6.64E-02	2.43E-02
Pachon 6	3.93E-02	-2.71E-03
Pachon 7	3.59E-02	1.27E-02
Surface 1	-9.78E-02	1.81E-02
Surface 2	-1.65E-02	2.43E-02
Surface 3	-1.59E-01	1.66E-02
Surface 4	-8.44E-02	-2.88E-02
Surface 5	-6.26E-02	-1.35E-02
Surface 6	-4.55E-02	-1.61E-02
Tinaja 1	6.08E-02	-2.39E-03
Tinaja 2	6.52E-02	6.87E-03
Tinaja 3	5.70E-02	-1.83E-03
Tinaja 4	2.54E-02	-1.32E-02
Tinaja 5	9.76E-02	-1.51E-02

The principal component analysis was used to highlight the differences in the parasphenoid bone among Mexican tetra cave and surface fish populations. According to the correlation values obtained under the PC1, all the positive values were corresponding to Pachon and Tinaja (Table: 4.1). Therefore, the PC1 (the correlation between fish types: Pachon and Tinaja, and PC1 component) increased with an increase in the shape of the parasphenoid bone in two cavefish populations. This suggested that the shape of the parasphenoid bone in these two cavefish varied together. All the negative values were corresponding to surface fish (Table: 4.1). This suggests that the shape of the parasphenoid bone of surface fish did not vary together with the shape of the parasphenoid bone of Pachon and Tinaja. These results indicated that the criteria in surface fish parasphenoid bone varies opposite to the two cavefish populations.

Fig 4.3: PCA analysis for the shape of the parasphenoid bone of the three different Mexican tetra populations. The x-axis indicates the PC1 and Y-axis indicates the PC3. Contour points for the parasphenoid bone are placed as below. 1) Anteriorly - the place that parasphenoid bone articulated to the ethmoid bone, 2) Posteriorly- the point that bone is articulated to the basioccipital bone, 3) Ventral margin of the bone and 4) Dorsal margin of the bone. Two cavefish populations occupied the same area in the scatter plot. Surface fish fell into a separate space in the scatter plot.

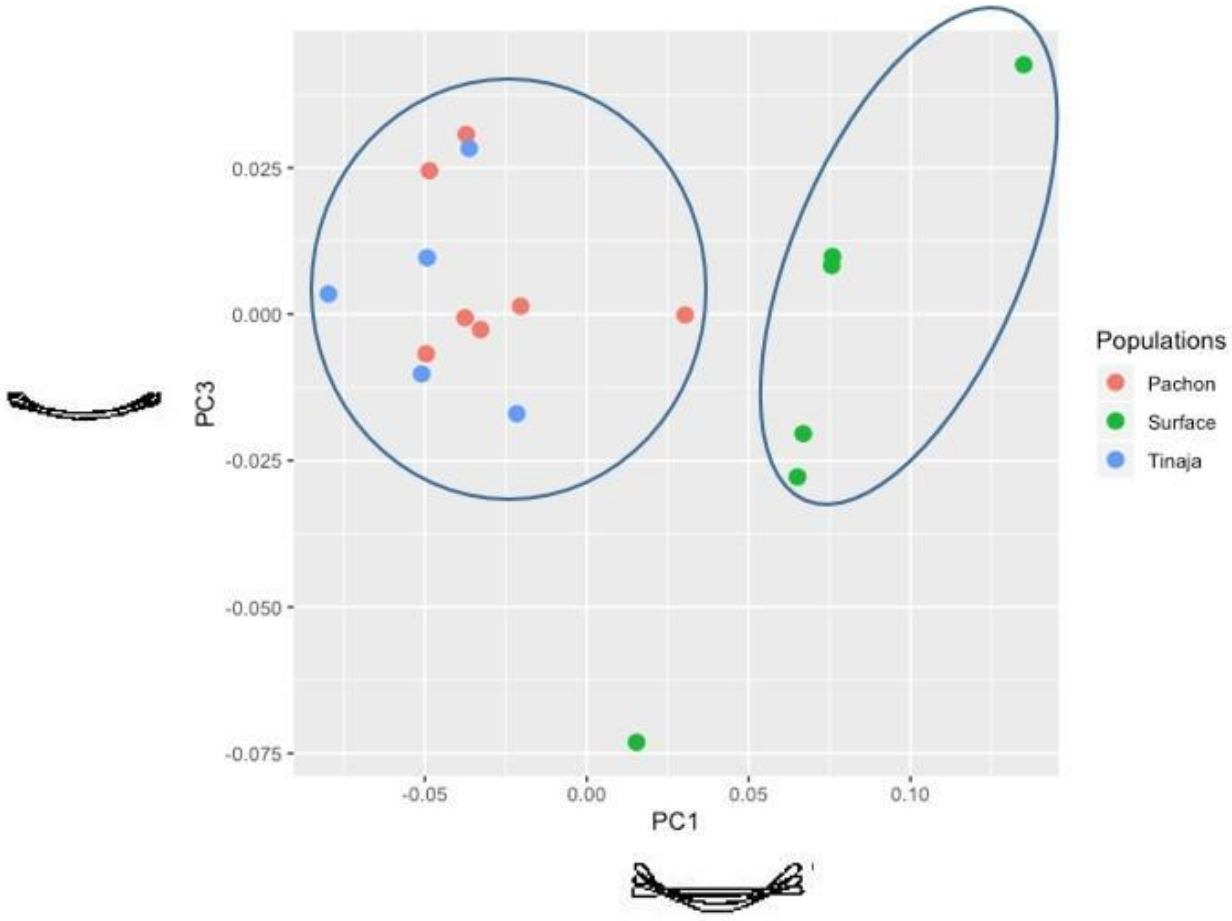

Principal Component values for the shape of the parasphenoid bone for three different populations has shown in the Table 4.1. and in the scatter plot in Figure 4.3. According to the PC1 the cavefish populations are distinctly separated from the surface fish in the scatter plot (Fig 4.3). Tinaja and Pachon occupied the same space in a scatter plot revealing that the shape of the parasphenoid bone of the two cavefish populations were similar but demonstrated a distinct difference compared to the surface fish (Fig 4.3). Concerning the PC3, all three samples of cavefish and surface were within the same range (Fig 4.3). In terms of the shape of the parasphenoid bone, two cavefish populations clearly distinguished from surface fish populations on the scatter plot.

Table 4.2: The Principal Component 1 (PC1) and Principal Component 2 (PC2) for the shape of the neurocranium in different Mexican tetra populations.

Populations	PC1	PC2
Pachon 1	3.04E-02	-1.50E-02
Pachon 2	-3.28E-02	-5.09E-03
Pachon 3	-2.04E-02	-2.15E-02
Pachon 5	-4.96E-02	-1.08E-02
Pachon 6	-4.86E-02	-1.05E-02
Pachon 7	-3.72E-02	-9.13E-03
Surface 1	-3.76E-02	-8.67E-03
Surface 2	7.57E-02	6.65E-02
Surface 3	1.54E-02	8.15E-02
Surface 4	1.35E-01	5.70E-02
Surface 5	6.51E-02	-5.89E-02
Surface 6	7.59E-02	-5.61E-02
Tinaja 1	6.69E-02	-6.10E-02
Tinaja 2	-3.63E-02	3.08E-02
Tinaja 3	-5.10E-02	5.10E-03
Tinaja 4	-4.93E-02	-5.94E-03
Tinaja 5	-2.16E-02	-1.39E-02

The shape of the neurocranium in three different populations of Mexican tetra was subjected to principal component analysis. According to the PC1 correlation values, most of the positive values corresponded to surface fish (Table 4.2). Therefore, the PC1 increased with increasing shape of the neurocranium in surface fish. In comparison, most of the negative values obtained under PC1 corresponded to Pachon and Tinaja (Table 4.2). PC1 variation in surface fish is directly opposed to PC1 variation in Pachon and Tinaja. This showed that the shape of the neurocranium of surface fish did not vary together with the shape of the neurocranium of Pachon and Tinaja. These results suggests that the criteria in the shape of the neurocranium of surface fish varied opposite to the cavefish populations.

Fig 4.4: PCA analysis for the shape of the neurocranium of the three different Mexican tetra populations. The x-axis indicates the PC1 and Y-axis indicates the PC2. The contour point for the selected area in the neurocranium is the dorsally highest end of the neurocranium, the ventrally lowest point of the neurocranium, anteriorly the anterior-most end of the neurocranium, and posterior-most end of the neurocranium. Two cavefish populations and surface fish occupied three different spaces in the scatter plot.

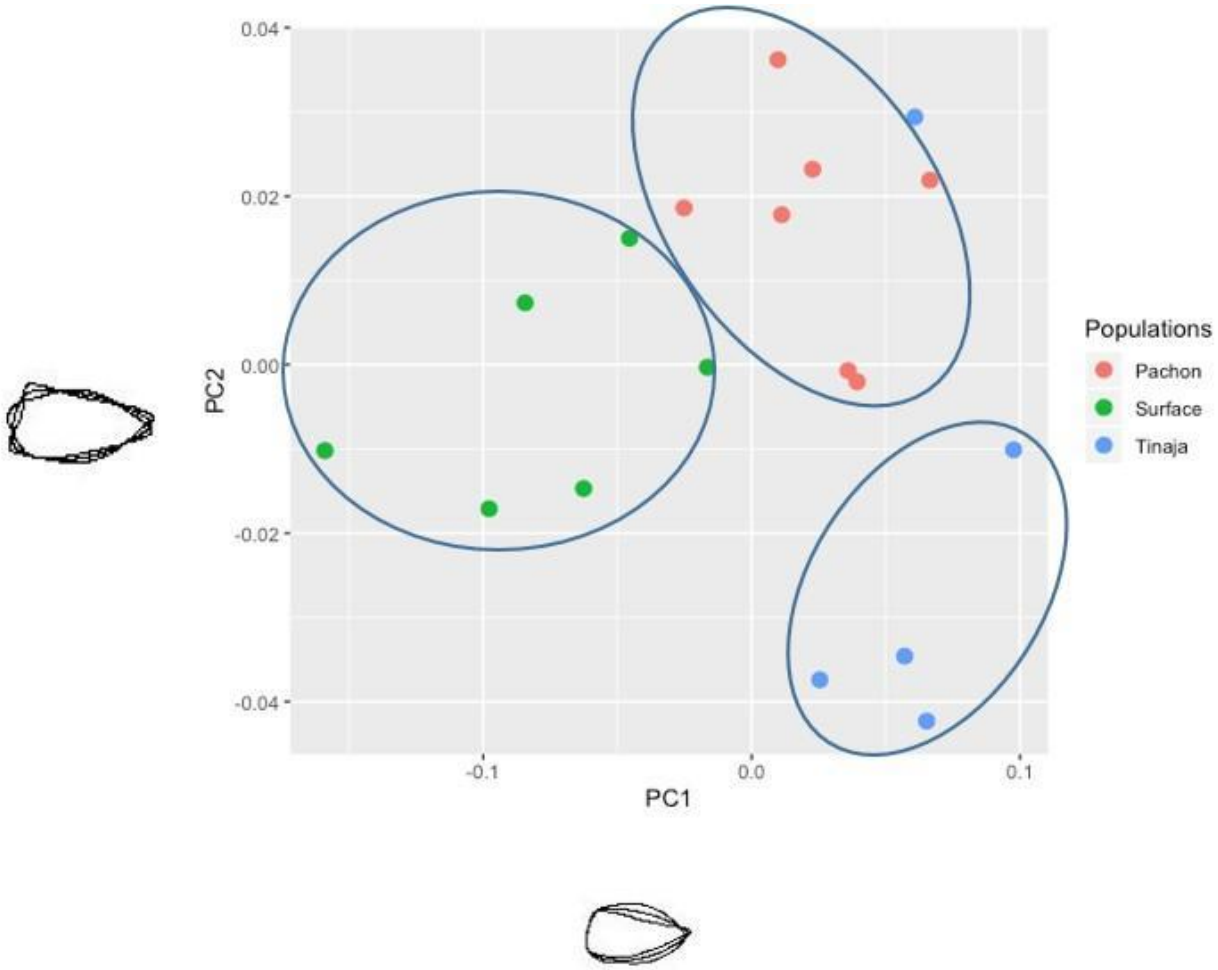

PCA was used to check whether the shape of the neurocranium in three Mexican tetra populations differs from one another. A scatter plot is drawn between the PC1 and PC2 (Fig 4.4). All three populations occupied the three different spaces in the scatter plot (Fig 4.4). Surface fish and two cavefish populations were different from each other based on the PC1 (Fig 4.4). Tinaja fish overlaped with the Pachon cavefish according to PC1, which differentiated the surface fish as a separate cluster (Fig 4.4). The neurocranium shapes of three populations of Mexican tetra varied among each other.

4.4. TRAP and ALP staining

4.4.1 TRAP staining

Fig 4.5: TRAP staining for 60 dpf Mexican tetra surface and cavefish. The image shows an enlarged view of the anterior, middle, and posterior region of the parasphenoid bone. Cavefish: **A, B,** & **C,** Surface: **D, E,** & **F**. **A** & **D**: Posterior region of the parasphenoid bone, **B** & **E**: Middle region of the parasphenoid bone, **C** & **F**: Anterior region of the parasphenoid bone. **P**: Parasphenoid, **Ep**: Epithelium. Osteoclast cells (red) were detected in the posterior and middle area of the parasphenoid bone of cavefish from the red color in **A** & **B** (margined area and marked with astrix). No sign of osteoclast cells were detected in surface fish **D, E** & **F**. Magnification is x 40. Scale bar indicates the 0.1 µm.

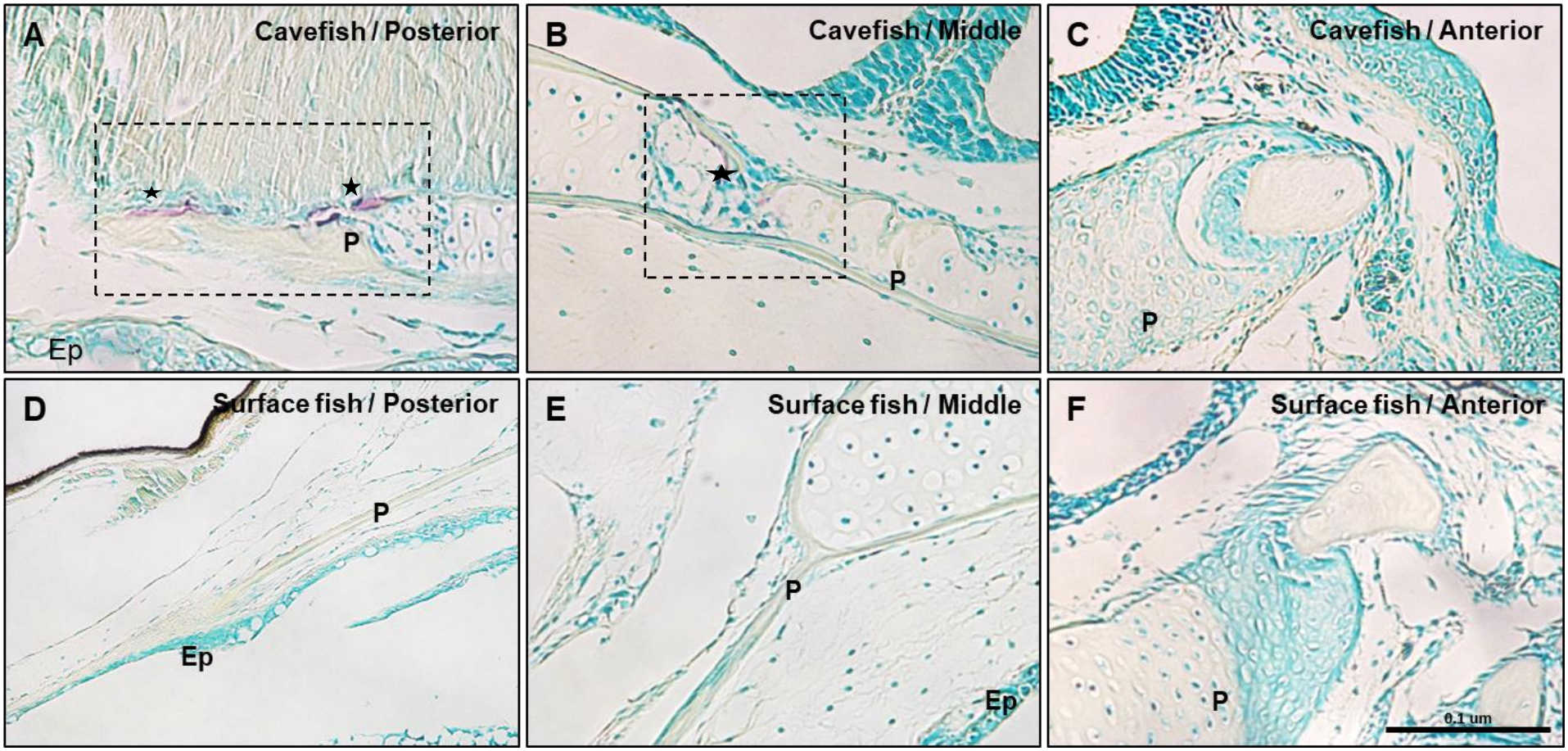
A
Cavefish / Posterior
P
Ep
B
Cavefish / Middle
P
C
Cavefish / Anterior
P
D
Surface fish / Posterior
P
Ep
E
Surface fish / Middle
P
Ep
F
Surface fish / Anterior
P
0.1 um

TRAP staining was used as a marker to identify the osteoclast cells in the bone-resorbing sites. Figure 4.5 depicted a lateral cross-section of the cavefish and surface fish skull stained with TRAP at 60 dpf. At 60 dpf in Pachon cavefish had high osteoclast cell activity in the middle and posterior ends of the parasphenoid bone (Fig: 4.5 A & B). The anterior area of the Pachon did not have a sign of osteoclast activity (Fig: 4.5 C). The anterior, middle and posterior areas of the parasphenoid bone in surface fish did not show any signs of osteoclast cells. (Fig: 4.5 D, E & F). High bone resorption was observed in cavefish at 60 dpf.

4.4.2 ALP staining

Fig 4.6: ALP staining for 60 dpf Mexican tetra surface and cavefish. The image shows an enlarged view of the anterior, middle, and posterior region of the parasphenoid bone. Cavefish: **A, B,** & **C,** Surface: **D, E,** & **F**. **A** & **D**: Posterior region of the parasphenoid bone, **B** & **E**: Middle region of the parasphenoid bone, **C** & **F**: Anterior region of the parasphenoid bone. **P**: Parasphenoid, **Ep**: Epithelium. Mineralization margin secret from the osteoblast cells were detected in the margin of the parasphenoid bone, indicated in brown color (double arrowhead). The highest osteoblast cell activity detected in the middle and posterior region of the parasphenoid bone in cavefish **A** & **B**. Magnification is x 40. Scale bar indicates the 0.1 µm.

1

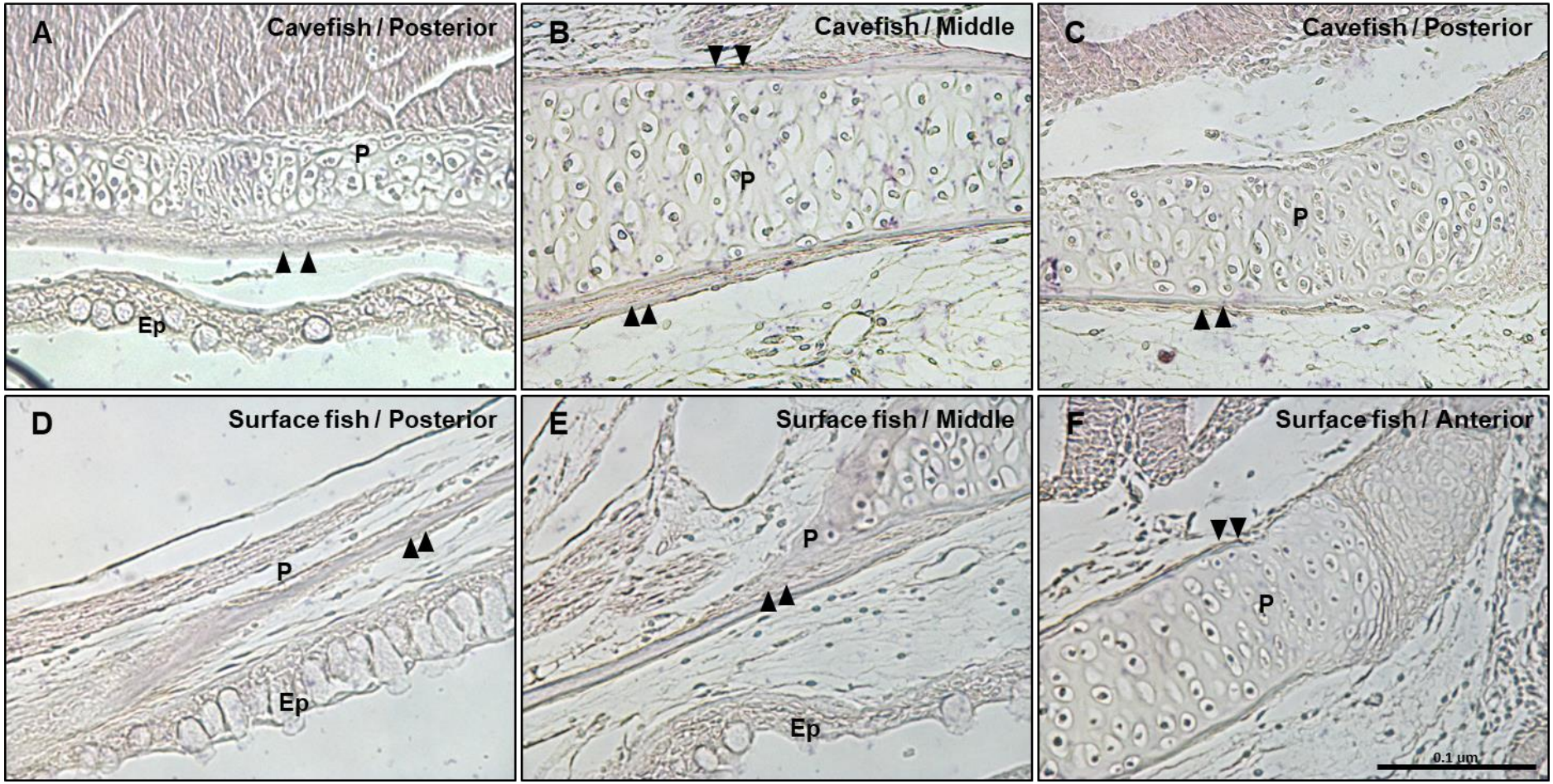
A
Cavefish / Posterior
P
Ep
B
Cavefish / Middle
P
C
Cavefish / Posterior
P
D
Surface fish / Posterior
P
Ep
E
Surface fish / Middle
P
Ep
F
Surface fish / Anterior
P
0.1 µm

ALP staining was used to examine bone-deposited osteoblasts cells. In this experiment, 60 dpf Mexican tetra surface and cavefish were subjected to the ALP staining. Brown color osteoblast cells were recognized on the bone margin (Fig 4.6: A, B, C, D, E & F). Both cave and surface fish had a thin layer of osteoblast cells in the anterior region (Fig 4.6: C & F). Bone density had risen in the middle in both fish (Fig 4.6: B & E). Relative to the surface fish, the appearance of brown color osteoblast cells in the cavefish was higher in the middle region (Fig 4.6: B). In the posterior region, higher number of osteoblast cells were observed in the cavefish (Fig 4.6: A). High bone deposition was observed in cavefish at 60 dpf.

4.5 Alcian blue cartilage staining of the ethmoid cartilage

Fig 4.7: Alcian blue-stained base of the neurocranium of 5 dpf zebrafish (*Danio rerio*). **LE:** Lateral ethmoid, **ME:** Median ethmoid, **N:** Notochord, **PC:** Polar cartilage, **PR:** Parachordal, **T:** Trabeculae. The ventral base of the neurocranium attached to the notochord. Ethmoid cartilage has lateral ethmoid and median ethmoid. Scale bar indicates the 100 µm.

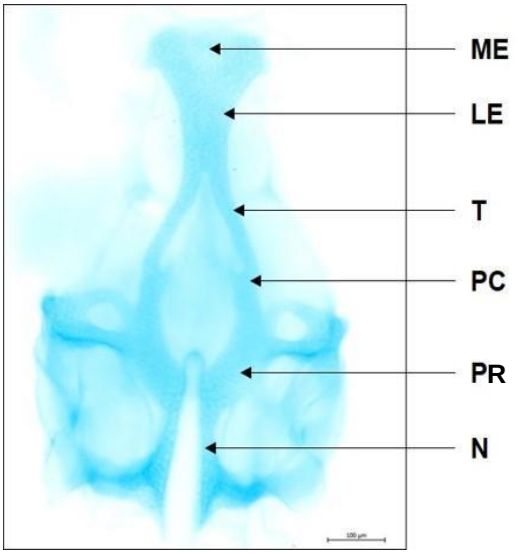

To understand the anatomy of the zebrafish ventral base of the neurocranium, 5 dpf zebrafish were subjected to the alcian blue cartilage staining. The base of the neurocranium of zebrafish was extracted from the dissected samples. The base of the neurocranium consisted the most ventrally to anterior as followed, notochord, parachondral, polar cartilage, trabeculae, and ethmoid cartilage. Ethmoid cartilage was formed by two basic areas; mid ethmoid region and lateral ethmoid region (Fig 4.7).

Fig 4.8: Alcian blue stained ethmoid cartilage of 5 dpf zebrafish after treatments. **A** & **E**: Control, **B** & **F**: 1% Ethanol, **C** & **G**: 10 µM Dorsomorphin and **D** & **H**: combined treatment (1% Ethanol + 10 µM Dorsomorphin). The median ethmoid region is highlighted with an arrowhead. Blue color staining in the medial ethmoid region was reduced in the treated samples compared to the control. In the control sample, both areas of lateral and medial ethmoid was stained in the same color intensity. Blue color stain in the medial ethmoid region in treated samples was reduced compared to the lateral ethmoid region. Magnification for **A, B, C,** and **D** is x20. Magnification for **E, F, G,** and **H** is x40. Scale bar for **A, B, C, D** indicates 100 nm. Scale bar for **E, F, G** & **H** indicates 20 nm.

1

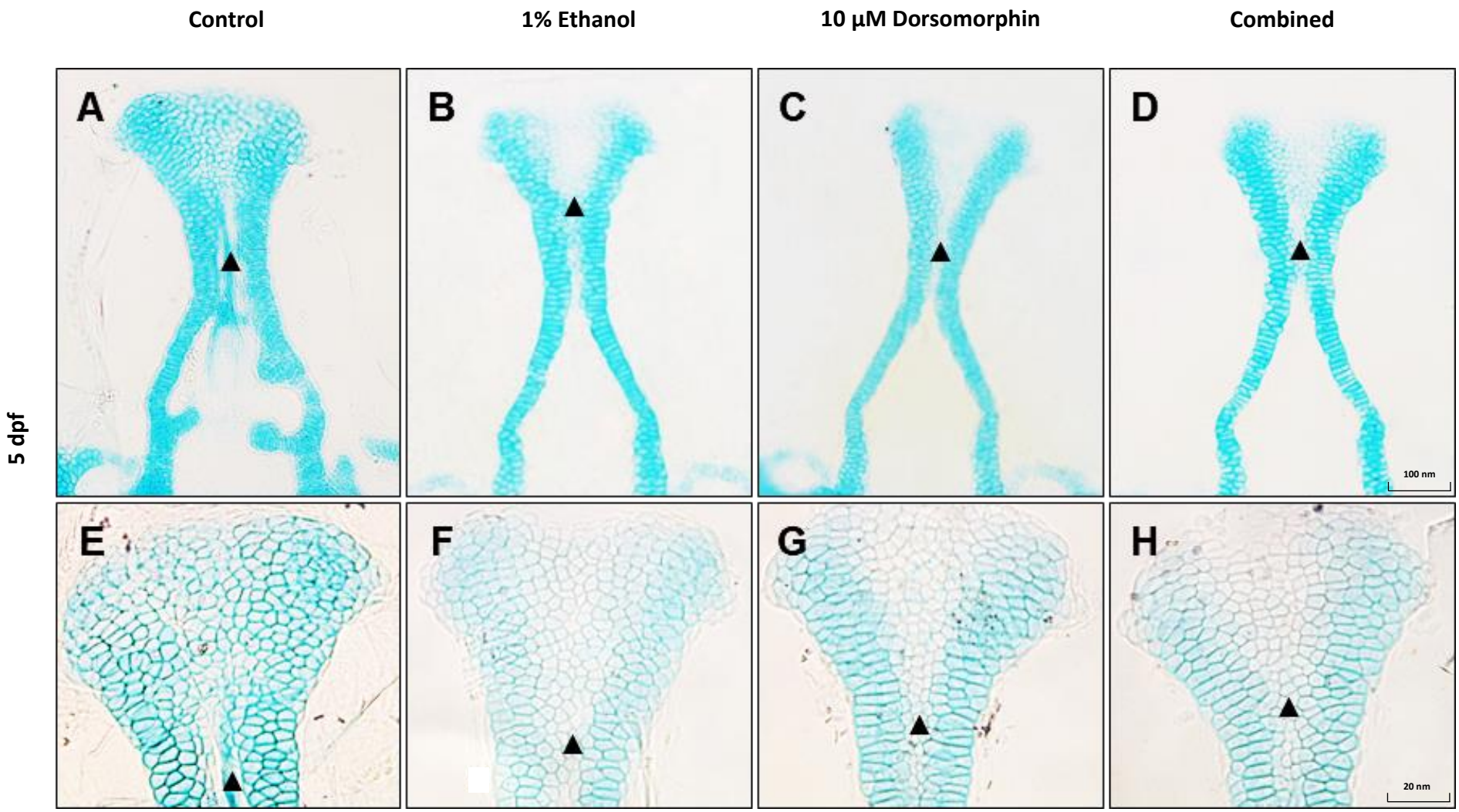
Control
1% Ethanol
10 µM Dorsomorphin
Combined
5 dpf
A
B
C
D
E
F
G
H
100 nm
20 nm

The effect of chemical exposure on ethmoid cartilage in zebrafish was studied using alcian blue cartilage staining. Upon the treatments from 10 hpf to 24 hpf; No apparent changes of shape and size of the ethmoid cartilage was observed under the stereomicroscope (Fig: 4.8). In the control sample, blue color cell stain in the median ethmoid region was prominent compared to the treated samples (Fig: 4.8 A & E). In the treated samples, blue color stain in the median ethmoid region was decreased relative to the control sample (Fig: 4.8 B, C, D, F, G & H). In the control sample blue color stain in the median ethmoid and lateral ethmoid area showed no difference whereas the same intensity of the blue color was noticed in both areas (Fig: 4.8 A & E). Blue color stains in the median ethmoid area in treated samples were reduced relative to the lateral ethmoid cartilage of the same sample (Fig: 4.8 B, C, D, F, G & H). This reduced blue color might indicate lower cell density in the median ethmoid region compared to the control sample. In 1% Ethanol-treated samples blue color stain in both lateral and median ethmoid area was reduced compared to the control and other treated samples (Fig: 4.8 B & F). Exposure to chemical treatments had no noticeable effect on the ethmoid cartilage shape and size that is visible by light microscopy.

4.6 Statistical analysis for height of the ethmoid cartilage

Statistical analyses were performed to better understand the effect of chemical exposure on the height of ethmoid cartilage. The mean height of the control samples was 263.3 ± 72.8 µm (Table 4.3) which is the longest length of all the other groups. The mean height of the ethmoid cartilage was decreased as a result of each different chemical treatment. With 1% Ethanol treatment, the mean height of the ethmoid cartilage was equal to the 161.55 ± 33.02 µm and in 10 µM Dorsomorphin treated samples it was 160.10 ± 20.97 µm. Interestingly, in the combined treated samples the ethmoid cartilage had the smallest mean height value, which was equal to 139.96 ± 13.68 µm.

Table 4.3: Mean height, standard deviation, and *P*-value obtained from one-way ANOVA for the ethmoid cartilage height in control and treated samples. Mean height of the ethmoid cartilage was measured by the maximum length from the tip of the ethmoid cartilage to the caudal end of the ethmoid cartilage marked with the widest point.

Treatment	**N**	**Mean height (µm)**	**SD**	***P*-value**
Control	8	263.3	72.8	$0.12x10^{-5}$
1% Ethanol	13	161.55	33.02	
10 µM Dorsomorphin	5	160.10	20.97	
Combined	11	139.96	13.68	

To better understand whether obtained mean heights were significantly different, one-way ANOVA was conducted. The one-way ANOVA results showed a significant difference in the mean heights ($P = 0.12x10^{-5}$, Table 4.3). This means that at least one mean height significantly differed from another considered group. Tukey's pairwise comparison was subsequently conducted to understand the differences in the mean height between each pair (Table: 4.4). The result showed that all treatment means differed significantly from the control mean (Table: 4.4). In contrast, mean height comparison of all the other possible pairs (1% Ethanol vs. 10 µM Dorsomorphin, 1% Ethanol vs. Combined, and 10 µM Dorsomorphin vs. Combined) were not significantly different (Table 4.4). The interval plot also showed that none of the potential pairs with the control sample had zero in their interval range (Fig 4.9). In comparison, all other

possible pairs with no control sample had a zero in their interval range (Fig 4.9). The height reduction observed in the treated samples were significant compared to the control.

Table 4.4: Tukey's pairwise comparison for the mean height of the ethmoid cartilage of control and treated samples.

Difference of Levels	***P*-value**
Control – 1% Ethanol	$0.18x10^{-4}$
Control – 10 µM Doromorphin	$0.47x10^{-3}$
Control – Combined	$0.11x10^{-5}$
1% Ethanol - 10 µM Doromorphin	1.00
1% Ethanol – Combined	0.57
10 µM Doromorphin – Combined	0.79

Fig 4.9: Interval plot of the Tukey's pairwise comparison for control and treated groups for the mean height of the ethmoid cartilage. Treatments include 1% ethanol, 10 µM Dorsomorphin and Combined.

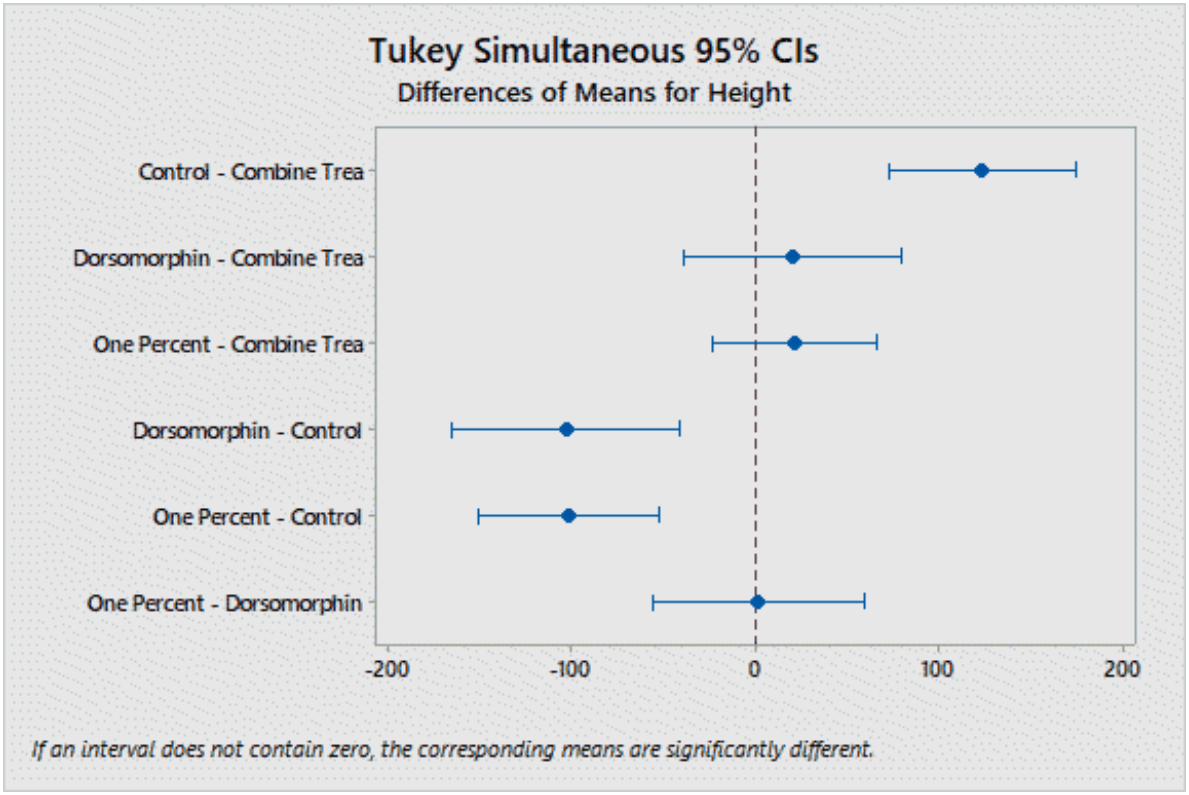

4.7 Statistical analysis for width of the ethmoid cartilage

To better understand the effect of chemical exposure on ethmoid cartilage, the mean width of the control and treated samples were calculated (Table 4.5). The mean width for the control samples was 246.4 ± 56.2 µm, which was the highest value for width from the rest of the samples. The mean width of the ethmoid cartilage has decreased with each different treatment. Interestingly the combined treated samples had the smallest mean ethmoid cartilage width, which was equal to 133.49 ± 9.75 µm. With 1% Ethanol treatment the mean width of the ethmoid cartilage was equal to 153.51 ± 32.82 µm and with the 10 µM Dorsomorphin treatment the mean width was equal to the 145.04 µm (SD ± 17.40).

Table 4.5: Mean width, standard deviation, and *P*-value obtained for the ethmoid cartilage in control and treated samples. Width of the ethmoid cartilage is measured by the maximum width of the ethmoid cartilage perpendicular to that of the rostral-caudal line drawn from the midline.

Treatment	**N**	**Mean width(µm)**	**SD**	***P*-value**
Control	8	246.4	56.2	$0.15x10^{-6}$
1% Ethanol	13	153.51	32.82	
10 µM Dorsomorphin	5	145.04	17.40	
Combined	11	133.49	9.75	

One-way ANOVA was used to determine if the obtained mean widths significantly differed. The results showed a significant difference between the recorded mean widths ($P = 0.15x10^{-6}$). Tukey's pairwise comparison was used to compare the differences in mean widths between each pair (Table 4.6). According to obtained *P*-values, all treatment mean widths were significantly different from the control mean as shown in Table 4.6. The mean width of the other possible pairs (1% Ethanol vs. 10 µM Dorsomorphin, 1% Ethanol vs. Combined, and 10 µM Dorsomorphin vs. Combined) were not significantly different. The interval plot also showed that none of the possible pairs with the control sample included zero in their interval range (Fig 4.10). All other possible pairs that did not include control had zero in their interval range (Fig 4.10). When compared to the control, the width reduction observed in the treated samples was significant.

Table 4.6: Tukey's pairwise comparison for control and treated groups for mean width of the ethmoid cartilage

Difference of Levels	P-Value
Control – 1% Ethanol	$0.18x10^{-4}$
Control – 10 µM Dorsomorphin	$0.47x10^{-3}$
Control – Combined	$0.11x10^{-5}$
1% Ethanol - 10 µM Dorsomorphin	0.963
1% Ethanol – Combined	0.476
10 µM Dorsomorphin – Combined	0.919

Fig 4.10: Interval plot of the Tukey's pairwise comparison for control and treated groups for mean width of the ethmoid cartilage. Treatments include 1% ethanol, 10 µM Dorsomorphin and Combined.

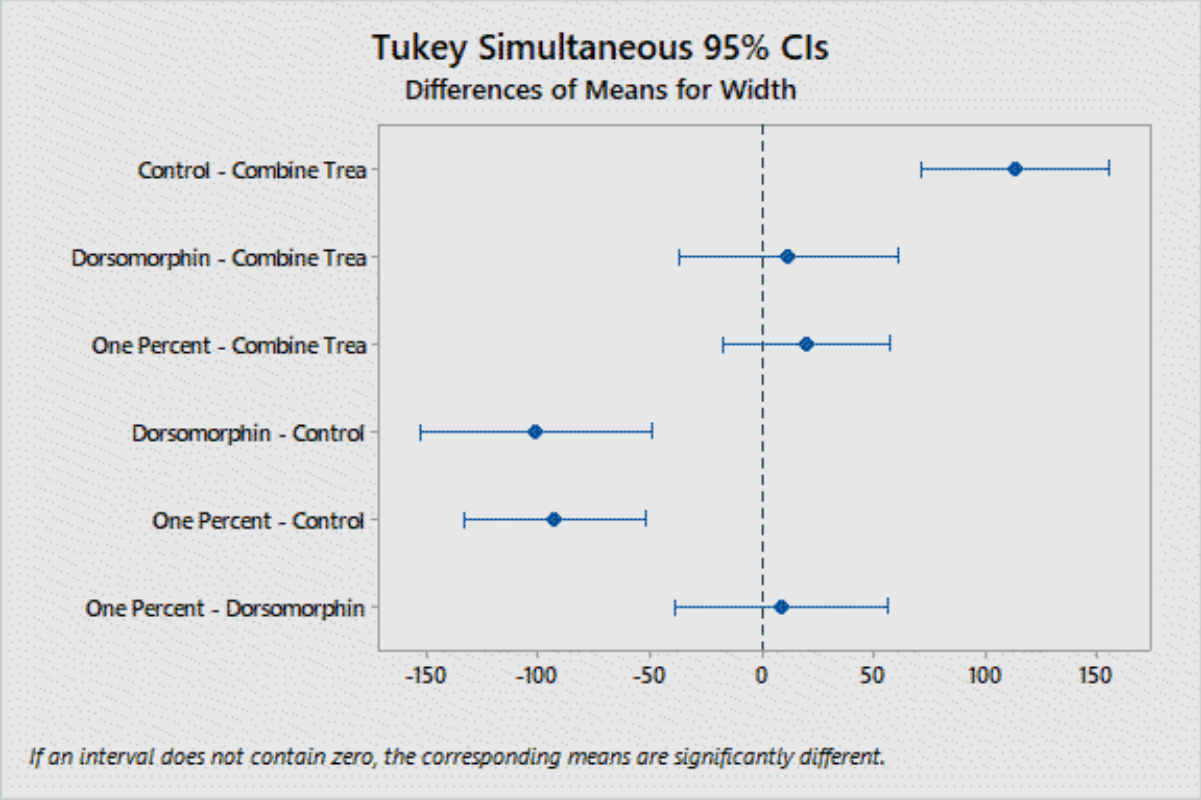

4.8 Whole-mount in situ hybridization (WMISH)

Fig 4.11: Whole-Mount in situ Hybridization of 48 hpf zebrafish for *bmp 4* probe. **A, B, C, D, E** Whole-mount sample, **F, G, H, I**: Cryosections. **A**: Negative control for the experiment, **B** & **F**: Control, **C** & **G**: 1% Ethanol, **D** & **H**: 10 µM Dorsomorphin, **E** & **I**: Combined treatment. Expression of *bmp 4* prominent in the control sample. The expression was detected around the eye and developing palatal region. With the treatment of **C, D**, and **E** from 10 hpf to 24 hpf overall expression of *bmp 4* has reduced. In cryosectioned samples, the expression of *bmp 4* has reduced in **C** and **E** areas of developing ethmoid cartilage. Scale bar for **A,B,C,D** indicates 100 nm. Scale bar for **E,F,G,H** indicates 20 nm.

1

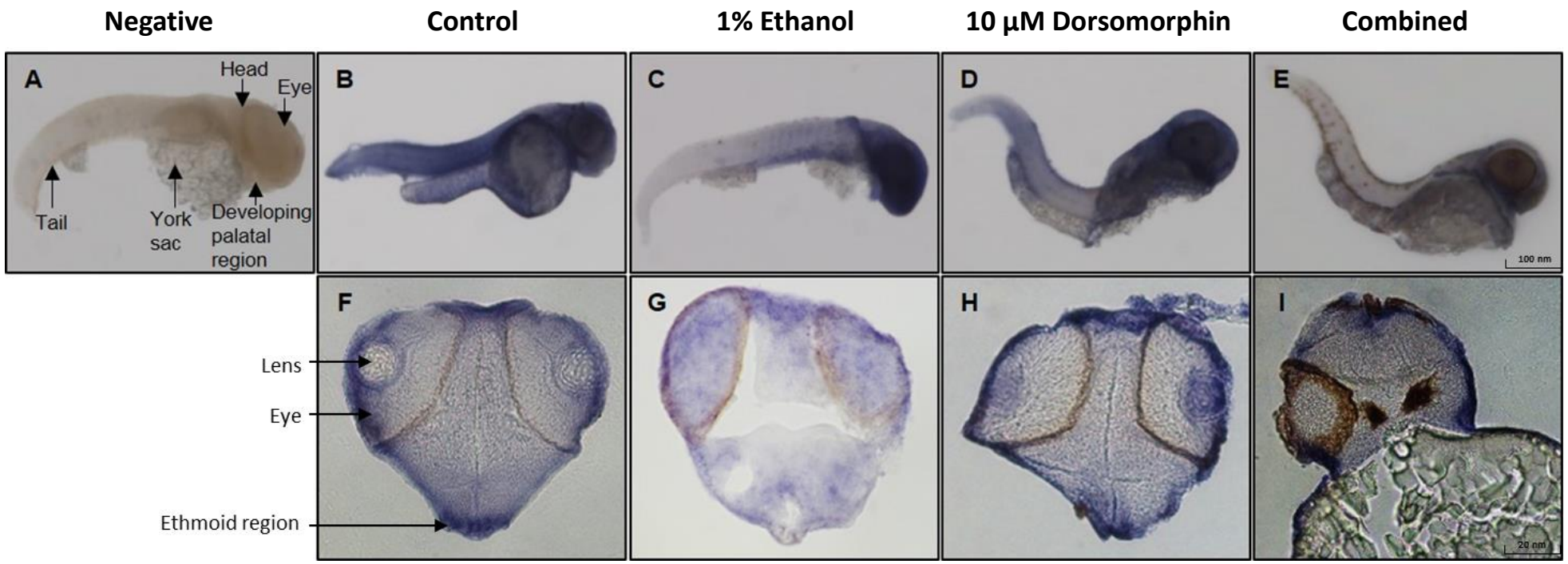
Negative
Control
1% Ethanol
10 µM Dorsomorphin
Combined
A
Head
Eye
Tail
York sac
Developing palatal region
B
C
D
E
100 nm
F
G
H
I
Lens
Eye
Ethmoid region
20 nm

WMISH was performed for the 48 hpf zebrafish using a *bmp 4* probe to identify the *bmp 4* expression in an area of developing ethmoid cartilage. The expression of the *bmp 4* upon the treatments was detected using the colorimetric method. Treatments include 1% Ethanol, 10 µM Dorsomorphin, and combined treatment. Each treatment was conducted from 10 hpf to 24 hpf. The area of the *bmp 4* expression was observed in purple color. The negative control was not treated with the *bmp 4* probe (Fig: 4.11 A). Expression of *bmp 4* detected in the developing oral region and around the eye in 48 hpf, control sample (Fig: 4.11 B). Cryosection of the control sample showed the *bmp 4* expression in the region of developing ethmoid cartilage with high intensity of the purple color (Fig: 4.11 F). In a 1% Ethanol-treated sample, overall *bmp 4* expression was reduced compared to the control sample (Fig: 4.11 C). However, compared to the other body region expression was prominent in the cranial region (Fig: 4.11 C). In the cryosections, 1% Ethanol-treated samples showed a reduction of *bmp 4* in the developing ethmoid cartilage which was observed from the lesser intensity of purple color. With the treatment of 10 µM Dorsomorphin, the overall *bmp 4* expression was reduced but the expression still noticed around the eye and developing oral region (Fig: 4.11 D). Cryosections showed the expression of *bmp 4* in the region of developing ethmoid cartilage (Fig: 4.11 G). The overall expression of *bmp 4* reduced in the combined treated sample compared to the control sample (Fig: 4.11 E). Unlike other treatments, expression around the cranial region (around the eye and developing oral region) has been reduced (Fig: 4.11 E). The cryosections further validated the reduced expression of *bmp 4* in the region of developing ethmoid cartilage (Fig: 4.11 I).

Collectively, the *bmp 4* expression in treated samples was reduced compared to the control sample. Except for the combined treatment, *bmp 4* expression around the eye and oral region was observed (Fig: 4.11. B, C, D & E). Cryosections of the dorsal to ventral directions of the zebrafish cranial region showed the expression of the *bmp 4* noticeably reduced in the 1% Ethanol treated and combined treated sample compared to the control sample (Fig: 4.11. F, G, H & I). Expression of *bmp 4* in 10 µM Dorsomorphin treated sample was closely similar to the intensity of purple color in the control sample. In the whole mount sample and developing palatal region at 48 hpf, *bmp 4* expression was less than in the control sample.

CHAPTER 5: DISCUSSION

5. Discussion

Here I studied the palatal bone development and evolution in response to environmental factors. I chose Mexican tetra to examine the impact of early eye degeneration on parasphenoid bone. The parasphenoid bone is a palatal bone that runs along the ventral side of the neurocranium. The development and articulation of the parasphenoid bone in cavefish and surface fish populations were nearly identical. However, I found some developmental delays in cavefish, which recapitulated later in bone development. Interestingly, with the micro-CT analysis I observed the shape of the parasphenoid bone varied between Mexican tetra populations. Surface fish had a curved parasphenoid bone, while cave populations showed a straightened parasphenoid bone. This study also discovered differences in bone remodeling activities between cave and surface fish populations where cavefish shows comparatively higher bone remodeling activity

Embryonic development is a delicate process influenced by the environment. I used zebrafish to examine the effect of ethanol exposure on zebrafish ethmoid cartilage development. With ethanol, Dorsomorphin, and combined treatment, hypo-stained area in the median ethmoid region was observed. Furthermore, I noticed a significant impact on ethmoid cartilage size in zebrafish with chemical treatments. The reduced expression of *bmp 4* in the developing ethmoid region was found with all the treatments except from the Dorsomorphin.

5.1 Parasphenoid bone development and ossification in Mexican tetra

The vertebrate cranial skeleton is developed from the CNCC derived ectomesenchymal cells and embryonic mesodermal cells [87]. Two modes of ossification can be found in the craniofacial skeleton, namely endochondral ossification and intramembranous ossification. In endochondral ossification, mesenchymal cells condense and differentiate into chondrocytes of cartilages. The skeletal structures are later replace by the bone-forming osteoblast cells. In intramembranous ossification, the mesenchymal cells condense and differentiate directly into osteoblast cells [1]. The anterior part of the neurocranium is derived from the CNCC, while the medial and posterior parts are of mesodermal origin [88]. Parasphenoid bone is a cranial bone that forms the base of the neurocranium. The parasphenoid bone has dual NCCs origin where it develops from the rhombo-mesencephalic NCCs and prosencephalon-mesencephalic NCCs [89]. Extensive research work on anatomy, development, and ossification of

parasphenoid bone in zebrafish is available but this is not well studied in, Mexican tetra fish (*Astyanax mexicanus).* Moreover, the developmental origin, anatomical location, and characteristics of Mexican tetra parasphenoid bone with regard to the development of the eye tissues have not yet been studied. Hence, in this study, we chose Mexican tetra as the model organism since it is an emerging species in evolutionarily developmental biology. We examined the effect of early eye degeneration on parasphenoid bone development using the Mexican tetra surface and cavefish.

We used alizarine red stained parasphenoid bone of the surface fish and Pachon cavefish to trace the growth and ossification sequence. Bones which are vital for survival have early ossification in the teleost skull. For example, bones that are needed for respiration and feeding, ossify earlier than other bones [90]. My results show that Mexican tetra parasphenoid bone ossifies as early as 5-10 dpf, while zebrafish parasphenoid bone ossifies as early as 4 dpf when the zebrafish is 3.4 mm in length (Fig 4.1 A & B) [90]. This early ossification of parasphenoid bone can be related to its functional importance of protection of the brain and other sensory organs from the ventral side of the neurocranium [1].

Parasphenoid bone in Mexican tetra ossifies from the endochondral ossification. The cartilaginous template is gradually replaced by the osteoblast cells that are responsible for the secretion of the bone matrix [91]. Then the cluster of cells develops into the skeletogenic condensation or the primary ossification center. Ossification centers are located in the middle of the developing bone as shown in figure 4.1 C & D. Thereafter the bone grows in multiple directions (ventral, dorsal, and lateral) [91]. We detected that the lateral wings of the parasphenoid bone have developed from the second pair of ossification centers on either side of parasphenoid bone (4.1 E & F). Unlike in mammals, ossification is not a common occurrence in small-sized adult teleost fish such as zebrafish and medaka. In these fish, two types of endochondral ossifications are found [92]. Type 1 ossification is similar to mammalian ossification where resorption of the cartilage and surrounding bone collar, which gives rise to the bone as seen in ceratohyal and the radials in zebrafish [92]. Type 2 ossification replaces the arising space in cartilage with bone collar cells and fill the bone marrow space with adipose tissue. But some bone shafts will remain without getting replaced by adipose tissue or by bone which later mineralized to form the bone [93]. However, in zebrafish, parasphenoid bone development occurs by type 1 endochondral occification. In our study, we observed type 1 endochondral ossification in Mexican tetra parasphenoid bone development.

5.2 Parasphenoid bone development and articulation in Mexican tetra

Bone growth and articulation in adult zebrafish and Mexican tetra cave, and surface morph, are almost identical, with the exception of a few developmental features that has been clarified in the following. In both Mexican tetra and zebrafish, parasphenoid bone is developed by the anterior spiny growth that merges in the midline to grow as one tapered projection into the anterior side. In Mexican tetra, the posterior bifurcates do not merge and instead converge as two elements into the basioccipital, while in zebrafish, the posterior bifurcates are fused in the posterior region and emerge as a tapering pointed projection [2].

Previous literature suggests that lateral wings of the parasphenoid bone are conserved in the teleost fish [2]. In zebrafish, the lateral wings of the parasphenoid bone develop when the total body length of the fish is equal to approximately 7.6 mm at an age of 14 dpf to 21 dpf [2]. Our finding revealed that the lateral wings of the parasphenoid bone in Mexican tetra is similar to zebrafish in morphology and articulation. Furthermore, we observed lateral wings of parasphenoid bone have appeared in 20 dpf surface fish. But in cavefish lateral wings of the parasphenoid bone appeared in the range of 20 - 35 dpf. The delayed lateral wings growth in Mexican tetra may caused due to the pressures exerted by biotic and abiotic factors in the cave environment during continuous evolution [94]. Further, this finding is supported by variations in parasphenoid bone shape and size observed in various taxa throughout evolutionary history due to the pressure of biotic and abiotic influences [94]. On the other hand, the delay in parasphenoid bone ossification might have been influenced by the optic nerve and the developing eye structures. In cavefish, degeneration of the eye and associated structures begins at 24 hpf; very early stages of development. Here onwards there is negative pressure and influence on the development of the eye-protecting tissues. The early bone fragmentation and malposition of circumorbital bones are directly associated with eye loss. Similarly, with the absence of eye structures, the inner parasphenoid bone might be getting a shock or sudden pause in development and later recapitulate the bone growth.

The parasphenoid bone is a highly variable bone in evolutionary terms. Further, a variation of parasphenoid bone observed in some amphibian classes such as caecilians, where they show devoid of parasphenoid bone to simplify the skull. However, in some fossils and extant salamanders, there is evidence of teeth development on the parasphenoid bone. In humans, parasphenoid bone has been replaced by the vomer bone [94]. However, the parasphenoid bones were present in some other mammals like monotremes and marsupials but

morphologically different from the other vertebrate groups where they lost lateral wings in the parasphenoid bone compared to the other vertebrate phyla [94]. The delayed ossification of the parasphenoid bone needs further investigations with increase sample size by adding more age groups to capture the exact time points of ossification.

5.3 Bone remodeling activity in the Mexican tetra

The activity of old bone removal and new bone addition is termed as the process of bone remodeling. Bone remodeling is a dynamic process where the old or damaged bone is being resorbed by the osteoclast cells and new bone is being formed by the osteoblast cells [95, 96]. In the present study, paraffin-embedded tissue sections of surface fish and cavefish samples were used to identify the bone remodeling sequence of the parasphenoid bone. Bone remodeling activity was found to be notably different in different eye morphs of Mexican tetra; cavefish and surface fish. Osteoblast cell activity was detected by ALP staining. ALP enzyme is produced by osteoblast cells which is capable of catalyzes the hydrolysis of phosphomonoesters at an alkaline pH which can detect by the ALP staining [97, 98]. Osteoblast activity was found in both surface fish and cavefish, but activity was slightly higher in cavefish (Fig. 4.6). The calcium phosphate produced by osteoblast cells can be converted to hydroxyapatite and organic material. These hydroxyapatite and organic material together with type 1 collagen secrete the new bone in the part of bone reabsorbed. In the bone-resorbing process, high osteoclast dissociation was observed in cavefish by secreting hydrochloric acid and lysosomal enzymes which were detected with TRAP staining (Fig 4.5) [99]. TRAP staining is a histochemical marker to identify the osteoclast cell activity in the site of bone resorption [32, 98]. According to literature the bone deposition is more prominent in most of the fish than bone absorption at most of the ages [100]. In the older samples, bone absorption is more frequent compared to bone deposition [100]. In the present study, the same age fish were used (60 dpf) (Fig. 4.5 & 4.6). Therefore, the differential expression of bone remodeling we observed could not be due to age.

Collectively, high osteoclast and high osteoblast cell activity in the cavefish explain the high bone remodeling activity in cavefish compared to the surface fish. The main ions involved in bone remodeling activity are calcium and phosphate, which are essential minerals in fish skeletons. Fish can absorb calcium directly from the environment other than dietary calcium. Absorption occurs through the gills, fins, gastrointestinal tract, and oral epithelia [101]. Major calcium regulation happens through the gills. Even though both fish belong to one species,

metabolic rate differences have already been discovered in surface and cavefish [101]. Due to this, the amount of metabolized calcium can be different in surface and cavefish. Another key element in bone development is phosphorous. The amount of phosphorous in the inhabiting water and the diet determine the phosphorus amount in the fish body [102]. The hydrological study conducted in the caves of Mexico revealed that cave water contains high amounts of calcium but less phosphate content [103]. As mentioned earlier, calcium phosphate is the key component for new bone development [30, 103]. The absence of the required amount of phosphate ions in the cave water might limit the amount of phosphate ions in the fish body. Therefore, the phosphate entrapped in the bones of cavefish can be released into the fish body rapidly than that in surface fish. Further, rapid bone resorption can be helpful to maintain plasma calcium levels. Other than calcium present in the bones, calcium is essential in the circulatory system, extracellular fluid, muscle, and other tissues. Calcium present in those tissues is essential for mediating vascular contraction, vasodilatation, muscle activity, nerve transmission, intracellular signaling, and hormonal secretion. Also, it plays an important role in hormone regulation by regulating the parathyroid hormone, calcitriol, and other growth hormones [104].

In this study, we used only one age group with limited sample numbers. It is worth repeating these experiments with different age groups with increased sample size. Further, the lateral view, which has been used for this study, did not give us an idea of the parasphenoid bone thickness. In the future, it is important to use coronal sections to recapitulate the bone thickness at different areas of the parasphenoid bone. Many research groups have extensively studied the skull and facial bone anatomy and fine genetics. Others have extensively studied morphological adaptation to the cave environment [12, 105-107]. The activity of bone remodeling in Mexican tetra needs further investigations. Therefore, it will be very important to characterize how bone remodeling activity differs in different Mexican tetra populations and how bone remodeling activity varies between different ages of Mexican tetra. Further, this will provide insight into the bone diseases such as osteoporosis in humans that occur by altered bone remodeling activity.

5.4 Shape difference of parasphenoid bone in three different morphs of adult Mexican tetra

Eye loss has a direct and/or indirect effect on bone development in the cavefish's cranial skeleton. Studies have found that eye loss in cavefish influences the size, shape, and

organization of the cranial bones, more precisely the bones around the eye orbit [108]. Here we used micro-CT analysis to investigate the three-dimensional structural differences of parasphenoid bone of surface fish, Pachon cavefish, and Tinaja cavefish (Fig. 4.2). The cavefish population is believed to have originated from the two surface fish populations [109]. Some cavefish populations were derived from the old surface fish population, while others originated from the new surface fish population. Tinaja and Pachon are considered derived from the old populations, phylogenetically based on the DNA microsatellite data analysis [109]. But with the mitochondrial DNA data, Pachon was identified as a more derived population and grouped with new surface fish population [109]. In other studies on cranial bones, the Pachon and Tinaja cavefish were used to compare with the surface fish [33]. We use both Pachon and Tinaja cavefish to get a better understanding of parasphenoid bone morphology, and the findings are compared to the population of surface fish. The asymmetry of the skull that was observed in two cavefish populations is due to the collapsed eye orbit in the cavefish and the opercula bone, which is located posterior to the eye orbit [33]. This asymmetry is always biased to the left side, which is called directional bending. Interestingly, in our results, other than skull asymmetry, we observed the asymmetrical parasphenoid bone in cavefish, which bends the anterior end of the parasphenoid bone to the left side (Fig. 4.2 G, H & I). This bending is increased in the Tinaja compared to the Pachon fish. This asymmetrical parasphenoid bone morphology has not been studied previously. Even though the exact reason for this asymmetry was not clear, studies have shown that asymmetrical NCC migration may cause skull asymmetry in cavefish. This could be the cause of the asymmetrical parasphenoid bone we saw in our experiments [13]. However, further studies are needed to identify the role of migratory NCCs on the development of the cranial tissues. NCCs tracing using live-cell markers would be an ideal experiment to identify the NCCs migration with regards to the asymmetry.

Many studies have been conducted on the effect of eye degeneration on facial bone and circumorbital bones. However, the effect of eye degeneration on the palatal bones were not broadly studied [32, 33]. We studied the effect of eye degeneration in cavefish on the parasphenoid bone formation (Fig. 4.2.D, E, & F). We observed straightened parasphenoid bone in two cavefish populations and curved parasphenoid bone beneath the eye socket in surface fish. In Pachon cavefish, parasphenoid bone is straight and it is raised towards the anterior-dorsal direction relative to the Tinaja, allowing approximately 20˚ ascending angels (Fig. 4.2 E). In Tinaja, the parasphenoid bone is perpendicular to the premaxilla (Fig. 4.2 D). Therefore, we can hypothesize that the absence of a functional eyeball leads to a lack of a

proper eye socket. The lateral view of micro-CT imaging revealed that the absence of an eye orbit in the cavefish population of Pachon and Tinaja moves the underside bone upward and reduces the curvature of the parasphenoid bone. On the contrary, the presence of an eye and the eye orbit in surface fish influences the parasphenoid bone curvature around the eye socket. Further, these findings were validated by the PCA analysis. In general, principal components help to determine which variables are correlated with each component. On the scatter plot (Fig ; 4.3 & 4.4), we used a combination of PC1, PC2, and PC1, PC3 to get a strong separation. According to the correlation values obtained, Pachon and Tinaja clustered as one group, and the surface fish differentiate into a separate group by the shape of the parasphenoid bone. Pachon and Tinaja cavefish are not only morphologically similar, but the literature also reveals that genetically constructive and regressive characteristics are more closely related in Pachon cavefish and Tinaja cavefish [110, 111]. By the area of the neurocranium three populations seem to occupy independent space in the scatter plot. This shows that the area of the neurocranium varies by population, even within cavefish populations.

Eye degeneration in cavefish directly or indirectly affects the determination of the shape of the parasphenoid bone. The morphological difference that we observed in the parasphenoid bone in three different Mexican tetra populations has not been studied thus far. This observed morphology of Pachon cavefish resembles that of the "high arched palate" condition in infants [112]. We suggest the Mexican tetra as a model organism to research the birth defects associated with the high arch palate studies because it has a valeted oral cavity, which is one of the characteristics of CLP [112].

Collectively, this objective of my study sheds light on a previously unknown aspect of Mexican tetra craniofacial growth, which will assist future researchers in developing comparisons based on the primary data we have provided. Furthermore, this study demonstrates how the limited resources in the cave environment affect species evolution and what structural adaptations in the craniofacial region are acquired by cave fishes to survive in the cave environment. Furthermore, the high arched palate observed in Pachon has a morphology that is similar to the high arched palate seen in infants with cleft palate. Understanding the genetic mechanism underlying the development of the high arch palate in Pachon cavefish will aid in the discovery of the mechanisms underlying the development of the high arch in cleft palate condition.

5.5 Ethmoid cartilage defects in zebrafish after exposure to differential chemicals

Zebrafish is an established model in craniofacial developmental biology. The zebrafish ethmoid plate is homologous to the human palate and the zebrafish ethmoid plate is composed of the median and lateral ethmoid plate. Zebrafish ethmoid plate and human palate develop from the bilateral groups of CNCC [51]. Because of these reasons zebrafish is now identified as an excellent model organism particularly for the CP [66].

In order to analyze ethmoid cartilage defects in the treatment of ethanol, Dorsomorphin, and combined, we performed the alcian blue cartilage staining. We chose the period of 10 hpf to 24 hpf for the study because this is the time where NCC migration, development of the neural tube, and organogenesis begins in the developing zebrafish embryo [113, 114]. Zebrafish has several wild-type fish strains. For example AB, EKW (Ekkwill),TU (Tubingen) and etc. According to previous studies, zebrafish exhibit a strain-dependent sensitivity to ethanol [115]. AB strain and EKW (Ekkwill) strain have higher survivability upon ethanol exposure. TU (Tubingen) strain in zebrafish was found to be more vulnerable for ethanol with a remarkably high mortality rate. However, AB larvae exhibit more skeletal defects compared to the EKW strain [115]. Therefore, we chose wild-type AB zebrafish strain to detect ethmoid plate defects in our study.

Exposure of zebrafish to ethanol can induce various defects to the fish body. Further, zebrafish exhibit a dose-dependent sensitivity to ethanol [115]. Exposure to the 1% or 1.5% ethanol dose reduces the overall body size by reducing the body length and width [116, 117]. Reduced body width reduces the distance of the eyes in zebrafish [116]. In this study, we exposed zebrafish to a dose of 1 % ethanol (171 mM) to study defects in ethmoid cartilage [114, 118]. The chondrocytes are well packed and stacked in the median and lateral ethmoid cartilage areas in the control sample (Fig 4.8 E). Alcian blue stain intensity was found to be the same between the median ethmoid and lateral ethmoid regions in control samples. In contrast, with 1% ethanol treated samples we observed a hypo-stain area in the median ethmoid region (Fig 4.8 B & F). Since alcian blue stain binds with sulfated Glycosaminoglycan or glycoproteins reduced stain can result from the less alcian blue binding with the glycoprotein in the cells in the median ethmoid region [119]. Also, studies have reported that ethanol can suppress the amount of CNCC migration from the prosencephalon, mesencephalon, and rhombencephalon areas of the developing neural tube [120]. Reduced cell migration can reduce the cell density and size in the area that develops from the corresponding CNCC as we observed a significant

reduction of height (Fig: 4.3, 4.4, & 4.8) and width (Fig: 4.5, 4.6 & 4.8) of the ethmoid cartilage with ethanol treatment in ANOVA and Tukey's pairwise comparison.

Dorsomorphin has been used as an antagonist for the BMP pathway [121]. Dorsomorphin was found to selectively inhibit the BMP pathway at low concentrations (5 µM). At high concentration (10-20 µM) it inhibits the AMPK signaling and mTOR signaling. Dorsomorphin found to inhibit the BMP 4 - induced phosphorylation in mice [122]. Generally, *bmp* induces the trabeculae and ethmoid plate formation in zebrafish. Furthermore, BMP's are involved in NCC induction, proliferation, cell survival, and differentiation [123]. In our results with the Dorsomorphin treatment, we observed a hypo-stain area in the median ethmoid region as we observed with ethanol treatment (Fig: 4.8 C & G). Further, significant reduction of the size of the ethmoid cartilage with regards to height (Fig: 4.3 & 4.4) and width (Fig: 4.5 & 4.6) was observed. This ethmoid cartilage defect may be caused by inhibition of *bmp 4* signaling following Dorsomorphin treatment.

Since both ethanol and Dorsomorphin act as a suppressor of cell migration and inhibit *bmp 4* signaling, adverse effects on height and width of the ethmoid cartilage could be due to the combined treatments (Fig: 4.8 D & H). Other than that, cell density reduction in the median ethmoid region was observed. This further confirms that exposure to both chemicals resulted in severe defects to the ethmoid cartilage by affecting *bmp 4* expression and CNCC migration. To avoid embryo mortality with the combined treatment of 1 % ethanol and 10 µM Dorsomorphin that I discovered in preliminary studies, the initial concentration of 1 % ethanol and 10 µM Dorsomorphin is diluted to half as the working solution. Further studies are needed to confirm the exact mechanism of *bmp 4* - ethanol on palate development. However, there are ongoing studies on the effect of other cell signaling pathways such as retinoic acid pathway, *wnt* signaling pathway, *shh* pathway and *fgf* signaling in plate development [117] [124-126].

According to the available literature, ethanol treatment is not only found to have an effect on ethmoid cartilage but also on other cranial bones. Among the most ethanol, sensitive structures are the eye, otic capsule, and ethmoid plate. This ethanol-induced craniofacial dysmorphogenesis was found to be mainly the result of increased cell apoptosis, regenerative capacity, and compensated facial primordial growth [127]. Further, in zebrafish after ethanol exposure, malformed body cavity and fin displacement were found [127]. Exposure of histone H4 transcription factor (*hinf*), polo-like kinase 1 (*plk1*), Forkhead box I1 (*foxi1*), and methionyl-tRNA synthetase (*mars*) mutant with ethanol exposure led to reduction of ventral viscerocranium along with microcephaly and microphthalmia [128]. Interestingly, severe

craniofacial defects were identified in the *plk1* mutant zebrafish which exhibit the complete loss of the craniofacial skeleton, localized cell death, and reduced axon projections [129].

Exposure to various other chemicals also can causes defects in the ethmoid cartilage in zebrafish [48, 130]. According to previous studies, exposure to chemicals such as methotrexate, dexamethasone, and chemicals present in the smoke was found to increase these defects. In detail, methotrexate causes the disorderly arrangement of chondrocytes in the ethmoid cartilage. Further, the cell morphology of the chondrocytes was observed to be different [48]. Exposure to dexamethasone showed severe defects of ethmoid cartilage [48]. Hypoxic conditions can occur inside the body by maternal smoking, living at high altitudes, and acardiac tining [130-132]. The PAHs, carbon monoxide (hypoxia), and nicotine are chemicals found in smoke that may increase the hypoxic condition inside the body, which results in severe ethmoid cartilage defects [48]. Further exposure of the ethmoid cartilage to mood stabilizer VAP resulted in shortened ethmoid cartilage [48]. Exposure to 17ß-estradiol resulted in cleft phenotype in the ethmoid cartilage in zebrafish [133].

We identified ethanol and Dorsomorphin individually has an effect on ethmoid cartilage further combination of both chemicals increases the severity. However, molecular analysis such as RNA sequencing is needed to precisely locate the gene alterations after the ethanol exposure. Further performing the above experiment on *bmp 4* knockdown zebrafish will provide further insights into the phenotype induced by *bmp 4*- ethanol interactions.

5.6 Chemical dependent differential expression of *bmp 4*

Different *bmp*s are expressed in different stages of development. The *bmp 4* has been identified as a major regulator for craniofacial shaping [122]. The *bmp 4* is found in the NCC and mesoderm-derived preosteoblast, thereby playing an important role in craniofacial development by maintaining the tissue-tissue interaction [122]. In our study, we exposed 10 hpf zebrafish larvae to the different treatments. In the segmentation period (10-24 hpf) and the *bmp 4* expression was determined in the hatching stage of 48 hpf (Fig. 4.11). The *bmp 4* expression has been observed in the frontonasal maxillary NCC and oral ectoderm in the 36 hpf to 44 hpf by Swartz *et* al,2011. This study revealed that the expression of *bmp 4* was reduced by 48 hpf in maxillary NCC [42]. But in our samples, we confirmed the expression of the *bmp 4* at 48 hpf in maxillary NCC and oral ectoderm (Fig. 4.11). In addition, we discovered the reduction of *bmp 4* expression in maxillary NCC and oral ectoderm upon 1% ethanol treatment and combined treatment of 1% ethanol and Dorsomorphin using the digoxigenin-labeled antisense RNA probes (Fig. 4.11). As previously mentioned, ethanol acts as a

suppressor for NCC migration and it increases cell apoptosis [93]. This might have resulted in the reduced expression of *bmp 4* in the area of maxillary CNCC and oral ectoderm [134].

We did not observe a reduction in *bmp 4* in the developing palatal region after Dorsomorphin treatment at 48 hpf. However, alcian blue staining and statistical data revealed a substantial reduction in ethmoid cartilage height and width, as well as a hypo-stained area of the medial ethmoid region. As a result, we can infer that Dorsomorphin has an effect on the ethmoid plate, but the observed *bmp 4* expression in the developing palatal region may be due to an error in the experiment.

The development of the palate is not only directly regulated by *bmp 4*, but by the regulatory gene network. Transforming Growth Factor β (TGFβ) was reported as an impactful genetic factor for the CLP [135]. During palatogenesis, the anterior palate in mice expresses the genes *Bmp 4, Msx 1, Bmp 2, Fgf 10,* and *Shox 2.* In addition, maxillary and mandibular posterior processes express the *Osr 1, Lhx 6, Lhx 8*, and *Tbx 22.* A remarkable similarity was observed regarding these genes in zebrafish ethmoid plate development and mouse palate development [42]. IRF6, MSX2, ABCA4, FOXE1, FGFR1, FGFR2, FGF8, MAFB, PDGFC, TBX10, CRISPLD2, PVRL1, GABRB3, SATB2, GLI2, JAG2, MTHFR, RARA, SKI, and SPRY2 genes identified as other candidate genes in cleft formation. In these regulatory loops, the alteration of at least one gene may result in altered gene expression [42]. In addition, it influences the regulation of the other genes that are mixed. It is therefore essential to research how *bmp 4* and the gene network operate on exposure to ethanol and Dorsomorphin. This will have a clearer explanation of the fact that we can compare our data with human CLP defects in humans.

This study highlighted the effect of ethanol, inhibition of *bmp 4* on plate development, and the combined effect of both chemicals on zebrafish palate development. This is the first study to show that combining the effects of ethanol and a *bmp 4* inhibitor can increase the severity. This research will contribute to a better understanding of the complex etiopathogenesis of cleft palate development by introducing ethanol-*bmp 4* interaction.

CHAPTER 6: CONCLUSION

Conclusion

Collectively, results from my thesis suggest that the Mexican tetra cavefish and surface fish is similar to the zebrafish in bone development, articulation, and ossification with certain exceptions. Among Mexican tetra cavefish and surface fish have different bone remodeling activities as an adaptation for their habitat. Further, both surface and cavefish have a direct or indirect effect on the development of bones in the cranial region. Parasphenoid bone, which makes the mid-ventral surface of the neurocranium, shows the shape difference in surface fish and cavefish population. The curved shape of parasphenoid bone in surface fish can be affected by the eye orbit and the straight bone in cavefish can be explained by the degeneration of the eye orbit in the absence of the eye. In addition, the limited resources in the cave environment and or as an adaptation to the constant darkness in the cave environment can cause these types and bone differences in cavefish.

Zebrafish ethmoid cartilage was affected by ethanol, Dorsomorphin, and combined treatment. Severe ethmoid cartilage defects observed upon the combined treatment resulted from the interaction of ethanol with *bmp 4.* The combined treatment has an effect on the shape and size of zebrafish ethmoid cartilage. Ethanol interactions have reduced the expression of *bmp 4* in maxillary CNCC and oral ectoderm. This indicates that the association of *bmp 4* gene-ethanol in zebrafish may have an effect on ethmoid plate formation. This will shed light on the increased occurrence of CLP in the prenatal stages after exposure to ethanol.

CHAPTER 7: APPENDIX

Appendix 1

Alizarin red bone staining

Day 1

- If the fish in 70% Ethanol

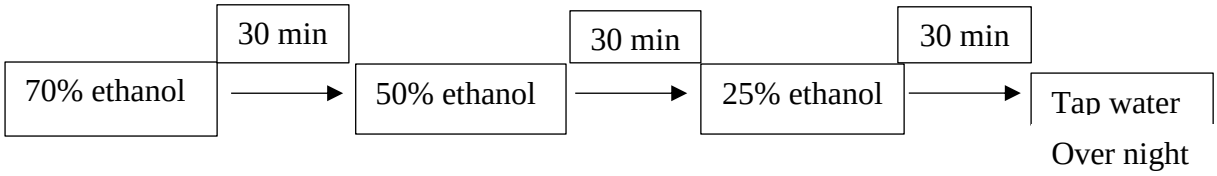

- If the fish in PBS

PBS ⟶ Tap water

1. Take fish out of water. Remove scales, gut contents wings blade & forceps

2. Bleaching

1% KOH + 3% H_2O_2

20 ml 1 ml

We put KOH as it enhance the stain absorption

Put the samples in 1% KOH + 3% h

We put KOH as it enhance the stain absorption

Put the samples in 1% KOH + 3% H_2O_2, keep them over night or eyes are coffee brown

1% KOH + 3% H_2O_2 overnight room temperature

Day 2

3. Remove the bleach solution

4. Rinse with the tap water

- Keep it in tap water 30 min.

5. Transfer to saturated Sodium Tetra borate (Saturated borax) overnight in room T

Day 4

6. Alizarin red stain on 1% KOH recipe

1% KOH – 20 ml

Alizarin red – 20 mg

7. Take sample out of Sodium Tetra borate (put the borax back to the container, It can reuse)

Put the fish to Alizarin red solution & keep over night at room temperature

Day 5

8. Rinse the sample in tap water. We have to make trypsin borax solution

1% Trypsin

2% Sodium tetra borate

Make with the distilled water

9. Keep in the trypsin / borax solution for three nights at room temperature

Day 8

10. After three nights if the soft tissue still there transfer to 37°C incubator for 2 hours

Day 9

11. Remove samples from trypsin borax. Discard the solution to sink.

12. Change to 20% Glycerol 80%, 1% KOH over night at room temperature.

Day 10

13. 100% Glycerol, room temperature for store & it clears more.

Appendix 2

Alcian Blue Staining of Cartilage (Modified by Nuwanthika)

1. Larvae fix in 3.7% neutral buffered formaldehyde at room temperature for several hours to overnight. Care should be taken not to over fix the preparation.
2. Wash the larvae 5 times with PBT for 5 min for each wash.
   - (PBT: PBS, 0.1% Tween-20)
3. Transfer into a 0.1% solution of Alcian blue for 8 hours to overnight.
   - (0.1% Alcian blue solution: 0.1% Alcian blue, 80% ethanol and 20% glacial acetic acid., Alcian solution should be syringe filtered)
4. Rinse larvae in ethanol and rehydrate gradually in to PBS. Use ethanol PBT solutions of 70%-30%, 50%-50%, and 30%-70% respectively.
5. Remove pigmentation by bleaching in bleach solution for 1 to 3 hours. Leave the tube cap open. This reaction should be monitored carefully and stopped once eye pigmentation has cleared. Bubbles may form within the embryo during clearing but will disappear in subsequent steps.
   - (Bleach solution, 3% Hydrogen peroxide, 1% potassium hydroxide.)
6. Clear tissue in trypsin solution for 1 to 2 hours at room temperature. Time taken for this step can be vary according to the density of the sample. Monitor tissue clearing closely. Stop the trypsin digestion once the brain tissue has cleared.
   - (Trypsin solution: 0.05% trypsin dissolved in PBS)
7. Transfer larvae into glycerol, gradually though a series of 30% and 50% dilution in PBS, and store in 70% glycerol.

Appendix 3

DIG High Prime DNA Labeling and Detection protocol

1. Make sure that oven is on and preheated to 120 ˚C
2. Cut out the membrane big enough to fit in the Petri dish. Cut a wedge out of one corner in order to indicate the top left corner.
3. Apply a 1 µl of your labeled probe and labeled control probe to the nylon membrane
4. Fix the nucleic acid by baking for 30 minutes at 120˚C in a sterile glass petri dish.
5. Transfer membrane into the plastic dish (sterile) with 10 ml of Maleic acid buffer (approx. ½ the depth of the dish, enough to cover the membrane). Incubate (20˚C) with shaking (40 RPM) for 2 min.
6. Incubate (20˚C) for 20 minutes in Blocking solution with shaking 40 RPM.
   Prepare antibody solution.
7. Wash for 5 minutes with TBST. Incubate (20˚C) with shaking (40 RPM)
8. Incubate (20˚C) with 10 ml Antibody solution for 30 minutes with shaking (40 RPM)
9. Wash with washing buffer. Incubate (20˚C) with shaking (40 RPM). Carry this out twice for 15 minutes each, the second time with fresh washing buffer, save the antibody solution
10. Prepare the color solution during the second wash above.
11. Equilibrate for 5 minutes in the Detection buffer. Incubate (20˚C) with shaking (40 RPM)
12. Incubated at room temperature in a dark drawer (due to light sensitivity) in 10 ml of substrate solution. No shaking. Check approximately every 2 minutes for any color change.

Appendix 4

Whole-Mount in situ Hybridization Protocol /

Important considerations before starting

- ✓ All solutions should be made with DEPC H_2O unless otherwise stated in protocol
- ✓ Gloves should be worn at all times to reduce contamination
- ✓ Countertop work surface should be RNAase zapped to reduce contamination before use
- ✓ All plastic containers/tubes should be DNAase/RNAase free
- ✓ Autoclaved pipette tips and Gilson Pipettes are to be used

Prep Day (Collection of embryo's and fish) (Approx. 2 hours + Overnights)

- Collect Embryos
  - □ Dechorinate 24 and 48 hpf embryos. For older embryos – anesthetize in .1% MS222.
  - □ Fix in 4% PFA (RNAase free) for 2 hours at room temperature or overnight at 4^{o}C.

- Dehydrate in series
  - □ 25% MeOH in PBS — 30 min at RT — 1x
  - □ 50% MeOH in PBS — 30 min at RT — 1x
  - □ 75% MeOH in PBS — 30 min at RT — 1x
  - □ 100% MeOH — At Least Overnight — Store in -20^{o}C

- Notes
  - □ MS222 is a powder that should be made into 0.01% and 0.1% solutions fresh for each day.
  - □ PFA is found in the -20^{o}C freezer

Day 1: Bleach Day (Approx. 1.5 hours, longer if older fish)

- Rehydrate embryos
  - □ 75% MeOH in PBS — 5 min at RT — 1x
  - □ 50% MeOH in PBS — 5 min at RT — 1x

- □ 25% MeOH in PBS 5 min at RT 1x

- Wash
  - □ PBST 5 min at RT 1x

- Bleach
  - □ Bleach according to times below, or until the embryo is a creamy white. Ensure eyes do not become bulgy.
  - □ General timeline for fish

Age	Approx. Bleach Time
24 hpf	10 min
48 hpf	25 min
72 hpf	40 min
5 dpf	50 min
6.7 mm	1 h 15 min
8.0 mm	1 h 30 min

  - □ Bleach Recipe – Make Fresh on the day

Total Amount	5 ml	Total Amount	20 ml
KOH (.5%)	0.025 g	KOH (.5%)	.1050G
H_2O_2 (3% of 30%)	150 ul	H_2O_2 (3% of 30%)	600 ul
DepC H_2O	To 5 ml	DepC H_2O	To 20 ml

- Wash
  - □ PBS 5 min at RT 1x
    - Note: Embryos can be very sticky in PBS/MeOH solutions

- Dehydrate in series
  - □ 25% MeOH in PBS 5 min at RT 1x
  - □ 50% MeOH in PBS 5 min at RT 1x
  - □ 75% MeOH in PBS 5 min at RT 1x

- □ Transfer into new 1.5 ml eppendorff tube
- □ 100% MeOH Store in -20° C Overnight

✓ Embryos can now be stored in 100% MeOH at -20° C for several weeks or at minimum of 2 hours before continuing on

Day 2: Pro-K and Treatment Day (Approximately 5 hours, longer if older fish)

- Rehydrate embryos in 1.5 ml eppendorf tubes
  - □ 75% MeOH in PBS 5 min at RT 1x
  - □ 50% MeOH in PBS 5 min at RT 1x
  - □ 25% MeOH in PBS 5 min at RT 1x

- Wash
  - □ PBST 5 min at RT 4x

- Permeabilize: With Proteinase K (10 ug/ml in DepC)
  - □ If using a 10 mg/ml stock, dilute by adding 1 ul of stock solution to 1000 ul of DepC H_2O

    Note: Pro-K in lower part of -20°C

Age	Approx. Pro-K Time
24 hpf	10 min
48 hpf	23 min
72 hpf	30 min
5 dpf	42 min
6.7 mm	1 h
8.0 mm	1 h 15 min

- Wash
  - □ PBST 5 min at RT 2x

- Fix (In fume hood)

□ 4% PFA (DepC Treated) 20 min at RT 1x

Note: PFA is found in the -20°C freezer

- Wash
  - □ PBST 5 min at RT 2x
- Treat (In fume hood) – Make fresh on the day
  - □ Acetic Anhydride 30 min at RT 1x

Acetic Anhydride Recipe	6 ml Batch
DepC Water	4.5 ml
Triethanolamamine (upstairs lab cabinet)	79.9 ul
pH to 7.0	
DepC Water	To 6 ml
Acidic anhydride (under fume hood)	15 ul

- Wash
  - □ PBST 10min at RT 2x
- Prehybridize
  - □ Hyb (-) 2 hours at 70°C/35 rpm

    Note: See last page for Hyb (-) recipe. There should be a premade stock in the -20°C at all times.

✓ **<u>Stop Point:</u>** Embryos can be stored in Hyb (-) for several weeks, or you can continue to the next step.

Continuing on or starting a new run

Note: If embryo's have been processed into Hyb (-) and stored, this is a good place to start a new in situ run. It allows you to effectively process many fish, and then run different genes on fewer numbers.

Day (1/3): Hyb (+) – Adding the probe (Approx. 2 hours)

- Pre Hyb (-)
  - □ Hyb (-) 2 hours at 70^{o}C/35rpm

  Note: We re-do this stage to ensure the embryos are at the same permeability /solubility as previous

- Adding Hyb (+)

  □ Add 1 ml of Hyb (+) to each sample

Hyb (+) Recipe	Per tube (1 ml)	For 4 ml
Hyb (-)	890 ul	3560 ul
Yeast tRNA (5 mg/ml)	100 ul of 50 mg/ml stock	400 ul
Heparin (50 ug/ml)	10 ul of 5 mg/ml stock	40 ul
pH to 6.0 with Citric Acid	9.2 ul of 1 M citric acid	36.8 ul

Note: Multiply each reagent by the number of samples you have.

- Adding probe
  - □ Add 2-3 ul of probe (depending on strength) to each of the sample tubes.

  - □ Notes
    - Probe should not be left out of the freezer long. Putting them on ice is recommended.

- Ensure probe is mixed – flick with finger and centrifuge liquid back down for 2-3 seconds.
- If using Fast Red probes – ensure samples are not exposed to light. Cover using tinfoil.

- Incubate overnight at 70°C/35rpm

Day (2/4): Washes and Antibody (Approx. 7 hours, with 3-4 hour break in middle)

- Washes
  - □ 75% Hyb (-) + 25% 2xSSC 15 min at 70°C/35 rpm 1x
  - □ 50% Hyb (-) + 50% 2xSSC 15 min at 70°C/35 rpm 1x
  - □ 25% Hyb (-) + 75% 2xSSC 15 min at 70°C/35 rpm 1x

    Note: These solutions should be premade and stored in the -20°C freezer

  - □ Change to fresh eppendorf tubes – Hyb (-) is very slippery and the tube caps tend not to stay in place at this point. The tubes will also likely have white precipitate throughout.

    Note: Going into this next stage – Embryos can become very sticky! Check pipette tip after each changeover!

  - □ 2xSSC 10 min at 70°C/35rpm 2x
  - □ 0.2xSSC 30 min at 70°C/35rpm 3x

  - □ Start sheep serum inactivation 30 min at 60°C
    (amount based on Blocking Buffer Recipe)

  - □ 75% 0.2xSSC + 25% PBST 10 min at Room temp/60 rpm 1x
  - □ 50% 0.2xSSC + 50% PBST 10 min at Room temp/60 rpm 1x
  - □ 25% 0.2xSSC + 75% PBST 10 min at Room temp/60 rpm 1x
  - □ 100% PBST 10 min at Room temp/60 rpm 1x

- Incubate in blocking buffer for 3-4 hours
    - □ Add 1 ml of Blocking buffer to each tube

Make Fresh on the day

Blocking Buffer recipe	1 ml/Sample	For 4 ml
1 x PBST	980 ul	3920 ul
2% Heat inactivated Sheep serum	20 ul	80 ul
Bovine serum albumin (2 mg/ml)	0.002 g	0.008 g

Note: Save at least 10 ul of blocking buffer. It is required in making the antibody recipe.

- Adding antibody

Antibody Recipe	
Blocking Buffer (saved from before)	9 ul
Anti-Dig Antibody	1 ul
Optional – Fish powder	A few pieces

- □ Allow antibody to sit in blocking buffer for at least 10 minutes before adding the antibody solution to the samples. This allows pre absorption to occur, and reduces background.
- □ Add 1 ul of above antibody recipe to each sample tube already containing the 1 ml of blocking buffer from 4-5 hours prior.

- Incubate overnight at 4^{o}C while shaking
    - □ Note: The incubator in the lower lab works well for this. Ensure the incubator is properly set and on early in the day, as it takes time to cool down.
    - □ The small “Mandel” shaker works well for this stage.

Day (3/5): Antibody and Color Reaction (Approx. 4 hours then overnight)

- Remove samples from incubator and discard antibody solution

- Washes
  - □ PBST 5 min at RT

  - □ PBST 15 min at RT on same "Mandel" Shaker 12x

- Place embryo's in sterile glass vials – Ensure proper labeling

- Incubate TRIS Staining Buffer
  - □ Add 1 ml of TRIS Staining Buffer to each sample 5 min at room temp 3x

  - □ Make Fresh on the day

Reagent	Stock	Final	20 ml Batch	10 ml Batch
TRIS pH 9.0	1 M	100 mM	2 ml	1 ml
$MgCl_2$	1 M	50 mM	1 ml	0.5 ml
NaCl	5 M	100 mM	400 ul	200 ul
Tween	10%	0.1%	20 ul	10 ul
Levamisole		2 mM	0.019 g	0.0095 g
DepC H_2O			To 20 ml	To 10 ml

Note: When determining batch size, allow for three change-over's per tube as well as enough for mixing NBT/BCIP staining solution

- Add Color Reaction Solution

NBT/BCIP Staining Solution	Amount needed per single sample	Amount for 4 tubes
TRIS staining buffer (from above)	1.2 ml	4.8 ml
BCIP	4.25 ul	17 ul
NBT	3.03 ul	12.12 ul

- □ **Very Important**! – Ensure staining solution remaining in dark. It is a light sensitive reagent.

- Remove TRIS staining buffer and Add Color Reaction Solution
  - □ Approximately 1.2 ml per sample
  - □ Place samples in incubator at 4^{o}C overnight or at 37^{o}C until expression shows.
    - Best results have been attained at 4^{o}C overnight

Day (4/6): Stopping Color Reaction (Approx. 2 hours)

- Wash
  - □ PBST 5 min at Room Temperature 6x

- Fix (in fume hood)
  - □ 4% PFA 20 mins at room temperature 1x

- Dehydrate (for NBT/BCIP Color reactions only!) – Skip to below for Fast Red
  - □ 25% MeOH in PBS 10 min at RT 1x
  - □ 50% MeOH in PBS 10 min at RT 1x
  - □ 75% MeOH in PBS 10 min at RT 1x
  - ✓ 100% MeOH Store in 4^{o}C in sample box

    Note: Photo's should be taken while sample is in 25% or 50% MeOH/PBS

Reagent Recipes

Hyb (-)

Reagent	% in final solution	50 ml Batch	250 ml Batch (ideal)
Deionized Formamide 100%	50	25 ml	125 ml
SSC 20x	5x	12.5 ml	62.5 ml
Tween 10% (stock solution)	0.1	50 ul	250 ul
DepC Water		Top to 50 ml	Top to 250 ml

Note: Make in fume hood. Ensure contents are well mixed. Aliquot into 50 ml flacon tube and store in -20^{o}C.

PBS

Reagent for 500 ml Batch	
NaCl	4.0 g
KCl	0.1 g
Na_2PO_4	0.693 g
KH_2PO_4	0.1 g
Top to 500 ml with DepC H_2O	
pH to 7	

To make PBST add 50 ul of Tween-10 to 50 ml of PBS

DepC H_2O

- ✓ Per 1 L of water add 100 ul of DepC (found in upstairs fridge).
- ✓ Carry out in fume hood.
- ✓ Shake for 30 minutes vigorously.
- ✓ Autoclave

CHAPTER 8: REFERENCE

REFERENCE

1. Kuratani, S., *The neural crest and origin of the neurocranium in vertebrates.* Genesis, 2018. **56**(6-7): p. e23213.
2. Cubbage, C.C. and P.M. Mabee, *Development of the cranium and paired fins in the zebrafish Danio rerio (Ostariophysi, Cyprinidae).* J Morphol, 1996. **229**(2): p. 121-160.
3. Helwany, M. and M. Rathee, *Anatomy, Head and Neck, Palate*, in *StatPearls [Internet]*. 2020, StatPearls Publishing.
4. Li, J., et al., *Regulatory Mechanisms of Soft Palate Development and Malformations.* J Dent Res, 2019. **98**(9): p. 959-967.
5. Hourfar, J., et al., *Three dimensional anatomical exploration of the anterior hard palate at the level of the third ruga for the placement of mini-implants--a cone-beam CT study.* Eur J Orthod, 2015. **37**(6): p. 589-95.
6. Abramyan, J. and J.M. Richman, *Recent insights into the morphological diversity in the amniote primary and secondary palates.* Dev Dyn, 2015. **244**(12): p. 1457-68.
7. Richman, J.M., M. Buchtová, and J.C. Boughner, *Comparative ontogeny and phylogeny of the upper jaw skeleton in amniotes.* Dev Dyn, 2006. **235**(5): p. 1230-43.
8. Volff, J.N., *Genome evolution and biodiversity in teleost fish.* Heredity (Edinb), 2005. **94**(3): p. 280-94.
9. Krishnan, J. and N. Rohner, *Cavefish and the basis for eye loss.* Philos Trans R Soc Lond B Biol Sci, 2017. **372**(1713).
10. Gregory, W.K., *Fish skullsa study of the evolution of natural mechanisms*. 1933.
11. Cooney, C.R., et al., *Mega-evolutionary dynamics of the adaptive radiation of birds.* Nature, 2017. **542**(7641): p. 344-347.
12. Jeffery, W.R., *Chapter 8. Evolution and development in the cavefish Astyanax.* Curr Top Dev Biol, 2009. **86**: p. 191-221.
13. Gross, J.B. and A.K. Powers, *A Natural Animal Model System of Craniofacial Anomalies: The Blind Mexican Cavefish.* Anat Rec (Hoboken), 2020. **303**(1): p. 24-29.
14. Heuzé, Y., et al., *Developmental and Evolutionary Significance of the Zygomatic Bone.* Anat Rec (Hoboken), 2016. **299**(12): p. 1616-1630.
15. Goudy, S., et al., *Conductive hearing loss and otopathology in cleft palate patients.* Otolaryngol Head Neck Surg, 2006. **134**(6): p. 946-8.
16. DeRoo, L.A., et al., *First-trimester maternal alcohol consumption and the risk of infant oral clefts in Norway: a population-based case-control study.* Am J Epidemiol, 2008. **168**(6): p. 638-46.
17. Atkins, J.B. and T.A. Franz-Odendaal, *The evolutionary and morphological history of the parasphenoid bone in vertebrates.* Acta Zoologica, 2016. **97**(2): p. 255-263.

18. Schoch, R.R., *Amphibian skull evolution: the developmental and functional context of simplification, bone loss and heterotopy.* J Exp Zool B Mol Dev Evol, 2014. **322**(8): p. 619-30.
19. Kuratani, S., Y. Oisi, and K.G. Ota, *Evolution of the vertebrate cranium: viewed from hagfish developmental studies.* Zoological science, 2016. **33**(3): p. 229-238.
20. Kuratani, S., Y. Oisi, and K.G. Ota, *Evolution of the Vertebrate Cranium: Viewed from Hagfish Developmental Studies.* Zoolog Sci, 2016. **33**(3): p. 229-38.
21. Ahi, E.P., *Signalling pathways in trophic skeletal development and morphogenesis: Insights from studies on teleost fish.* Dev Biol, 2016. **420**(1): p. 11-31.
22. Atukorala, A.D.S. and R.K. Ratnayake, *Cellular and molecular mechanisms in the development of a cleft lip and/or cleft palate; insights from zebrafish (Danio rerio).* The Anatomical Record, 2020.
23. Harris, M., et al., *Fish is Fish: the use of experimental model species to reveal causes of skeletal diversity in evolution and disease.* Journal of Applied Ichthyology, 2014. **30**(4): p. 616-629.
24. Machado, R.G. and B.F. Eames, *Using zebrafish to test the genetic basis of human craniofacial diseases.* Journal of Dental Research, 2017. **96**(11): p. 1192-1199.
25. Jeffery, W.R., *Cavefish as a model system in evolutionary developmental biology.* Dev Biol, 2001. **231**(1): p. 1-12.
26. Jeffery, W.R., *Emerging model systems in evo-devo: cavefish and microevolution of development.* Evol Dev, 2008. **10**(3): p. 265-72.
27. Atukorala, A.D.S. and T.A. Franz-Odendaal, *Genetic linkage between altered tooth and eye development in lens-ablated Astyanax mexicanus.* Developmental biology, 2018. **441**(2): p. 235-241.
28. Kowalko, J., *Utilizing the blind cavefish Astyanax mexicanus to understand the genetic basis of behavioral evolution.* J Exp Biol, 2020. **223**(Pt Suppl 1).
29. Bradic, M., et al., *Gene flow and population structure in the Mexican blind cavefish complex (Astyanax mexicanus).* BMC Evol Biol, 2012. **12**: p. 9.
30. Hambli, R., *Connecting mechanics and bone cell activities in the bone remodeling process: an integrated finite element modeling.* Front Bioeng Biotechnol, 2014. **2**: p. 6.
31. McGaugh, S.E., et al., *The cavefish genome reveals candidate genes for eye loss.* Nat Commun, 2014. **5**: p. 5307.
32. Powers, A.K., et al., *Facial bone fragmentation in blind cavefish arises through two unusual ossification processes.* Sci Rep, 2018. **8**(1): p. 7015.
33. Powers, A.K., et al., *Cranial asymmetry arises later in the life history of the blind Mexican cavefish, Astyanax mexicanus.* PLoS One, 2017. **12**(5): p. e0177419.

34. Atukorala, A.D.S., V. Bhatia, and R. Ratnayake, *Craniofacial skeleton of MEXICAN tetra (Astyanax mexicanus): As a bone disease model.* Dev Dyn, 2019. **248**(2): p. 153-161.
35. Fernandes, V.F.L., et al., *Evolution of the developmental plasticity and a coupling between left mechanosensory neuromasts and an adaptive foraging behavior.* Dev Biol, 2018. **441**(2): p. 262-271.
36. Casane, D. and S. Rétaux, *Evolutionary Genetics of the Cavefish Astyanax mexicanus.* Adv Genet, 2016. **95**: p. 117-59.
37. Veldman, M.B. and S. Lin, *Zebrafish as a developmental model organism for pediatric research.* Pediatr Res, 2008. **64**(5): p. 470-6.
38. Howe, K., et al., *The zebrafish reference genome sequence and its relationship to the human genome.* Nature, 2013. **496**(7446): p. 498-503.
39. Abbate, F., et al., *The oral cavity of the adult zebrafish (Danio rerio).* Anat Histol Embryol, 2006. **35**(5): p. 299-304.
40. Bruneel, B., et al., *Imaging the zebrafish dentition: from traditional approaches to emerging technologies.* Zebrafish, 2015. **12**(1): p. 1-10.
41. Curtin, E., et al., *Zebrafish wnt9a is expressed in pharyngeal ectoderm and is required for palate and lower jaw development.* Mechanisms of development, 2011. **128**(1-2): p. 104-115.
42. Swartz, M.E., et al., *Examination of a palatogenic gene program in zebrafish.* Dev Dyn, 2011. **240**(9): p. 2204-20.
43. Chiquet, B.T., et al., *Knockdown of Crispld2 in zebrafish identifies a novel network for nonsyndromic cleft lip with or without cleft palate candidate genes.* European Journal of Human Genetics, 2018. **26**(10): p. 1441-1450.
44. Schilling, T.F. and C.B. Kimmel, *Musculoskeletal patterning in the pharyngeal segments of the zebrafish embryo.* Development, 1997. **124**(15): p. 2945-60.
45. Atukorala, A.D.S. and R.K. Ratnayake, *Cellular and molecular mechanisms in the development of a cleft lip and/or cleft palate; insights from zebrafish (Danio rerio).* Anat Rec (Hoboken), 2020.
46. Mork, L. and G. Crump, *Zebrafish Craniofacial Development: A Window into Early Patterning.* Curr Top Dev Biol, 2015. **115**: p. 235-69.
47. Dougherty, M., et al., *Distinct requirements for wnt9a and irf6 in extension and integration mechanisms during zebrafish palate morphogenesis.* Development, 2013. **140**(1): p. 76-81.
48. Raterman, S.T., et al., *Zebrafish Models of Craniofacial Malformations: Interactions of Environmental Factors.* Front Cell Dev Biol, 2020. **8**: p. 600926.
49. Kague, E., et al., *Skeletogenic fate of zebrafish cranial and trunk neural crest.* PLoS One, 2012. **7**(11): p. e47394.
50. Smith, T.M., et al., *Molecular signaling along the anterior-posterior axis of early palate development.* Front Physiol, 2012. **3**: p. 488.

51. Bush, J.O. and R. Jiang, *Palatogenesis: morphogenetic and molecular mechanisms of secondary palate development.* Development, 2012. **139**(2): p. 231-43.
52. Acs, N., et al., *Maternal influenza during pregnancy and risk of congenital abnormalities in offspring.* Birth Defects Res A Clin Mol Teratol, 2005. **73**(12): p. 989-96.
53. Jalali, A., et al., *Induction of palate epithelial mesenchymal transition by transforming growth factor β3 signaling.* Dev Growth Differ, 2012. **54**(6): p. 633-48.
54. Shu, X., Z. Dong, and S. Shu, *AMBRA1-mediated autophagy and apoptosis associated with an epithelial-mesenchymal transition in the development of cleft palate induced by all-trans retinoic acid.* Ann Transl Med, 2019. **7**(7): p. 128.
55. Yılmaz, H.N., E.Ö. Özbilen, and T. Üstün, *The Prevalence of Cleft Lip and Palate Patients: A Single-Center Experience for 17 Years.* Turkish Journal of Orthodontics, 2019. **32**(3): p. 139.
56. Saad, A.N., et al., *Incidence of oral clefts among different ethnicities in the state of California.* Annals of plastic surgery, 2014. **72**: p. S81-S83.
57. Martín-Del-Campo, M., R. Rosales-Ibañez, and L. Rojo, *Biomaterials for Cleft Lip and Palate Regeneration.* Int J Mol Sci, 2019. **20**(9).
58. Ghassibe-Sabbagh, M., et al., *FAF1, a gene that is disrupted in cleft palate and has conserved function in zebrafish.* Am J Hum Genet, 2011. **88**(2): p. 150-61.
59. Ke, C.Y., et al., *IRF6 and TAK1 coordinately promote the activation of HIPK2 to stimulate apoptosis during palate fusion.* Sci Signal, 2019. **12**(593).
60. Wong, F.K. and U. Hagg, *An update on the aetiology of orofacial clefts.* Hong Kong Med J, 2004. **10**(5): p. 331-6.
61. Wu, T., et al., *Evidence of gene–environment interaction for the IRF6 gene and maternal multivitamin supplementation in controlling the risk of cleft lip with/without cleft palate.* Human genetics, 2010. **128**(4): p. 401-410.
62. Martínez-Sanz, E., et al., *Alteration of medial-edge epithelium cell adhesion in two Tgf-beta3 null mouse strains.* Differentiation, 2008. **76**(4): p. 417-30.
63. Graf, D., et al., *Common mechanisms in development and disease: BMP signaling in craniofacial development.* Cytokine Growth Factor Rev, 2016. **27**: p. 129-39.
64. Loffredo, L.C., et al., *Oral clefts and vitamin supplementation.* Cleft Palate Craniofac J, 2001. **38**(1): p. 76-83.
65. Park-Wyllie, L., et al., *Birth defects after maternal exposure to corticosteroids: prospective cohort study and meta-analysis of epidemiological studies.* Teratology, 2000. **62**(6): p. 385-92.
66. Duncan, K.M., et al., *Zebrafish models of orofacial clefts.* Dev Dyn, 2017. **246**(11): p. 897-914.

67. Ornoy, A. and Z. Ergaz, *Alcohol abuse in pregnant women: effects on the fetus and newborn, mode of action and maternal treatment.* Int J Environ Res Public Health, 2010. **7**(2): p. 364-79.
68. Zhou, F.C., et al., *Alteration of gene expression by alcohol exposure at early neurulation.* BMC genomics, 2011. **12**(1): p. 124.
69. Burd, L., J. Blair, and K. Dropps, *Prenatal alcohol exposure, blood alcohol concentrations and alcohol elimination rates for the mother, fetus and newborn.* J Perinatol, 2012. **32**(9): p. 652-9.
70. Gemma, S., S. Vichi, and E. Testai, *Metabolic and genetic factors contributing to alcohol induced effects and fetal alcohol syndrome.* Neuroscience & Biobehavioral Reviews, 2007. **31**(2): p. 221-229.
71. Lowery, J.W. and V. Rosen, *The BMP Pathway and Its Inhibitors in the Skeleton.* Physiol Rev, 2018. **98**(4): p. 2431-2452.
72. Ducy, P. and G. Karsenty, *The family of bone morphogenetic proteins.* Kidney Int, 2000. **57**(6): p. 2207-14.
73. Parada, C. and Y. Chai, *Roles of BMP signaling pathway in lip and palate development.* Front Oral Biol, 2012. **16**: p. 60-70.
74. Antebi, Y.E., et al., *Combinatorial Signal Perception in the BMP Pathway.* Cell, 2017. **170**(6): p. 1184-1196.e24.
75. Chen, D., M. Zhao, and G.R. Mundy, *Bone morphogenetic proteins.* Growth Factors, 2004. **22**(4): p. 233-41.
76. Baek, J.-A., et al., *Bmpr1a signaling plays critical roles in palatal shelf growth and palatal bone formation.* Developmental biology, 2011. **350**(2): p. 520-531.
77. Nie, X.G., *Differential expression of Bmp2, Bmp4 and Bmp3 in embryonic development of mouse anterior and posterior palate.* Chin Med J (Engl), 2005. **118**(20): p. 1710-6.
78. Lee, J.M., et al., *Modulation of cell proliferation during palatogenesis by the interplay between Tbx3 and Bmp4.* Cell Tissue Res, 2007. **327**(2): p. 285-92.
79. Thomason, H.A., M.J. Dixon, and J. Dixon, *Facial clefting in Tp63 deficient mice results from altered Bmp4, Fgf8 and Shh signaling.* Dev Biol, 2008. **321**(1): p. 273-82.
80. He, F., et al., *Wnt5a regulates directional cell migration and cell proliferation via Ror2-mediated noncanonical pathway in mammalian palate development.* Development, 2008. **135**(23): p. 3871-9.
81. Paul, B.Y., et al., *Dorsomorphin inhibits BMP signals required for embryogenesis and iron metabolism.* Nature chemical biology, 2008. **4**(1): p. 33-41.
82. Lovely, C.B., et al., *Bmp signaling mediates endoderm pouch morphogenesis by regulating Fgf signaling in zebrafish.* Development, 2016. **143**(11): p. 2000-11.

83. Javidan, Y. and T.F. Schilling, *Development of cartilage and bone.* Methods Cell Biol, 2004. **76**: p. 415-36.
84. Edsall, S.C. and T.A. Franz-Odendaal, *A quick whole-mount staining protocol for bone deposition and resorption.* Zebrafish, 2010. **7**(3): p. 275-80.
85. Walker, M.B. and C.B. Kimmel, *A two-color acid-free cartilage and bone stain for zebrafish larvae.* Biotech Histochem, 2007. **82**(1): p. 23-8.
86. Thisse, B. and C. Thisse, *In situ hybridization on whole-mount zebrafish embryos and young larvae.* Methods Mol Biol, 2014. **1211**: p. 53-67.
87. Wada, N., et al., *Hedgehog signaling is required for cranial neural crest morphogenesis and chondrogenesis at the midline in the zebrafish skull.* Development, 2005. **132**(17): p. 3977-3988.
88. Yu, T., et al., *Stem Cells in Tooth Development, Growth, Repair, and Regeneration.* Curr Top Dev Biol, 2015. **115**: p. 187-212.
89. Le Lièvre, C.S., *Participation of neural crest-derived cells in the genesis of the skull in birds.* Development, 1978. **47**(1): p. 17-37.
90. Cubbage, C.C. and P.M. Mabee, *Development of the cranium and paired fins in the zebrafish Danio rerio (Ostariophysi, Cyprinidae).* Journal of Morphology, 1996. **229**(2): p. 121-160.
91. BR, O., *Reginato AM. Wang W. Bone development.* Annu Rev Cell Dev Biol, 2000. **16**: p. 191-220.
92. Weigele, J. and T.A. Franz-Odendaal, *Functional bone histology of zebrafish reveals two types of endochondral ossification, different types of osteoblast clusters and a new bone type.* Journal of Anatomy, 2016. **229**(1): p. 92-103.
93. Witten, P.E. and A. Huysseune, *A comparative view on mechanisms and functions of skeletal remodelling in teleost fish, with special emphasis on osteoclasts and their function.* Biological Reviews, 2009. **84**(2): p. 315-346.
94. Richman, J.M., M. Buchtová, and J.C. Boughner, *Comparative ontogeny and phylogeny of the upper jaw skeleton in amniotes.* Developmental Dynamics: An Official Publication of the American Association of Anatomists, 2006. **235**(5): p. 1230-1243.
95. Powers, A.K., et al., *Facial bone fragmentation in blind cavefish arises through two unusual ossification processes.* Scientific reports, 2018. **8**(1): p. 1-10.
96. Weigele, J. and T.A. Franz-Odendaal, *Functional bone histology of zebrafish reveals two types of endochondral ossification, different types of osteoblast clusters and a new bone type.* J Anat, 2016. **229**(1): p. 92-103.
97. Anderson, H.C., et al., *Impaired calcification around matrix vesicles of growth plate and bone in alkaline phosphatase-deficient mice.* The American journal of pathology, 2004. **164**(3): p. 841-847.

98. Miao, D. and A. Scutt, *Histochemical localization of alkaline phosphatase activity in decalcified bone and cartilage.* Journal of Histochemistry & Cytochemistry, 2002. **50**(3): p. 333-340.
99. Hambli, R., *Connecting mechanics and bone cell activities in the bone remodeling process: an integrated finite element modeling.* Frontiers in bioengineering and biotechnology, 2014. **2**: p. 6.
100. Edsall, S.C. and T.A. Franz-Odendaal, *A quick whole-mount staining protocol for bone deposition and resorption.* Zebrafish, 2010. **7**(3): p. 275-280.
101. Moran, D., R. Softley, and E.J. Warrant, *Eyeless Mexican cavefish save energy by eliminating the circadian rhythm in metabolism.* PloS one, 2014. **9**(9): p. e107877.
102. Antony Jesu Prabhu, P., J. Schrama, and S. Kaushik, *Quantifying dietary phosphorus requirement of fish–a meta-analytic approach.* Aquaculture Nutrition, 2013. **19**(3): p. 233-249.
103. Elliott, W.R., *The Astyanax Caves of Mexico: Cavefishes of Tamaulipas, San Luis Potosí, and Guerrero*. 2018: Association for Mexican Cave Studies.
104. Institute of Medicine Committee to Review Dietary Reference Intakes for Vitamin, D. and Calcium, *The National Academies Collection: Reports funded by National Institutes of Health,* in *Dietary Reference Intakes for Calcium and Vitamin D,* A.C. Ross, et al., Editors. 2011, National Academies Press (US)

105. Berning, D., et al., *In-Frame Indel Mutations in the Genome of the Blind Mexican Cavefish, Astyanax mexicanus.* Genome Biol Evol, 2019. **11**(9): p. 2563-2573.
106. Bradic, M., H. Teotónio, and R.L. Borowsky, *The population genomics of repeated evolution in the blind cavefish Astyanax mexicanus.* Mol Biol Evol, 2013. **30**(11): p. 2383-400.
107. Krishnan, J. and N. Rohner, *Sweet fish: Fish models for the study of hyperglycemia and diabetes.* J Diabetes, 2019. **11**(3): p. 193-203.
108. Yamamoto, Y., et al., *Development and evolution of craniofacial patterning is mediated by eye-dependent and-independent processes in the cavefish Astyanax.* Evolution & development, 2003. **5**(5): p. 435-446.
109. Gross, J.B., *The complex origin of Astyanax cavefish.* BMC Evol Biol, 2012. **12**: p. 105.
110. Dowling, T.E., D.P. Martasian, and W.R. Jeffery, *Evidence for multiple genetic forms with similar eyeless phenotypes in the blind cavefish, Astyanax mexicanus.* Mol Biol Evol, 2002. **19**(4): p. 446-55.
111. Strecker, U., L. Bernatchez, and H. Wilkens, *Genetic divergence between cave and surface populations of Astyanax in Mexico (Characidae, Teleostei).* Molecular ecology, 2003. **12**(3): p. 699-710.

112. Conley, Z.R., et al., *A quantitative method for defining high-arched palate using the Tcof1(+/-) mutant mouse as a model.* Dev Biol, 2016. **415**(2): p. 296-305.
113. Kimmel, C.B., et al., *Stages of embryonic development of the zebrafish.* Developmental dynamics, 1995. **203**(3): p. 253-310.
114. McCarthy, N., et al., *Pdgfra protects against ethanol-induced craniofacial defects in a zebrafish model of FASD.* Development, 2013. **140**(15): p. 3254-3265.
115. Loucks, E. and M.J. Carvan III, *Strain-dependent effects of developmental ethanol exposure in zebrafish.* Neurotoxicology and teratology, 2004. **26**(6): p. 745-755.
116. Fernandes, Y., D.M. Buckley, and J.K. Eberhart, *Diving into the world of alcohol teratogenesis: a review of zebrafish models of fetal alcohol spectrum disorder.* Biochem Cell Biol, 2018. **96**(2): p. 88-97.
117. Lovely, C.B., Y. Fernandes, and J.K. Eberhart, *Fishing for Fetal Alcohol Spectrum Disorders: Zebrafish as a Model for Ethanol Teratogenesis.* Zebrafish, 2016. **13**(5): p. 391-8.
118. Lovely, C.B., *Quantification of Ethanol Levels in Zebrafish Embryos Using Head Space Gas Chromatography.* Journal of visualized experiments: JoVE, 2020(156).
119. Terry, D.E., et al., *Differential use of Alcian blue and toluidine blue dyes for the quantification and isolation of anionic glycoconjugates from cell cultures: application to proteoglycans and a high-molecular-weight glycoprotein synthesized by articular chondrocytes.* Anal Biochem, 2000. **285**(2): p. 211-9.
120. Witten, P.E. and A. Huysseune, *A comparative view on mechanisms and functions of skeletal remodelling in teleost fish, with special emphasis on osteoclasts and their function.* Biol Rev Camb Philos Soc, 2009. **84**(2): p. 315-46.
121. Juergens, R.A. and A. Forastiere, *Combined modality therapy of esophageal cancer.* J Natl Compr Canc Netw, 2008. **6**(9): p. 851-60; quiz 861.
122. Chen, G., et al., *BMP signaling in the development and regeneration of cranium bones and maintenance of calvarial stem cells.* Frontiers in Cell and Developmental Biology, 2020. **8**: p. 135.
123. Bond, A.M., O.G. Bhalala, and J.A. Kessler, *The dynamic role of bone morphogenetic proteins in neural stem cell fate and maturation.* Dev Neurobiol, 2012. **72**(7): p. 1068-84.
124. Marrs, J.A., et al., *Zebrafish fetal alcohol syndrome model: effects of ethanol are rescued by retinoic acid supplement.* Alcohol, 2010. **44**(7-8): p. 707-715.
125. Kietzman, H.W., et al., *The teratogenic effects of prenatal ethanol exposure are exacerbated by Sonic Hedgehog or GLI2 haploinsufficiency in the mouse.* PLoS One, 2014. **9**(2): p. e89448.
126. Hu, X., et al., *Retinoic acid alters the proliferation and survival of the epithelium and mesenchyme and suppresses Wnt/β-catenin signaling in developing cleft palate.* Cell Death Dis, 2013. **4**(10): p. e898.

127. Murawski, N.J., et al., *Advances in Diagnosis and Treatment of Fetal Alcohol Spectrum Disorders: From Animal Models to Human Studies.* Alcohol Res, 2015. **37**(1): p. 97-108.
128. Lovely, C.B., *Animal models of gene-alcohol interactions.* Birth Defects Res, 2020. **112**(4): p. 367-379.
129. Becker, H.C., J.L. Diaz-Granados, and C.L. Randall, *Teratogenic actions of ethanol in the mouse: a minireview.* Pharmacol Biochem Behav, 1996. **55**(4): p. 501-13.
130. Küchler, E.C., et al., *Assessing the association between hypoxia during craniofacial development and oral clefts.* J Appl Oral Sci, 2018. **26**: p. e20170234.
131. Castilla, E.E., J.S. Lopez-Camelo, and H. Campaña, *Altitude as a risk factor for congenital anomalies.* Am J Med Genet, 1999. **86**(1): p. 9-14.
132. Jones, K.L., et al., *Acardiac fetus: evidence in support of a vascular/hypoxia pathogenesis for isolated oral clefting.* Birth Defects Res A Clin Mol Teratol, 2008. **82**(8): p. 597-600.
133. Fushimi, S., et al., *17beta-Estradiol inhibits chondrogenesis in the skull development of zebrafish embryos.* Aquat Toxicol, 2009. **95**(4): p. 292-8.
134. Iyyanar, P.P.R. and A.J. Nazarali, *Hoxa2 Inhibits Bone Morphogenetic Protein Signaling during Osteogenic Differentiation of the Palatal Mesenchyme.* Front Physiol, 2017. **8**: p. 929.
135. Ardinger, H.H., et al., *Association of genetic variation of the transforming growth factor-alpha gene with cleft lip and palate.* Am J Hum Genet, 1989. **45**(3): p. 348-53.